

MASTER

Numerical investigation of the urban heat island effect on outdoor and indoor climate conditions and thermal comfort case study for a care center in Rotterdam

Nugteren, I.M.

Award date:
2013

[Link to publication](#)

Disclaimer

This document contains a student thesis (bachelor's or master's), as authored by a student at Eindhoven University of Technology. Student theses are made available in the TU/e repository upon obtaining the required degree. The grade received is not published on the document as presented in the repository. The required complexity or quality of research of student theses may vary by program, and the required minimum study period may vary in duration.

General rights

Copyright and moral rights for the publications made accessible in the public portal are retained by the authors and/or other copyright owners and it is a condition of accessing publications that users recognise and abide by the legal requirements associated with these rights.

- Users may download and print one copy of any publication from the public portal for the purpose of private study or research.
- You may not further distribute the material or use it for any profit-making activity or commercial gain

Numerical investigation of the urban heat island effect on outdoor and indoor climate conditions and thermal comfort

Case study for a care center in Rotterdam

...
Graduation report

8 November, 2013

I.M. Dijkstra - Nugteren BSc

0631589

i.m.nugteren@student.tue.nl

TU/e Technische Universiteit
Eindhoven
University of Technology

Colofon

Document information

Document title: Graduation report

Project title: Numerical investigation of the urban heat island effect on outdoor and indoor climate conditions and thermal comfort - case study for a care center in Rotterdam

Date: 8 November, 2013

Personal information

Name: I.M. Dijkstra - Nugteren BSc

Mail: i.m.nugteren@student.tue.nl

Student number: 0631589

Master track: Architecture, Building and Planning (ABP), Building Physics and Services (BPS)

Graduation committee

Chairman: prof. dr. ir. B. Blocken (b.j.e.blocken@tue.nl)

Daily supervisor: ir. W. Janssen (w.d.janssen@tue.nl)

Extra supervisor: dr. ir. T. van Hooff (t.a.j.v.hooff@tue.nl)

Acknowledgements

The last year I have been working on my graduation project of the Master track Building Physics and Services at Eindhoven University of Technology. A special thanks goes to my research committee for their supervision: prof. dr. ir. Bert Blocken (chairman of committee), dr. ir. Twan van Hooff and ir. Wendy Janssen (daily supervisors). Besides, I would like to express my appreciation to all the people present at the urban physics progress meetings. Furthermore, I would like to thank the following PhD candidates/Postdocs for their support with some specific problems in the research: Christof Gromke, Mike van der Heijden, Hamid Montazeri, Rubina Ramponi and Yasin Toparlar.

Finally, I would like to thank my friends and family. In particular, I would like to thank my parents who supported me during my entire study. Last but not least, I would like to thank Rutger for supporting me with love and care.

Ilse Dijkstra - Nugteren

8 November, 2013

Abstract

The phenomenon of urban heat islands (UHI's), being urban areas which are much warmer than the surrounding rural areas, was long thought not to be significant in the Netherlands. However, several researches in the last decades have proven that the UHI effect is present in the Netherlands, especially for the larger cities. Combined with the prospects of climate change and increased urbanization, urban heat islands are expected to be even more significant in the future. Therefore, more research is dedicated to this topic.

The significance of the UHI effect and its consequences for outdoor and indoor temperatures are investigated for a case study, being a care center and its surroundings in the city centre of Rotterdam. Also the effects on thermal comfort of the elderly, who form a sensitive group for heat stress, are taken into account.

A literature study is performed on the UHI effect, the effects of excessive heat on the elderly and thermal comfort models. As a next step, a care center in Rotterdam is selected for evaluation and building documentation is being collected. For the calculation of the UHI effect, Computational Fluid Dynamics (CFD) is used. Detailed models are developed of the care center in Rotterdam and the same care center placed in a rural surrounding. A validation study is performed of both average surface temperatures of the city centre and the air temperature on a fixed position.

Surface heat island intensities (SHI intensities) and atmospheric urban heat island intensities (UHI intensities) are calculated for 3 moments during a hot day of the 2nd heat wave of 2006. UHI intensities are lower than the SHI intensities and also the variation (in time and place) is smaller. Highest values are found for the noon case, followed by the morning case. The late afternoon case shows the lowest UHI and SHI intensities. UHI intensities are more dependent on their distance from building facades and local air velocities than whether these positions are in sunlit or shaded areas. SHI intensities are highly dependent on solar radiation and the grounds surface properties. The effect of air velocities on SHI intensities is visible, but less pronounced than for the UHI intensities.

The Universal Thermal Climate Index (UTCI) equivalent temperature is used as a performance indicator of outdoor thermal comfort of the elderly. At noon, strong heat stress occurs in most regions around the care center. In the morning, the UTCI equivalent temperatures are the lowest. When air temperatures are high, which is the case for a heat wave, thermal comfort is highly dependent on the relative humidity.

Initial results about the indoor environment are as follows. For the care center placed in the rural environment, indoor temperatures are highly overestimated. Better results might be achieved with transient simulations.

Large initialization times are found for the models including the indoor environment of the care center because of the use of the solar load model. A parameter study on initialization times is performed. The initialization time seems to be highly dependent on 3 parameters: the type of walls, the number of cells in the domain and the number of boundaries in the domain. Furthermore, an increase of interfaces also leads to an increase of the initialization time.

Table of contents

1. Introduction	11
1.1 Urban heat islands	11
1.2 Relevance and problem statement	11
1.3 Research aim	12
1.4 Research questions	12
1.5 Research approach	13
2. Literature study	15
2.1 Urban heat island effect	15
2.2 Effects of excessive heat on the elderly	16
2.3 Thermal comfort models	19
3. Case selection and description	25
3.1 Selection procedure	25
3.2 Building description care center Atrium	28
4. CFD simulations: settings and parameters	33
4.1 Strategy	33
4.2 Geometry	34
4.3 Initial and boundary conditions	50
4.4 Solution parameters	57
4.5 Thermal model	58
4.6 Summary settings	58
5. CFD simulations: validation study	61
5.1 Validation of surface temperatures	61
5.2 Validation of air temperatures	68
6. Results: outdoor environment	75
6.1 UHI intensity	75
6.2 SHI intensity	78
6.3 Outdoor thermal comfort	81
7. Results: indoor environment	91
7.1 Calculation procedure and initialization problem	91
7.2 Parameter study	94
8. Discussion	99
8.1 CFD settings and parameters	99
8.2 Validation study	99
8.3 UTCI equivalent temperature	100
8.4 Initialization time	101
8.5 Recommendations for further research	101
9. Conclusions	103
Nomenclature	105

References	109
Appendix 1: subdomains	117
Appendix 2: inlet profiles	121
Appendix 3: UTCI MATLAB script	123

1. Introduction

This is a report for the graduation project of the master track '*Building Physics and Services*'. Topic of the research is the urban heat island effect and its consequences for the temperatures in and around a care center in Rotterdam. Also the effects of increased temperatures on thermal comfort of the elderly will be taken into account.

The report starts with an introduction in which the relevance, research questions, goals and approach will be explained. In chapter 2, a literature study can be found. Then, the selection procedure of a care center and its properties will be described in chapter 3. Chapter 4 - 7 are dedicated to the CFD simulation part. In chapter 4, the settings and parameters of the simulations will be explained. In the next chapter, the validation study will be described in detail. Results will be presented and discussed in chapter 6 and 7. At the end of the report a discussion chapter and a chapter with conclusions can be found.

1.1 Urban heat islands

The topic of this research is the urban heat island effect. This is the effect that an urban area is significantly warmer than its surrounding rural areas (Dorland & Saunders, 2007). In the city, materials are used with larger storage capacities and other transfer properties than rural materials. Waste heat from human activities and a higher air pollution rate also result in higher temperatures in urban environments. Research has shown that the UHI effect is most pronounced during summer nights with little wind and a clear sky (Steenefeld & van Hove, 2010; van Hove et al., 2011a). Especially during heat waves, the temperature difference between the city and the rural area can be significant. The UHI effect will be described in more detail in the literature study in chapter 2.

Excessive heat can have negative effects on indoor and outdoor thermal comfort during summer. Also health problems and death rate might increase, as was noticed during heat waves. During the heat waves of 2003 and 2006, there were between 2400 and 3200 heat-related deaths in the Netherlands and hospitalizations in Spain and France increased (Vanheems et al., 2003; Cajato et al., 2005; Rahola et al., 2009). People who are most sensitive to high temperatures are elderly and ill people, because of the reduced temperature perception, use of medication, presence of illnesses, reduced thirst stimulus and reduced transpiration ability (Döpp, 2011). Another consequence of the UHI effect is that the energy usage in summer will increase: because of the higher temperatures more air conditioning is used (Döpp, 2011).

1.2 Relevance and problem statement

It was long thought that the urban heat island effect was only present in large foreign urban cities such as Washington or Los Angeles. However, recent research has shown that the urban heat island effect is also present in Dutch cities. For example, in a research performed by Heusinkveld et al. (2010) maximum air temperature differences of 7°C were found between the city centre of Rotterdam and a weather station at Rotterdam airport. These results were based on air temperatures measured during a hot summer day in August 2009 with a bicycle equipped with a weather station. Also in a research by Steenefeld et al. (2011), where the UHI intensity of 20 Dutch cities with varying populations from 1.000 to 1.000.000 inhabitants was being investigated, the urban heat island effect was found to be present particularly in the larger cities in the Netherlands. The results were based on meteorological observations by hobby meteorologists.

KNMI (Royal Dutch meteorological institute) has predicted four different scenarios for the temperatures in the Netherlands in 2050. The scenarios are different, but the conclusions are similar (Döpp, 2011):

- Summer temperatures will rise
- The number of heat waves will increase; in the Netherlands heat waves are defined as a period of five consecutive days with maximum air temperatures > 25°C of which on three days maximum air temperatures of ≥ 30°C are reached (KNMI).
- The number of tropical days (max. temperature > 30°C) will increase.

Furthermore, it is predicted that 60% of the world population will be living in urban areas, compared to 49% in 2005 (Kim & Baik, 2004; Choi et al., 2009). Also for the Netherlands, it is expected that the process of urbanization will continue (Nijs et al., 2002). Therefore, the urban heat island effect will be more pronounced in the future. This makes research concerning the consequences of the urban heat island effect of great importance.

Until now, little research has been done on the UHI effect in the Netherlands. The focus of recently performed UHI studies was on the outdoor temperature rise in Dutch cities such as Utrecht and Rotterdam. Because people spend more than 90% of their life in buildings and because of the mentioned negative effects of UHI's on thermal comfort and human health, research on the UHI effect on the indoor climate could be of great value as well (Duijm et al., 2007). Powerful numerical simulation tools could be used to make the translation of the UHI effect to the outdoor temperatures, the indoor temperatures and finally on thermal comfort and health.

1.3 Research aim

At the moment, weather forecasts only give temperatures in rural areas (because this is the place where the weather stations are located), so the UHI effect is not taken into account (Döpp, 2011). The goal of this research is to calculate the UHI effect for the 2nd heat wave of 2006 for a part of Rotterdam making use of CFD. The higher outdoor temperatures caused by the UHI effect will lead to higher indoor temperatures, assuming no air conditioning. Although the heat wave of 2003 got much more media attention due to the high related mortality rate in different European countries, the 2nd heat wave of 2006 was chosen for evaluation because of its longer duration and higher corresponding air temperatures measured at Rotterdam airport (see Table 1.1). Furthermore, it was not the heat wave of 2003 but the 2nd heat wave of 2006 which reached a top four position of the Netherlands in the yearly world ranking of countries with most deaths caused by natural disasters (Gruyter, 2007). The hottest day of this heat wave was July 19th with a maximum day temperature of 34.6°C at Rotterdam airport (KNMI).

Table 1.1: Information about the heat waves of 2003 and 2006 for Rotterdam (KNMI)

Heat wave	Summer days	Tropical days	Duration	T _{max} Rotterdam airport [°C]
August 2003	7	7	14	32.9
July 2006 - I	4	3	7	31.6
July 2006 - II	8	8	16	34.6

The rise of indoor temperatures due to the UHI effect will be simulated for a case study in the chosen district of Rotterdam. The case study will be a care center without air conditioning. These building types are relevant, because the elderly are most sensitive to high temperatures (Döpp, 2011). Finally, the effect of the temperature rise on thermal comfort will be investigated.

1.4 Research questions

In order to reach the research aim, some research questions have been defined. The research questions with their sub questions are given below.

- 1) *What is the contribution of Rotterdam (UHI effect) on the temperature rise and thermal comfort around a care center in Rotterdam for the 2nd heat wave of 2006?*
 - a. *How significant is the UHI effect around the care center during the heat wave?*
 - b. *What is the effect of the temperature rise on outdoor thermal comfort of the elderly?*

Initially, the following research question was formulated about the indoor environment of the care center:

- 2) *What is the contribution of Rotterdam (UHI effect) on the temperature rise and thermal comfort in the care center in Rotterdam for the 2nd heat wave of 2006?*
 - a. *How significant is the UHI effect for the chosen care center during the heat wave?*
 - b. *What is the effect of the indoor temperature rise on thermal comfort of the elderly?*

However, during the progress of the project it was found that this question about the indoor environment of the care center was not feasible in time for this graduation research. This is especially caused because of the occurrence of large initialization times of large CFD models using the solar load model (this will be discussed in more detail in the results chapter). Nevertheless, a detailed CFD model of the care center in Rotterdam has been developed in this research. The modeling approach and applied settings and parameters of this model will be described in detail. Furthermore, a study about the impact of different simulation parameters on the initialization time will be given. Therefore, the following research question will be answered in this research:

- 2) *Which parameters have the greatest impact on the initialization time and how could the time needed for initialization of a CFD simulation combined with the solar load model be decreased?*

1.5 Research approach

The research questions will be answered by following the next steps. First of all, a literature study will be performed on the urban heat island effect, its consequences on thermal comfort, morbidity and mortality of elderly, and thermal comfort models.

Secondly, a care center will be selected for this research. It should be located in Rotterdam: for this city, useful weather data is available of the heat wave of 2006 which is needed for the simulation part. In addition, several studies have shown that the UHI effect is present in Rotterdam (Heusinkveld et al., 2010; Steeneveld et al., 2011; Klok et al., 2012).

Then, data of the care center and its surroundings will be collected. For simulating the outdoor temperatures and indoor temperatures of the care center, CFD shall be used. In total, three different models will be made.

A model of Rotterdam without the indoor environment of the care center will be used for the validation of the outdoor temperatures. The model will be validated with measurement data. These are average surface temperatures of Rotterdam based on satellite data as reported in an article by Klok et al. (2012) and air temperature measurements of a weather station of the Dutch national research program 'Knowledge for Climate' located in the city centre of Rotterdam.

The model used for the validation study will also be used to give an answer on the first research question and its sub questions. The UHI intensity will be calculated by comparing the simulated air and surface temperatures in the city with air temperature and surface temperatures of the surrounding rural area as found in literature. Thermal comfort models will be used to investigate the effect of the outdoor temperatures on thermal comfort of the elderly.

For the investigation of the UHI effect on temperatures and thermal comfort inside the care center, 2 models are needed: (1) a model of Rotterdam including the indoor environment of the care center and (2) a model of the same care center including the indoor environment placed in a rural environment. In this way, the contribution of the city to the indoor temperatures can be calculated.

2. Literature study

This research is focused on the urban heat island effect. In this paragraph, both the causes and consequences of the UHI effect will be described. Special attention is given to the negative consequences of excessive heat on the elderly in terms of thermal comfort, morbidity and mortality.

2.1 Urban heat island effect

2.1.1 Types

An urban heat island is defined as an urban area which is significantly warmer than its surrounding rural areas (Dorland & Saunders, 2007). A distinction can be made between surface urban heat islands (SHI) and atmospheric urban heat islands (UHI), where the SHI intensity is the difference between urban and surrounding rural surface temperatures and the UHI intensity the difference between air temperatures measured in a city and in the surrounding rural area (Klok et al., 2012). SHI intensities are defined based on satellite data or surface temperature measurements, while UHI intensities are measured with mobile or fixed weather stations. Surface heat islands are most pronounced during the day when the sun is shining, while the peak in the atmospheric urban heat island is typically measured after sunset due to the slow release of heat from urban structures (van Hove et al., 2011b).

Atmospheric urban heat islands can be further subdivided into urban canopy layer (UCL) heat islands and urban boundary layer (UBL) heat islands. In research on UCL heat islands, the layer between ground and rooftops is being observed, which is the layer of the air where people live. In UBL heat island research, the region between rooftop and the point where the urban landscape no longer influences the atmosphere is being observed (van Hove et al., 2011b). In this research, focus is on SHI's and UCL heat islands.

2.1.2 Causes

UCL heat islands occur because of a changed energy balance caused by the different urban properties compared to rural properties.

First of all, the effect occurs due to the replacement of vegetation by urban materials such as concrete and asphalt for roads, buildings and other structures (Wong et al., 2008). These urban materials have different radiation and thermal properties than vegetation. Typically, albedo values of urban surfaces are lower which means that more radiation is being absorbed, than reflected. Furthermore, radiation levels in urban areas are higher due to the lower overall urban thermal emissivity being a measure for a surface's ability to lose heat. In urban areas, more heat is being stored due to higher heat capacities of the used materials (van Hove et al., 2011b). Because of a reduction of vegetation, less cooling is provided by evapotranspiration (Rahola et al., 2009).

Secondly, the urban heat island effect is caused by the geometry of a city. Urban canyons with high rise buildings and small streets cause more solar radiation to be absorbed because of the greater surface area and 'trapping' of heat by multiple reflections (Oke, 1995). Urban areas also have lower Sky View Factors (SVFs) than rural areas as can be seen in Figure 2.1. This means that a smaller part of the sky is visible from ground level. Therefore, the long-wave radiation loss is being reduced (Brandsma, 2010). Finally, wind speeds are lower in wake regions of buildings compared to open areas, resulting in a decreased total turbulent heat transport (Oke, 1995).

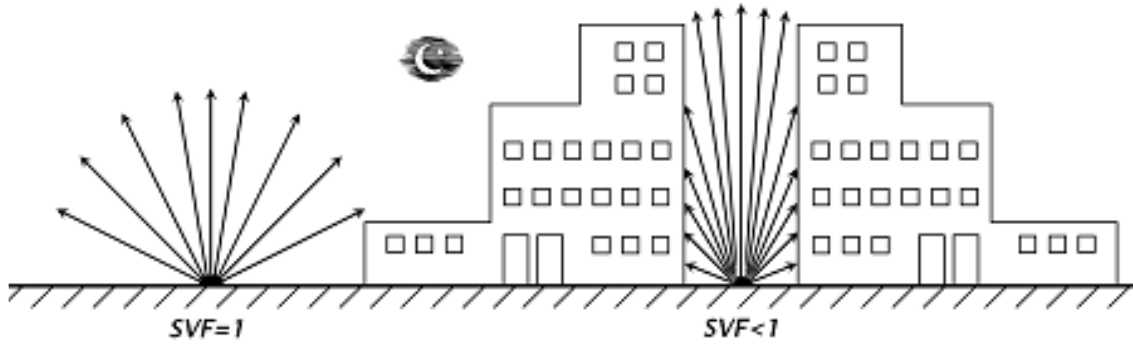


Figure 2.1: Urban geometries are identified by low Sky View Factors (retrieved from KNMI on November 1st, 2013)

The UHI effect is also caused by the anthropogenic waste heat released during energy conversion by human activities such as industry, households and traffic (Döpp, 2011).

Finally, air pollution should be mentioned. Particles in the air absorb infrared radiation resulting in an increased long-wave radiation from the sky (Oke, 1995). An overview of the different urban properties causing urban heat islands to form and their effects on the urban energy balance is given in Table 2.1.

Table 2.1: Overview of urban properties and their effects on the urban energy balance based on Oke (1995)

Cause		Change in urban energy balance
1) Properties of urban materials	<ul style="list-style-type: none"> * Lower overall albedo values * Higher overall thermal emissivity * Higher heat capacities * Surface 'water proofing' 	<ul style="list-style-type: none"> Increased solar absorption Increased storage of sensible heat Increased storage of sensible heat Decreased evapotranspiration
2) Urban geometry	<ul style="list-style-type: none"> * Greater surface area and 'trapping' by multiple reflection * Smaller sky view factors * Increased wind shelter 	<ul style="list-style-type: none"> Increased solar absorption Decreased net long-wave radiation loss Decreased total turbulent heat transport
3) Anthropogenic heat	<ul style="list-style-type: none"> * Industry, households, traffic 	<ul style="list-style-type: none"> Anthropogenic heat release
4) Air pollution	<ul style="list-style-type: none"> * Greater infrared absorption and re-emission 	<ul style="list-style-type: none"> Increased long-wave radiation from the sky

2.1.3 Consequences

The UHI effect combined with climate change and prospected trends in urbanization, has several negative consequences. First of all, energy usage in summer will increase because more air conditioning is used due to higher urban temperatures (Döpp, 2011). Besides, the higher temperatures add pressure to the electricity grid during peak periods of demand such as hot summer weekdays. Higher energy consumption in turn results in more air pollution and greenhouse gas emissions. Also a deteriorating water quality is a result of the UHI effect. It is caused by thermal pollution because the runoff water has higher temperatures due to the higher surface temperatures of concrete and asphalt. Finally, the higher temperatures can have negative effects on productivity, thermal comfort, health problems and death rate (Wong et al., 2008). People who are very sensitive to high temperatures are elderly and ill people (Döpp, 2011). The effects of excessive heat on elderly will be discussed in more detail in the next paragraph.

2.2 Effects of excessive heat on the elderly

2.2.1 Human heat balance

In order to understand the effects of excessive heat on the elderly, it is important to realize how the thermal heat balance of the human body works. The thermal heat balance consists of all heat fluxes between the

human body and its environment (Fanger, 1972). The thermal heat balance is shown in the following equation as defined by Fanger (1972):

$$M + W + \overbrace{C + R + E_{re} + E_{sw} + E_d}^{\text{heat fluxes}} + L = 0 \quad (2.1)$$

With:

M =	rate of metabolic heat production	[W/m ²]
W =	rate of mechanical work accomplished	[W/m ²]
C =	convective heat transfer	[W/m ²]
R =	heat loss by radiation	[W/m ²]
E _{sw} =	evaporation heat loss due to sweating	[W/m ²]
E _d =	heat loss by water vapor diffusion through the skin	[W/m ²]
E _{re} =	latent heat loss due to respiration	[W/m ²]
L =	sensible (dry) heat loss due to respiration	[W/m ²]

The metabolic heat production and mechanical work accomplished are dependent on personal characteristics and the activity rate. The heat fluxes of the thermal balance depend on climatic variables: air temperature, mean radiant temperature, air speed and relative humidity (Fanger, 1972).

The heat production and release over a longer period should be in balance in order to keep the core temperature of the body in a narrow range of 36.8 to 37.7°C (Döpp, 2011; Daanen & Herweijer, 2012). The core temperature is being regulated by constriction and dilating of our skin blood vessels. During cold, the heat production will be increased through shivering and in a lesser extent by fat burning. At high temperatures, the heat release will be increased by a higher sweat rate.

Especially the elderly are sensitive to higher temperatures because of several reasons. First of all, they have a reduced ability to sweat which makes them less capable of losing heat. Furthermore, they have a reduced thirst stimulus. This means that they do not drink extra at higher temperatures, while younger people would. Furthermore, the use of medication can have negative effects on the thermoregulation. Finally, mental disorders such as dementia negatively affect their risk perception. For example, they do not adapt their clothes when indoor temperatures increase (Rahola et al., 2009; Oudin Astrom et al., 2011).

Excessive heat can, in range of severity, lead to:

- thermal discomfort and heat stress
- heat related diseases and a higher morbidity rate
- increase of mortality rate

2.2.2. Thermal discomfort and heat stress

Thermal comfort can be defined as the expression of mind which expresses satisfaction with the thermal environment (ASHRAE, 2010). Because people are different, both psychological and physiological, an environment experienced as thermally comfortable for one person could be thermally uncomfortable for the other (Schellen et al., 2013). Thermal comfort is being influenced by air temperature, humidity levels, wind speed and solar radiation. Also a person's individual behavior, clothing, gender, age and activity level can influence the thermal comfort level (Rahola et al., 2009). In order to perceive thermal comfort, heat gains and losses of the human body must be in balance, the body should experience no local discomfort and the mean skin temperature and sweat rate must be within certain limits (van Hoof & Hensen, 2006). When this is not the case, one speaks about discomfort.

At a certain temperature threshold, the human body is not able to lose the excess heat anymore. In that case, the issue is not thermal discomfort but heat stress. In case of heat stress, high air temperatures lead to an increase of the core temperature which is called hyperthermia (Daanen, 2004). As a result, symptoms occur such as irritability, thirst, exhaustion and dizziness. An increase of the core temperature was also found in a study performed by Daanen et al. (2011): high core temperatures of $> 38^{\circ}\text{C}$ were measured for an elderly lady who stayed in a room with indoor temperatures between 25 and 31°C .

2.2.3 Heat related morbidity

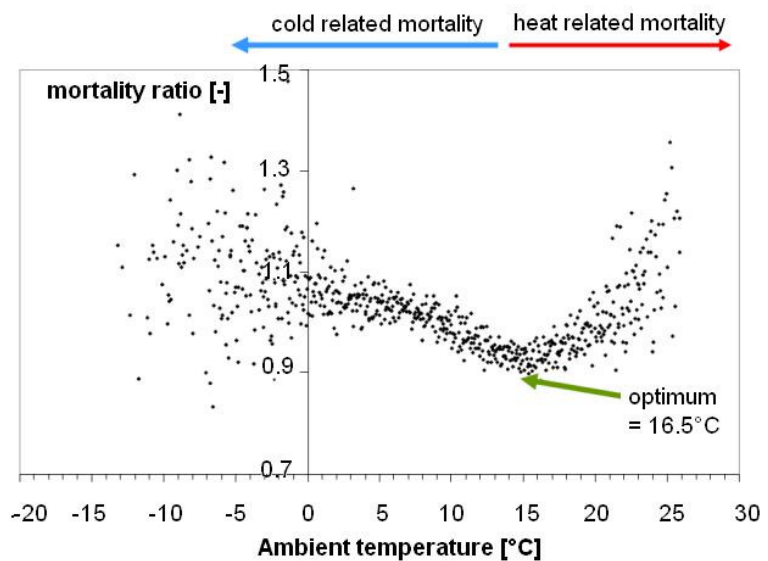
There are several illnesses that can occur because of excessive heat. In order of severity these are heat rash, heat cramps, heat exhaustion and heat strokes (Rahola et al., 2009).

In morbidity studies, the number of hospitalizations is used as an indicator for morbidity. In a study performed by Hansen et al. (2008), the amount of hospitalizations among the Australian population during heat waves was compared with non-heat wave periods. During heat waves, an increased amount of hospitalizations was found for the elderly aged over 75 years suffering from mental and behavioral disorders. Also in other studies, increased hospitalizations were found in particular for the elderly. A majority of morbidity studies, report an increase of hospitalizations for cardiovascular and especially respiratory diseases (Oudin Astrom et al., 2011).

Parsons et al. (2011) found a relationship between ambient temperatures and hospital admissions for the United Kingdom: each $^{\circ}\text{C}$ temperature rise above 18°C results in an extra 0.36% of hospital admissions and each $^{\circ}\text{C}$ drop in temperature below 18°C means a drop of hospital admissions of 0.64%. It is thought that these numbers can also be applied to the Netherlands (Stone et al., 2013). The increase in hospitalizations is not as dramatic as the increase in death rate caused by excessive heat. This could have 2 reasons: (1) during a heat wave, people die suddenly and do not get medical help in time. The fact that many elderly live alone contributes to this hypothesis (Döpp, 2011; Oudin Astrom et al., 2011) or (2) due to the ceiling effect in hospital admissions which can only increase to a maximum number of beds available (Oudin Astrom et al., 2011).

2.2.4 Heat related mortality

The effect of ambient temperatures on death rate can be described with a v-shaped curve. Death rate is lowest at an optimum temperature. Above and below that optimal temperature, mortality increases. The optimum temperature differs per country (Döpp, 2011). The relation between the average day temperature and excess mortality for the Netherlands, as described in Huynen et al. (2001), is given in Figure 2.2.



At 16.5°C the lowest values were found for total mortality, cardiovascular mortality, respiratory mortality as well as mortality among

Figure 2.2: Relation between the average ambient day temperature $[^{\circ}\text{C}]$ and excess mortality in the Netherlands. The mortality ratio equals the observed number of deaths on day $i \pm$ mean number of deaths over the whole study period (modified from Huynen et al., 2001)

people aged 65 years and older. For excess heat mortality a higher slope was found than for cold related mortality: an increase of 2.72% and respectively 1.37% for each degree Celsius above or below the optimum temperature. The average total heat related mortality found during a heat wave was 12.1% or 39.8 deaths/day for the Netherlands. Excess mortality is being influenced by climatic conditions such as wind speed and relative humidity rate: increased wind speeds reduce heat related mortality, while high humidity levels increase mortality (Kunst et al., 1991).

In 1997, Mackenbach et al. studied the heat-related mortality among Dutch nursing-home patients. In this study, national registered data about death rate in nursing homes during the years 1993 and 1994 were observed. For each week, the weekly averages of maximum daily temperatures in De Bilt were collected. The results more or less correspond with the v-shaped mortality curve of Figure 2.2. It was found, that mortality rates are lowest in weeks with average outside temperatures between 15 and 20°C. In the hottest weeks with temperatures between 25 and 30°C, mortality rates increased with 50% compared to the minimum rates. This means that 10 additional elderly die every week in Dutch nursery homes when ambient temperatures are between 25 and 30°C compared to 15 - 20°C (Daanen & Herweijer, 2012).

Several studies have concluded that heat related mortality is mainly observed with elderly of over 75 years of age (Diaz et al., 2002; Kovats & Hajat, 2008). This can also be seen in Figure 2.3, which shows a much larger peak in death rate in London among the elderly aged over 75 years compared to the younger people during the heat wave of 2003.

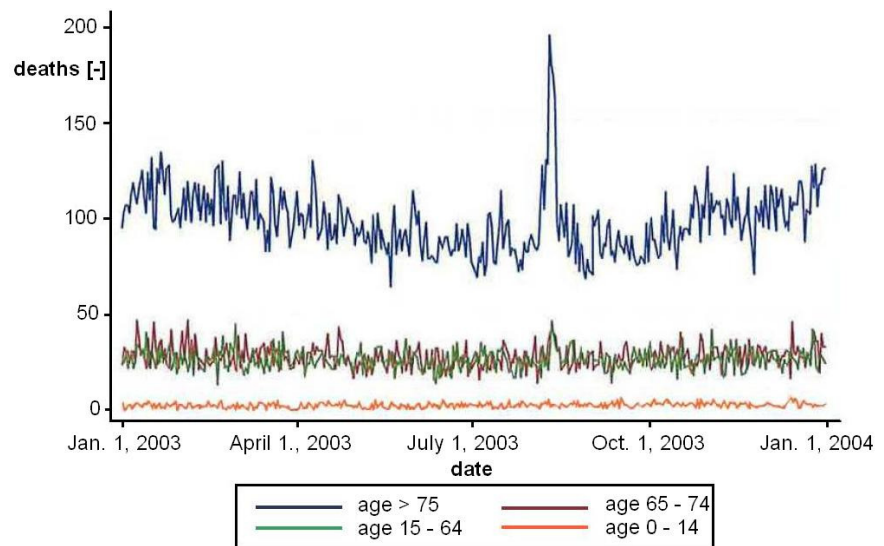


Figure 2.3: Mortality in greater London in 2003 (modified from Kovats & Hajat, 2008)

Because heat related mortality is particularly

observed among the elderly, increased death rate during heat waves is in some studies referred as 'harvesting'. This means a temporal increase of mortality among vulnerable persons being compensated by decreased mortality within the upcoming period (Rahola et al., 2009). This is only partly true: after a heat wave only half of the heat related deaths are compensated by a reduced death rate in a period of 7 - 30 days after the heat wave (Daanen, 2004).

2.3 Thermal comfort models

In this paragraph, thermal comfort models will be described as well as their applicability for the thermal comfort assessment of the elderly. Both models for indoor and outdoor applications will be discussed.

2.3.1 PMV/PPD model

Several studies have been performed to create models which could predict thermal comfort or heat stress in the design stage of a building. One of the first developed thermal comfort models is the Predicted Mean Vote model (PMV model) by Fanger (1972). This model predicts the mean thermal sensation vote (PMV) of a group of people with comparable activity levels (metabolism) and clothing resistance. The PMV is linked to

thermal comfort through the Predicted Percentage of people who will be Dissatisfied (PPD) with the thermal environment. The results of the PMV model are given on the seven-point thermal sensation scale of ASHRAE (see Figure 2.4). Fanger defined that the thermal neutral condition is the most comfortable condition. This is the condition in which a person does not prefer either a colder or warmer environment (Fanger, 1972). In thermophysiology, which is the study of the thermoregulation of the human body (Dorland & Saunders, 2007), the thermal neutral region is defined as the range of ambient temperatures without regulatory changes in metabolic heat production or evaporative heat loss.

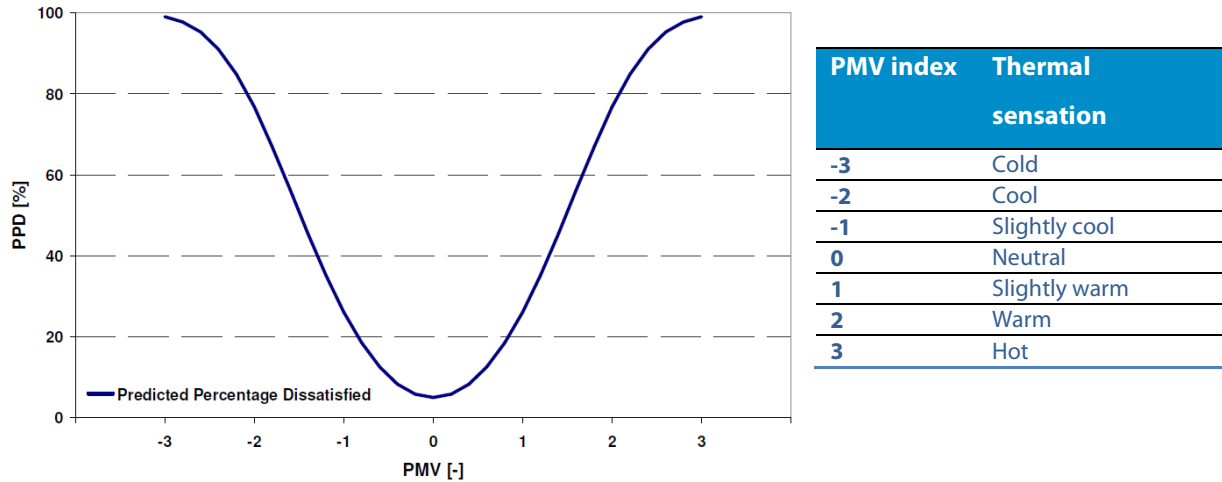


Figure 2.4: PPD as function of the PMV value (left) and seven-point thermal sensation scale of PMV-index (right) (Fanger, 1972)

In 2003, Rutten & Hensen used Fanger’s model for the prediction of the optimum indoor temperature in nursery homes based on a literature review of clothing resistances and activity levels of elderly. Because of the thermal insulation effect of a bed, the effective thermal resistance is in the range of 1.8 - 2.5 clo for bedridden people compared to a much lower resistance of 0.4 - 0.7 clo when being out of bed. The optimum temperatures (PMV = 0) for different combinations of clothing types and activity levels in the summer period are depicted in Table 2.2.

Table 2.2: Thermal comfortable indoor temperatures [°C] based on clothing resistance and metabolism (Rutten & Hensen, 2002)

Summer situation			
- patient in bed - sheet + blanket	Clothing resistance [Clo]	2.0	2.5
	Metabolism [MET]	0.8	0.9
	T _o (PMV = -0.5) [°C]	21.0	18.5
	T _o (PMV = 0) [°C]	23.0	21.0
	T _o (PMV = 0.5) [°C]	25.0	23.5
- patient in bed - sheet only	Clothing resistance [Clo]	1.8	1.9
	Metabolism [MET]	0.8	0.9
	T _o (PMV = -0.5) [°C]	21.5	19.5
	T _o (PMV = 0) [°C]	23.5	22.0
	T _o (PMV = 0.5) [°C]	25.5	24.0
- patient out of bed - sitting in a chair	Clothing resistance [Clo]	0.5	0.7
	Metabolism [MET]	1.0	1.6
	T _o (PMV = -0.5) [°C]	25.5	22.5
	T _o (PMV = 0) [°C]	27.0	24.0
	T _o (PMV = 0.5) [°C]	28.0	26.0
- patient out of bed - moving	Clothing resistance [Clo]	0.4	0.7
	Metabolism [MET]	1.4	1.6
	T _o (PMV = -0.5) [°C]	22.5	19.5
	T _o (PMV = 0) [°C]	24.5	22.0
	T _o (PMV = 0.5) [°C]	26.0	24.5

Normally, a predicted mean vote > -0.5 and < 0.5 equals a PPD of less than 10%. However, in a research of Parsons & Webb (1997) it was found that this percentage is higher among people with physical disorders.

The PMV/PPD model is not applicable in every situation. Because the PMV/PPD model is based on a steady-state human heat balance, it is intended for steady-state situations with temperatures close to the neutral temperature (Spagnolo & de Dear, 2003). De Dear et al. (1997) found that the PMV/PPD model is too restrictive for naturally ventilated buildings.

2.3.2 PET model

Another model used for thermal comfort assessment is the Physiological Equivalent Temperature model (PET model). It is based on the equations of the Munich Energy-balance Model for Individuals (MEMI) (Höppe, 1999). A value called PET is calculated based on these MEMI equations. PET is the air temperature at which the human balance is maintained with core and skin temperatures equal to those under the conditions being assessed (Höppe, 1999). Unfortunately, this model is also intended for steady-state situations. However, thermophysiological processes are taken into account which makes it a more sophisticated model than the PMV model. It is unknown if this model is also suitable for the thermal comfort assessment of elderly.

2.3.3 UTCI index

The Universal Thermal Climate Index is based on the combination of a thermophysiological model of Fiala and an adaptive clothing model. The index is expressed as an UTCI equivalent temperature which is defined as the air temperature of a reference environment that produces the same strain index value for a given combination of wind, radiation, humidity and air temperature (Bröde et al., 2011a). The UTCI equivalent temperature then gives information about the category of heat stress that will occur.

The multi-node Fiala model consists of a passive and an active system. The passive system represents the reference person. This passive system consists of 12 body elements which are subdivided into 63 sectors. The skin is modeled as 2 layers. The active system predicts the thermoregulatory reactions of the central nervous system for a certain atmospheric condition (Blazejczyk et al., 2011). The passive system of the Fiala model represents an average person with a body surface area of 1.85 m^2 , and body weight of 73.4 kg (Fiala et al., 2011). Based on data from the anthropometric database DINED about the Dutch population, an average length and weight of respectively 1.66 m and 73.3 kg was found for elderly over 65 years old (DINED anthropometric database). With the Body Surface Area (BSA) formula of Mosteller ($BSA = (\text{height} \cdot \text{weight}/36)^{0.725}$), this results in a BSA of 1.84 m^2 (Mosteller, 1987). The average person used for the Fiala-model therefore also represents an average Dutch person of 65+ years old.

Because the UTCI is developed for outdoor applications, the thermal index should cover the entire climate range from heat to cold. Therefore it was necessary to consider clothing as the interface between the person and the environment (Havenith et al., 2011). For this reason the Fiala model was coupled with a clothing model. Based on observations in the field of dressing behavior for different temperatures, a model was developed of the clothing distribution over the different body parts in relation to the ambient temperature (Havenith et al., 2011). Also changes in clothing insulation and vapor resistance caused by body movement and wind are taken into account in the clothing model (Havenith et al., 2011).

For the UTCI, a reference condition is described. The non-meteorological reference conditions are defined as a person walking 4 km/hr ($\pm 1.1 \text{ m/s}$) at a metabolic rate of 135 W/m^2 (Blazejczyk et al., 2013). For the meteorological reference condition the following values were assumed (Blazejczyk et al., 2013):

- Wind speed (u) of 0.5 m/s at 10 m height;
- a mean radiant temperature equal to the air temperature ($T_{mrt} = T_{air}$);
- a reference humidity (RH) of 50% for air temperatures $< 29^\circ\text{C}$ and 20 hPa above.

The calculated UTCI equivalent temperature values can be categorized in terms of heat (or cold) stress. The heat stress categories and their corresponding physiological responses are given in Table 2.3. The concept of UTCI is presented in Figure 2.5.

Table 2.3: UTCI equivalent temperatures categorized by the amount of heat stress and corresponding physiological responses (Blazejczyk et al., 2013)

UTCI [$^\circ\text{C}$] Range	Stress category	Physiological responses
Above +46	Extreme heat stress	- increase in T_{re} (rectal temperature) time gradient - steep decrease in total net loss - averaged sweat rate > 650 g/h, steep increase
+38 to +46	Very strong heat stress	- core to skin temperature gradient $< 1\text{K}$ (at 30 min) - increase in T_{re} at 30 min
+32 to +38	Strong heat stress	- Dynamic Thermal Sensation (DTS) at 120 min $> +2$ - averaged sweat rate > 200 g/h - increase in T_{re} at 120 min - latent heat loss > 40 W at 30 min - instantaneous change in skin temperature $> 0\text{K}/\text{min}$
+26 to +32	Moderate heat stress	- change of slopes in sweat rate, T_{re} and skin temperature: mean (T_{skm}), face (T_{skfc}), hand (T_{skhn}) - occurrence of sweating at 30 min - steep increase in skin wettedness
+ 9 to +26	No thermal stress	- averaged sweat rate > 100 g/h - DTS at 120 min < 1 - DTS between -0.5 and $+0.5$ (averaged value) - latent heat loss > 40 W, averaged over time - plateau in T_{re} time gradient

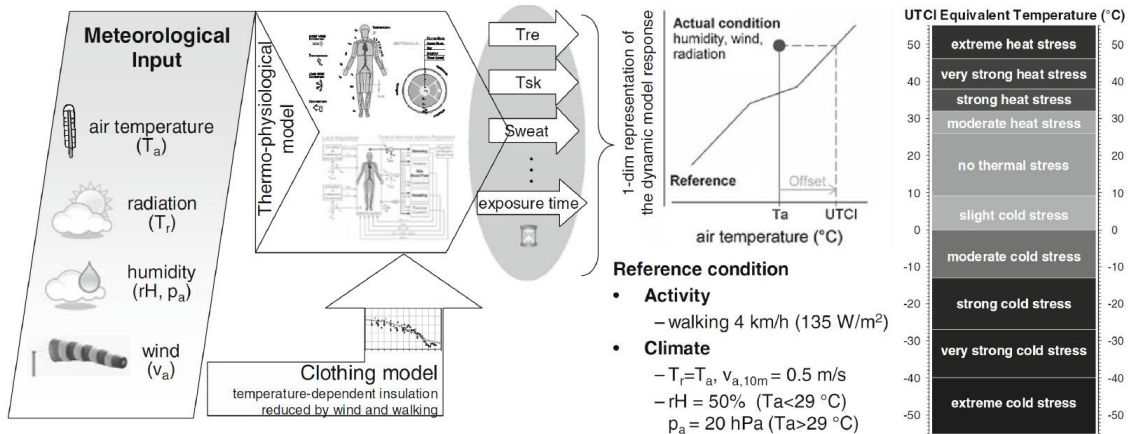


Figure 2.5: Concept of UTCI (Bröde et al., 2011a)

In a study of Bröde et al. (2011b), the UTCI was used to assess the thermal climate in Curitiba, Brazil. They analyzed different subgroups and concluded that the appropriateness of the UTCI is independent of gender or age. Based on these conclusions, the UTCI should be applicable on the thermal comfort assessment of elderly as well. The UTCI is intended for outdoor thermal conditions. It is unknown whether it gives reliable results for the indoor environment.

2.3.4 ATG Indicator

In 2004, a new performance indicator was developed called 'Adaptieve Temperatuur Grenswaarde Indicator' (ATG) or Adaptive Temperature Limit Indicator (ISSO, 2004). This indicator can be used for both mechanically and naturally ventilated office buildings. It is based on the findings of De Dear et al. in 1997, who performed

an analysis of 160 buildings in different climate zones. They found that occupants in naturally ventilated buildings were tolerant of a wider range of temperatures than occupants in HVAC buildings. The ATG chart for naturally ventilated buildings is provided in Figure 2.6.

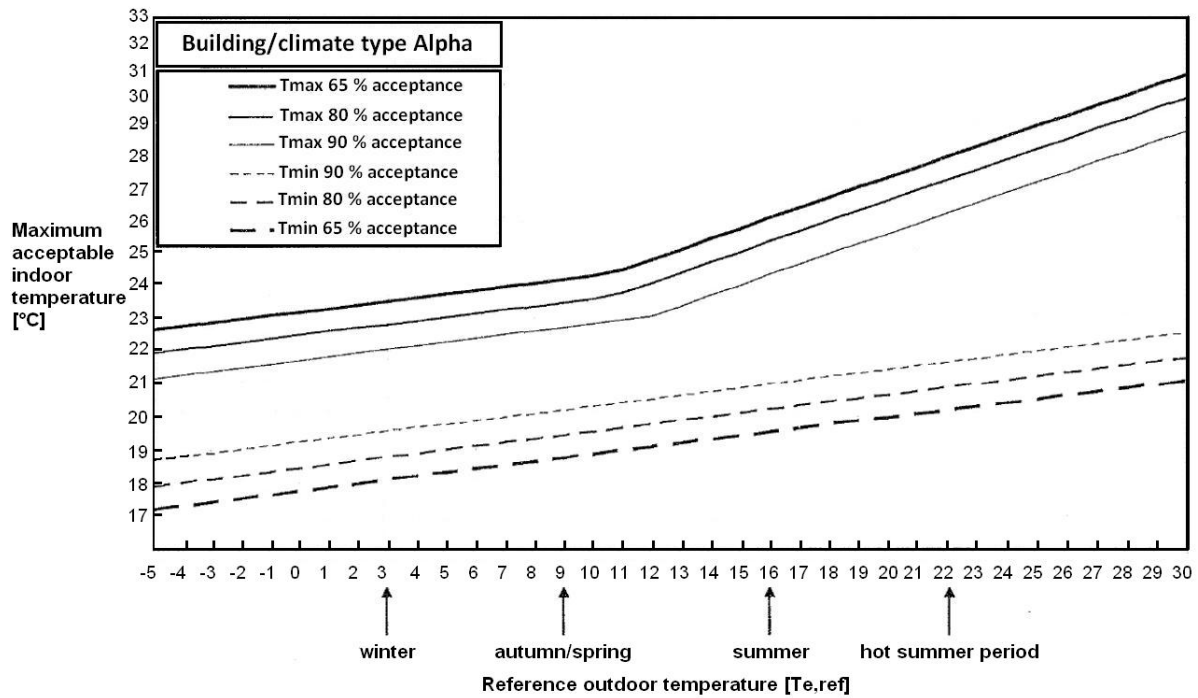


Figure 2.6: ATG chart for naturally ventilated office buildings (modified from ISSO, 2004)

The minimum and maximum indoor temperatures are given for the 90%, 80% and 65% acceptance level, based on the reference outdoor temperature. This reference outdoor temperature is based on the temperature of the past four days. According to Arbodienst, an indoor climate is comfortable when there is an 80% acceptance level of the indoor climate (van Hooff et al., 2012). The model is intended for indoor conditions. No information was found on the applicability of this model for the thermal comfort assessment of older people.

Because people in residential buildings have more adaptive options compared to offices (change clothes, go to another room, absence of dress codes etc.), the neutral temperature is more dependent on outdoor temperatures. This makes the ATG chart less suitable for the assessment of thermal comfort in residential buildings with adaptability possibilities. In a study of Peeters et al. (2009) thermal comfort ranges have been defined for residential buildings. The requirements are based on a literature review of several comfort studies about thermal comfort in residential buildings. The requirements are split up in comfort ranges for three different zones: bedrooms, bathrooms and other rooms. The defined upper and lower temperatures of a comfort band for these different zones are provided in Table 2.4. In Table 2.5 and 2.6, the values of the related parameters as a function of the PPD are given as well as the assumed neutral temperatures.

Table 2.4 & 2.5: Temperature limits of comfort band and parameter values as function of PPD (Peeters et al., 2009)

Bedroom	Bathroom and other rooms	10% PPD	20% PPD
$T_{upper} = \min(26^{\circ}\text{C}, T_n + w \cdot \alpha)$	$T_{upper} = T_n + w \cdot \alpha$	$w^* = 5^{\circ}\text{C}$	$w = 7^{\circ}\text{C}$
$T_{lower} = \max(16^{\circ}\text{C}, T_n - (1-w) \cdot \alpha)$	$T_{lower} = \max(18^{\circ}\text{C}, T_n - w \cdot (1 - \alpha))$	$\alpha^{**} = 0.7$	$\alpha = 0.7$
		* w = width of comfort band	
		** α = constant (≤ 1)	

Table 2.6: Neutral temperatures for different rooms (Peeters et al., 2009)

Room	Neutral temperature T_n
Bedroom	26°C for $T_{e,ref} \geq 21.8^\circ\text{C}$
Bathroom	$0.306 \cdot T_{e,ref} + 20.32^\circ\text{C}$ for $T_{e,ref} \geq 11^\circ\text{C}$
Other rooms	$16.63 + 0.36 \cdot T_{e,ref}$ for $T_{e,ref} \geq 12.5^\circ\text{C}$

Even though the guidelines of Peeters et al. (2009) are especially defined for residential buildings, it is doubted whether these guidelines should be chosen instead of the ATG model for the assessment of thermal comfort of the elderly. This because elderly seem to adapt their behavior less to the environment than younger people do (Rahola et al., 2009) and have an activity rate which is more in correspondence with seated employees in office buildings.

2.3.5 Applied model

For the outdoor thermal comfort assessment in this research, the UTCI index will be used because: (1) it is the only one based on a thermophysiological model taken into account all heat transfer mechanisms of the human heat balance; (2) it is suitable for transient situations; (3) it gives reliable results for the thermal comfort prediction of elderly. Besides, it is the only thermal comfort model especially developed for outdoor applications.

3. Case selection and description

3.1 Selection procedure

As described in the introduction of this report, the goal of this research is to calculate the UHI effect for a part of Rotterdam on temperatures and thermal comfort in and around a care center in Rotterdam. Because it would be too time consuming to perform simulations for multiple buildings, this will be done for a case study being a building where heat sensitive people live. In the previous chapter, it is described that especially the elderly are a group of risk. Therefore, it is decided to investigate the UHI effect on temperatures in and around a care center, located in Rotterdam. This care center should be representative of other Dutch care centers, allowing the results to be applicable on a larger scale.

Different types of care centers can be defined. In Table 3.1, an overview is provided of the amount of retirement homes, nursing homes and service flats in Rotterdam in 2011. Because of the large number of care centers in Rotterdam, a systematic approach is used to select a care center for further research. First, the residential district will be selected where the UHI effect is most pronounced based on a literature review of previously performed UHI research in Rotterdam. Then, a care center in this district will be selected based on present UHI indicators on a local scale and the care center characteristics.

Table 3.1: Number of different care center types in Rotterdam (VVZS Adresboek, 2011)

Building type	Number
Retirement homes	52
Nursing homes	30
Service flats	64
Total	146

3.1.1 UHI research Rotterdam

The first study on the UHI intensity in Rotterdam dates back to the year 1983. In this study of Roodenburg (1983), minimum air temperatures obtained from a thermograph at a fixed location in the centre of Rotterdam were compared with air temperatures measured at Zestienhoven Airport, situated at four kilometers north-west of the centre of Rotterdam. The data includes the years 1971 - 1973. Maximum UHI intensity of 8°C was found in September. However, the exact location of the urban measuring site is not mentioned and therefore this research cannot be taken into account when determining the district with the greatest UHI intensity.

The spatial distribution of heat islands can be assessed with thermal infrared remote sensing techniques. This method was used by Klok et al. (2012) to map the surface heat island intensity for Rotterdam. Remote sensing data from Landsat sensors of 15 summer days in the period of 1984 - 2007 were used to determine the average surface temperature of each district within the city. These temperatures were then compared to rural surface temperatures outside the city, resulting in the SHI intensity of each district. An overview of the different districts is provided in Figure 3.1.

Differences in SHI intensity between the districts can be explained by their surface characteristics: scarce vegetation, high fraction of impervious surfaces and a low albedo result in the highest SHI intensity. The highest daytime SHI intensity was found for districts Nieuw Mathenesse, Spaanse Polder, and Vondelingenplaat having SHI intensities of 10, 9 and 8°C respectively. The city centre of Rotterdam had an SHI intensity of 6°C (Klok et al., 2012).

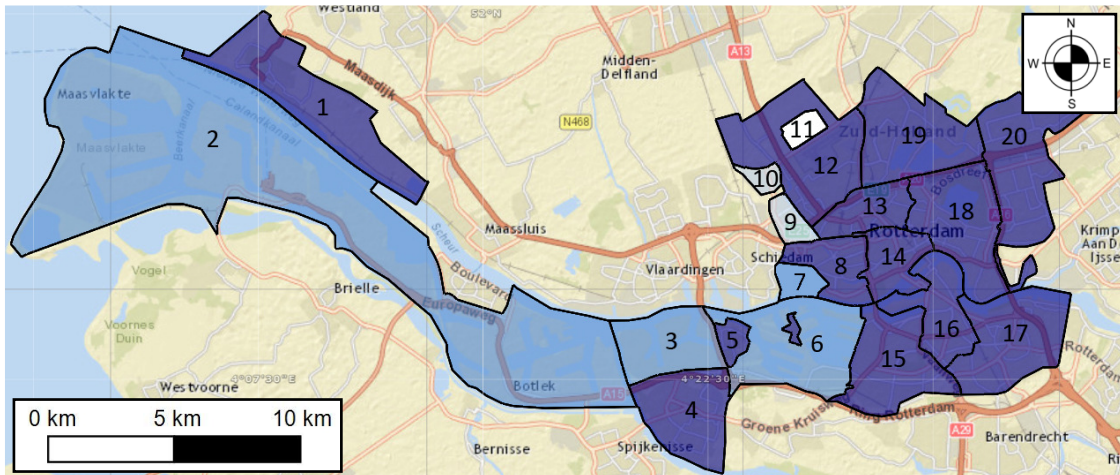


Figure 3.1: Districts of Rotterdam categorized by primary land use type: rural district (white), industrial districts (light blue), harbor districts (medium blue), residential districts (dark blue)

- | | | | |
|---------------------|---------------------------|-------------------------|-------------------------------|
| 1. Hoek van Holland | 6. Waalhaven | 11. Ind. area Schieveen | 16. Feijenoord |
| 2. Botlek | 7. Nieuw Mathenesse | 12. Overschie | 17. IJsselmonde |
| 3. Vondelingenplaat | 8. Delfshaven | 13. Noord | 18. Kralingen-Crooswijk |
| 4. Hoogvliet | 9. Spaanse Polder | 14. City centre | 19. Hillegersberg- Schiebroek |
| 5. Pernis | 10. Ind. area: North West | 15. Charlois | 20. Prins Alexander |

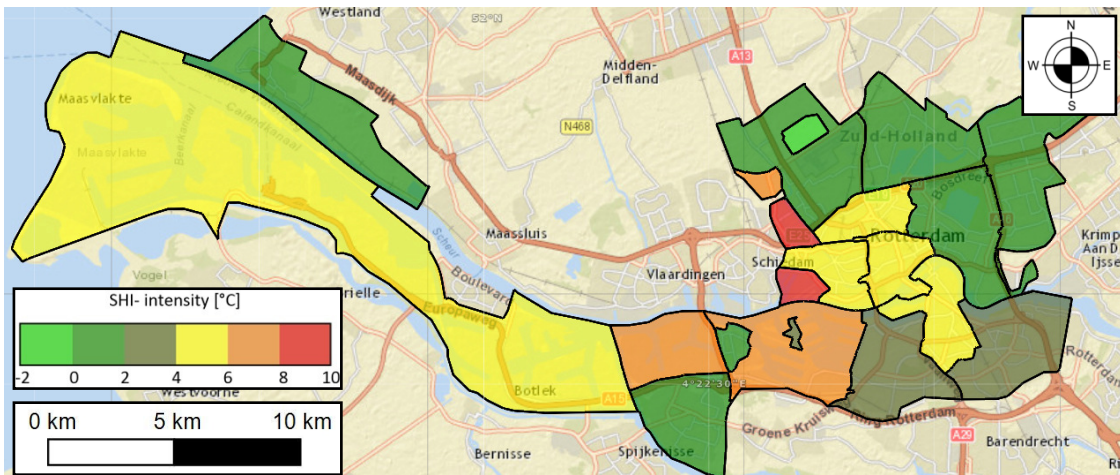


Figure 3.2: Average SHI intensities for each district based on the research of Klok et al. (2012)

Klok et al. (2012) also evaluated the diurnal variation in surface temperatures for the heat wave of 2006, making use of NOAA-AVHRR satellite images. NOAA-AVHRR stands for images from Advanced Very High Resolution Radiometer (AVHRR) operated by the US National Oceanic and Atmospheric Administration (NOAA). Daytime surface temperatures were the highest for Spaanse Polder, City centre and Delfshaven: respectively, 44, 43 and 42°C on 17 July 2007. The highest nighttime surface temperatures were found for City centre, Delfshaven, Nieuw Mathenesse, Heijplaat and Eem-Waalhaven, whereas the surface temperatures of Spaanse Polder were quite low at night.

Recently, the UHI intensity was measured making use of a mobile measuring platform on two bicycles (Heusinkveld et al., 2010). The bicycles were equipped with a thermometer, humidity sensor, anemometer and radiation sensors. The measurements were performed on a hot summer day in August 2009 along two routes through different urban districts. The first measurements were performed between 14:00 – 16:00 pm, the second set of measurements after sunset. The acquired data was compared with recordings from weather station Zestienhoven airport. At night, highest UHI intensity was found at the route through district City centre, followed by districts Delfshaven, Feijenoord and North. The highest UHI intensity at daytime was

found in City centre, Feijenoord, Kralingen-Krooswijk, Spaanse Polder, Overschie and industrial site North-West.

For the Knowledge for Climate research program, measurements have been performed on 3 fixed positions in different districts of Rotterdam since September 2009: in the city centre, in district Charlois and Prins-Alexander. The weather station in the city centre represents a densely built commercial area, the one in Charlois represents a densely built up residential neighborhood and the one in Prins-Alexander represents a relatively green suburban residential neighborhood (van Hove et al., 2011b). The maximum UHI intensity is reached during the evening hours in the summer months in June, July and August (Table 3.2). The measurement location in the City centre shows the largest UHI intensity followed by the measurement locations in Charlois and Prins-Alexander (van Hove et al., 2011b).

Table 3.2: Median and 95 percentile values for UHI_{max} for the summer of 2010 (June, July, August) for the monitoring locations City centre, Prins-Alexander and Charlois (van Hove et al., 2011b).

Measurement location	Median	95 percentile
City centre	4.7	7.9
Prins-Alexander	3.2	4.8
Charlois	4.5	6.9

In Table 3.3, an overview is presented of the different UHI-studies and their results. According to the results from the NOAA-AVHRR remote sensing data in Klok et al. (2012), the residential districts with highest SHI intensities at both day and night are Delfshaven and City centre. Also high UHI intensities were found for these districts in other studies. Therefore, a care center in these districts will be selected.

Table 3.3: Overview of urban heat island research in Rotterdam

Research	Maximum daytime intensity	Maximum nighttime intensity
Surface Urban Heat Island	Districts	Districts
Landsat remote sensing data (Klok et al., 2012)	Vondelingenplaat, Spaanse Polder, Nieuw Mathenesse	-
NOAA-AVHRR remote sensing data (Klok et al., 2012)	Delfshaven, City centre and Spaanse Polder	Delfshaven, City centre, Nieuw Mathenesse, Heijlplaat, Waalhaven
Atmospheric Urban Heat Island	Districts	Districts
Mobile measurements (Heusinkveld et al., 2010)	City centre, Feijenoord, Kralingen-Krooswijk, Spaanse Polder, Overschie and ind. Area North-West	City centre, Delfshaven, Feijenoord and North
In situ measurements (van Hove et al., 2011b)	City centre	City centre

3.1.2 Care center selection

In the districts Delfshaven and City centre, 9 care centers can be found. In order to select one of those care centers, some criteria have been defined. The care center for further research should meet the following criteria:

- 1) Located close to weather station: as mentioned in the previous paragraph, there is a weather station situated in the city centre district of Rotterdam. The weather station provides hourly data such as air temperatures, wind directions and wind speeds for the last four years. This data could be used for the validation of the CFD model. Therefore, the closer, the care center is located to this weather station, the smaller the models can be and the less computational demanding the

simulations will be. The location of this weather station is indicated with a blue dot in Figure 3.3. The locations of the care centers are also presented on this figure.

- 2) No air conditioning system applied: there is no UHI effect on indoor temperatures when an air conditioning system is applied. In case of air conditioning, higher outdoor temperatures only have an effect on the energy demand for cooling.
- 3) UHI indicators: high average UHI intensities were found in Delfshaven and City centre in previously performed UHI studies. However, the UHI intensity on different locations in these districts could vary significantly. UHI indicators such as scarce vegetation coverage or surrounding water surface give more information on the possible UHI intensity on a smaller scale.
- 4) Repetition in floor plans: this makes the modeling part easier. Furthermore, better comparisons can be made between the UHI effect on indoor temperatures of apartments on different orientations or floor levels.

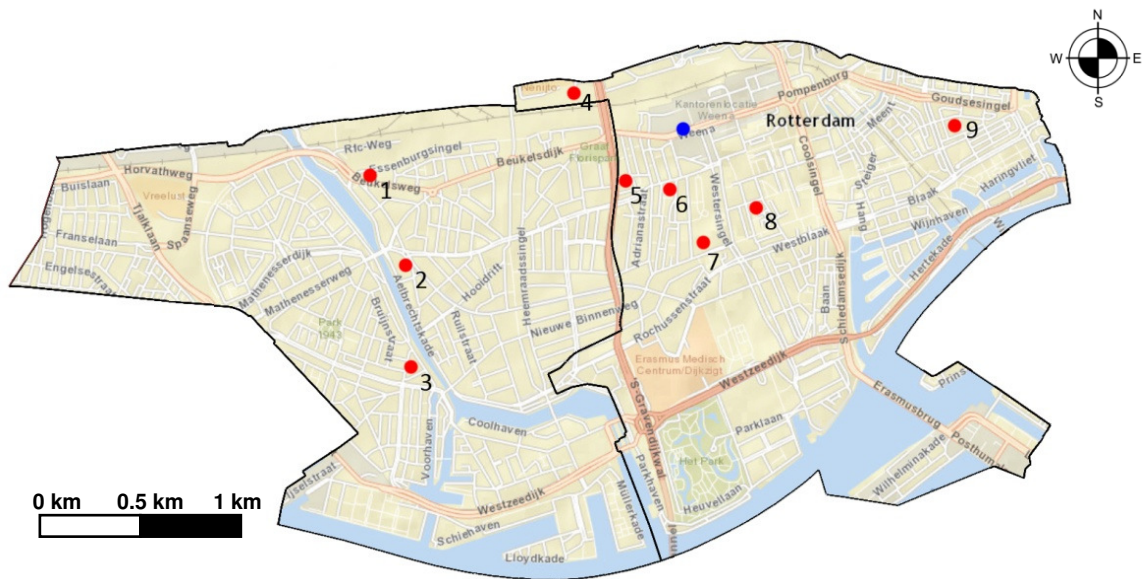


Figure 3.3: Location of care centers in district Delfshaven (left) and district City centre (right). The blue dot represents the Knowledge for Climate weather station. Number 8 is the position of care center Atrium.

Based on these criteria, care center Atrium has been selected for further research. This choice was mainly made because of its relatively close distance to the weather station and because of the absence of an air conditioning system in the apartments of the care center. In addition, the closest water pond is 200 m away and there are only some trees in the streets and some small parks. Compared to the other care centers, there is a high rate of repetition in the floor plans. In the following paragraph, the building and its properties will be described in more detail.

3.2 Building description care center Atrium

3.2.1 General information

During the Second World War, Rotterdam was severely affected. During the bombardments of May 1940, a protestant church and a care center in the city centre were also destroyed. As a replacement, care center Atrium was built some years after the war. At that time, the care center included a church hall. In 1987, the layout of the different floors was changed and the façade was renovated extensively. The church hall was transformed into a building with rooms for elderly residents. Figure 3.4a and Figure 3.4b give an impression of the care center in the current condition.



Figure 3.4: Aerial view of the care center (a) and front façade of the care center (b)

The care center is located in district Cool in the city centre of Rotterdam. This quarter of Rotterdam was almost completely destroyed during the Second World War. Therefore, it is a neighborhood with relatively new buildings. Well known are the Schouwburg square and shopping street Lijnbaan. Care center Atrium is located in the Karel Doormanlaan, which is also a shopping street. The front façade is oriented to the east. The care center is part of a building block consisting of low-rise buildings up to six storeys high. At the back of the care center, there is a courtyard with a parking area and a small play ground. The Karel Doormanlaan is mainly covered with impervious surfaces such as street tiles and paving stones. Vegetation is formed by 2 rows of trees at either side of the road. At 100 m north-east of the care center there is a small park.



Figure 3.5: Karel Doormanstraat (a), aerial view of care center in building block (b)

3.2.2 Building lay-out

The care center consists of a rectangular main building connected by a hallway with a smaller square building at the back. On the ground floor, 4 apartments as well as all the common rooms such as offices, the kitchen, reception and recreation room can be found. All the other apartments can be found on the 1st to 5th floor. These floors have identical floor plans with 12 apartments on each floor as can also be seen in Figure 3.6.

Most of the apartments are inhabited by one person. These apartments have one room equipped with a kitchen block, a bed and a living area. Besides, there is a bathroom with shower and toilet. The two persons-apartments also have a separate bedroom.

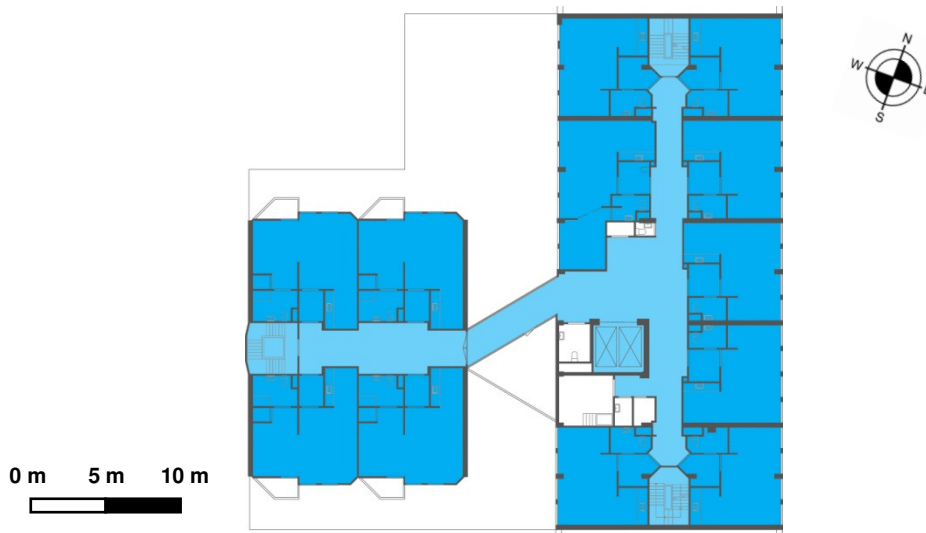


Figure 3.6: Floor plan of 1st - 5th floor with apartments (dark blue), hall (light blue) and other rooms (white)

3.2.3 Construction

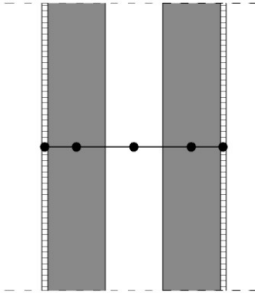
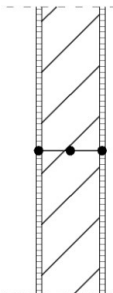
The highest indoor temperatures are expected on the top floor. It is decided to only investigate the indoor temperatures of the eight apartments on the top floor of the main building. Therefore, only this part will be described in more detail.

The building envelope consists of a concrete slab with outdoor insulation with a plaster finishing. At the inside there is a wooden frame with plaster or wallpaper as finishing layer. The floors are also made out of concrete covered with a cement layer and carpet or linoleum. The roof has a wooden construction with an insulation layer on top of it with a bituminous top layer. The internal walls between the apartments are cavity walls, while the other internal walls consist of one layer concrete bricks. In the bathrooms, the floor and walls are covered with ceramic tiles. The external walls of the hallway between the main building and the square building are made out of sandwich panels with an aluminum top layer at the outside. The construction layers are described in more detail in Table 3.4 and 3.5.

Table 3.4: Used materials for the different building components of the top floor apartments (part 1)

Building component	Material layer	Building component	Material layer
Roof	<ul style="list-style-type: none"> - 10 mm bitumen - 60 mm insulation + vapor barrier - 10 mm multiplex - 170 mm cavity + 170 x 71 mm wooden beams - 10 mm multiplex - 10 mm plaster 	Floors	<ul style="list-style-type: none"> - 10 mm carpet/linoleum - 30 mm cement - 100 mm concrete - 10 mm plaster
External wall of apartments	<ul style="list-style-type: none"> - 8 mm plaster - 60 mm insulation - 200 mm concrete - 10 mm multiplex - 55 mm wooden frame + vapor barrier - 10 mm multiplex - plaster/ wallpaper 	External wall of hallway	<ul style="list-style-type: none"> - aluminum top layer - 60 mm insulation (sandwich panel) - finishing layer

Table 3.5: Used materials for the different building components of the top floor apartments (part 2)

Building component	Material layer	Building component	Material layer
<p>Internal wall between apartments</p> 	<ul style="list-style-type: none"> - 10 mm plaster/wallpaper - 100 mm concrete - 100 mm cavity - 100 mm concrete - 10 mm plaster/wallpaper 	<p>Internal wall between hallway and apartments</p> 	<ul style="list-style-type: none"> - 10 mm plaster/wallpaper - 100 mm concrete bricks - 10 mm plaster/wallpaper

At the front of the main building, there are four windows per apartment. The windows have wooden frames with double glazing and vertical screens at the outside which can be controlled manually. Two of the windows can be opened. At the back of the main building, two larger windows are applied with orange sun screens at the outside which can also be controlled manually.

3.2.4 Ventilation, heating and cooling

In all the apartments, fresh air is being supplied by two Climacoust ventilation grilles in the upper corners of the façade. There is a mechanical exhaust in the bathroom and in the kitchen with installed ventilation rates of 75 respectively 50 m³/hr. These ventilation rates were measured by installation company Breijer in June 2012. At night, the ventilation rates are slightly reduced. There are two panel radiators below the windows. There is no cooling system applied. Internal heat sources are formed by the people, a television, lighting and some kitchen equipment.

4. CFD simulations: settings and parameters

For the calculation of the UHI effect CFD will be used. CFD stands for the solution of fluid flow problems by numerical simulation (Blocken, 2011). Over the last decades, CFD has gained dominance in all kinds of working fields because of its advantages over full-scale experimental testing, the increase of computational computer resources and the availability of user-friendly software (Blocken, 2011). This, however, also led to improper use of CFD by unskilled users. In order to avoid mistakes and improve the quality and reliability of CFD analyses, guidelines have been created for several applications.

For urban flow analysis and the assessment of pedestrian wind comfort, guidelines have been provided by Franke et al. (2007) and Tominaga et al. (2008). A ten steps approach for the model development and evaluation applied to CFD for environmental fluid mechanics can be found in a study by Blocken & Gualtieri (2012).

Although this research is more related to temperatures than wind velocities, the flow should be modeled correctly as well. Therefore, the above guidelines will be used in combination with adjustments and recommendations found in other research on the use of CFD for heat transfer problems in general or the UHI effect in particular. Little research has been performed on the evaluation of the UHI effect with CFD. In a study of Robitu et al. (2006), the beneficial influence of vegetation and water ponds on urban microclimate was investigated with CFD. In 2008, Priyadarsini et al. studied the effect of building geometry, façade materials and the location of air-conditioning condensers on the thermal environment of Singapore with CFD simulations. In a more recent study, performed by Toparlar (2012), CFD was used to investigate the effect of evaporative cooling for the Bergpolder Zuid region in Rotterdam. Especially the study of Toparlar (2012) provides useful information for this research.

In this chapter, subsequently the strategy, geometry, initial and boundary conditions, solution parameters and applied additional models will be described.

4.1 Strategy

4.1.1 Target variables

As a first step, target variables should be defined. These are the variables that are representative of the goals of the simulations (Franke et al., 2007). The target variable of the CFD analysis is the temperature. First, for the calculation of the UHI effect around the care center, UHI intensities as well as SHI intensities should be evaluated. Therefore, the target variables are outdoor air temperatures at pedestrian height (1.5 m) and outdoor surface temperatures in the city centre around the care center. Secondly, these temperatures are used in combination with the UTCI index for the thermal comfort assessment. Finally, indoor air temperatures on the top floor of the care center should be evaluated for the investigation of the UHI effect on indoor temperatures.

4.1.2 Approximate equations describing the physics of the flow.

Reynolds-Averaged Navier-Stokes (RANS) equations are used for solving the turbulent flow. These are based on averaging the Navier-Stokes equations. RANS equations are the expressions of three fundamental physical principles: (1) conservation of mass; (2) Newton's 2nd law: resulting force equals mass times acceleration and; (3) conservation of energy (Blocken, 2011). In this research, steady RANS simulations will be performed. Energy and radiation equations are used within the simulation for the temperature calculations.

The RANS equations are combined with a turbulence model. In this case, the realizable $k-\epsilon$ turbulence model is used. According to Franke et al. (2007) this is the mostly used and validated turbulence model for urban flow analysis. Furthermore, $k-\epsilon$ models have shown good results for indoor air flow as well (Linden, 1999; Sørensen & Nielsen, 2003).

4.2 Geometry

As described in the first chapter, 3 computational models are needed for the research: (1) a model of the care center in Rotterdam without the indoor environment of the care center, (2) a model of the care center in Rotterdam including the indoor environment and (3) a model of the care center with the indoor environment placed in a rural environment. These computational models will be described one by one in this paragraph.

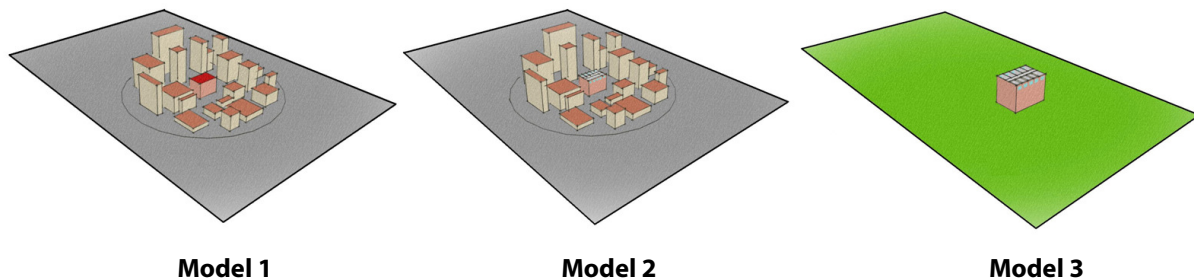


Figure 4.1: Schematic presentation of the 3 different models

4.2.1 Model 1: Care center in Rotterdam (indoor environment excluded)

Explicitly modeled urban area

As illustrated in Figure 4.2a, a computational domain with an urban area consists of three different regions (Blocken et al., 2007):

- 1) the region of interest in the centre of the domain with the buildings modeled explicitly;
- 2) the upstream region with the obstacles modeled implicitly and;
- 3) the downstream region where the obstacles are also modeled implicitly.

The dimensions of the explicitly modeled urban region are based on the evaluated wind direction(s) and the previously mentioned guidelines.

In general, south-western wind is the prevailing wind direction for the Netherlands (KNMI). However, when looking at heat wave periods, high temperatures are caused by wind coming from land directions instead of sea directions. Therefore, easterly wind is the prevailing wind direction during a heat wave. This can also be seen when looking at the wind directions measured at Rotterdam airport during the hottest period (temperatures $> 25^{\circ}\text{C}$) of the heat waves of 2003 and 2006 (Figure 4.2b): the wind is mostly coming from north-east to south-east directions. This is taken into account for the choice of the explicitly modeled urban region.

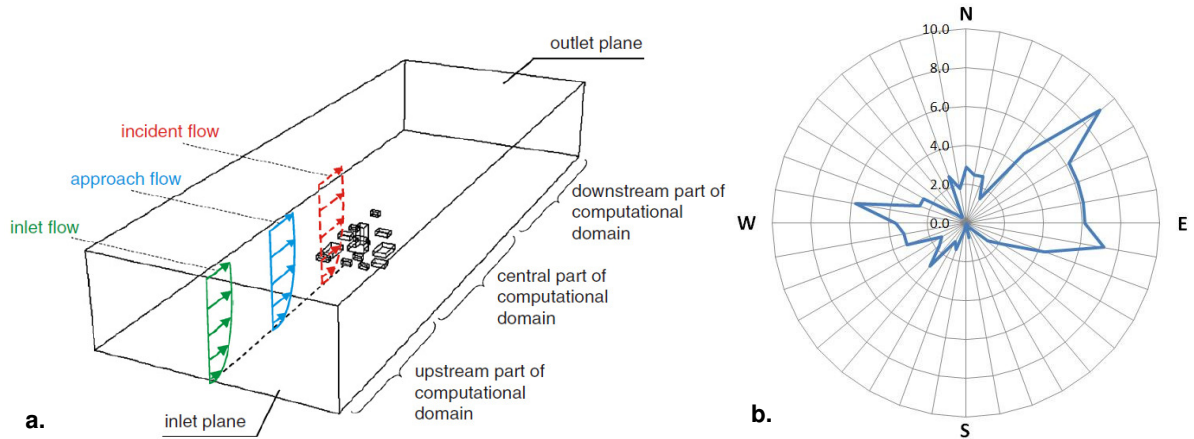


Figure 4.2: Computational domain with region of interest, upstream and downstream part of the domain (a) (retrieved from Blocken et al., 2007), distribution wind direction [%] during the heat waves of August 2003 and July 2006 for the periods with temperatures > 25°C (b) (modified from KNMI)

According to Tominaga et al. (2008), the highest level of detail is required at the building of interest. In this research, the care center and the location of the weather station require the highest level of detail. Because the distribution of buildings normally has the greatest impact on wind flow patterns, it is also advised to model at least one additional street block in each direction around the assessment region. Furthermore, the explicitly modeled area should be large enough to predict the UHI intensity correctly. In a CFD study on the UHI effect of the Bergpolder Zuid region in Rotterdam performed by Toparlar (2012), an urban area with a diameter of 1.2 km was modeled explicitly. Because the care center and the weather station are 700 m away from each other, a larger area is being modeled explicitly in this study.

The explicitly modeled region is depicted in Figure 4.3. It has dimensions of 1.2 x 2.1 km². Because wind directions vary between north-east to south-east, a larger urban area is modeled on these sides of the care center and the weather station. At the leeward side of the care center and the weather station, buildings are modeled as simple building blocks, while the buildings at the other side are modeled in more detail. Obstacles such as trees, cars, street poles and sign boards have not been modeled. Building heights of low rise buildings are rounded to a multiple of 3 to 4 m, while the high rise buildings of 40 - 150 m are rounded to a multiple of 5 to 10 m depending on the most common building heights in the urban area. The explicitly modeled buildings are shown in Figure 4.4. It also gives an impression of the distribution of high rise and low rise buildings over the modeled urban area.

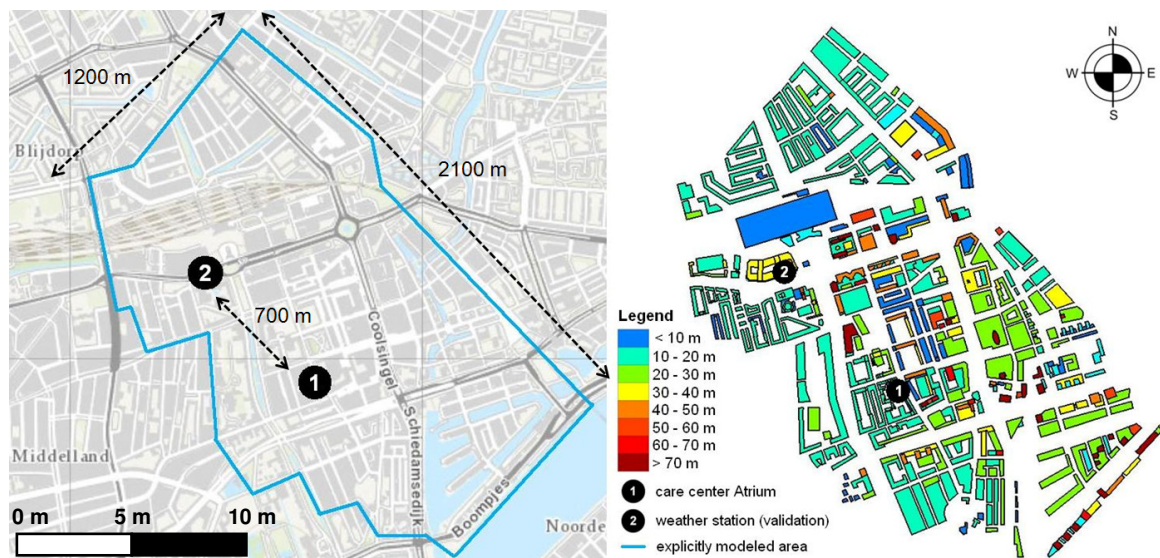


Figure 4.3: Explicitly modeled urban area (left) and corresponding building heights (right)

Computational domain

The size of the computational domain should be based on the area that shall be represented as well as the boundary conditions that will be used (Franke et al., 2007). The boundaries should be on a sufficient distance from the urban area in order to avoid its influence on the flow field. For an urban area with multiple buildings, it is advised to have a distance of 5 times H_{\max} between the top of the domain and the roof level of the tallest building ($= H_{\max}$) in order to avoid an artificial acceleration of the flow over the buildings (Franke et al., 2007). The highest building in the domain is Delfse Poort, located at the north-east side of the weather station. One of its towers has a height of 150 m. Therefore the height of the domain is set to 900 m.



Figure 4.4: Building Delfse Poort: height of left tower is 150 m

According to Tominaga et al. (2008), the distance between the sides of the domain and the building should be set on $5H$ or more. For an urban area with multiple buildings, Franke et al. (2007) suggests that the lateral boundaries of the computational domain can be placed closer to the explicitly modeled built area. However, the choice of the domain should also be based on the blockage ratio which is defined as the ratio of the projected area of the building in the flow direction to the free cross section of the computational domain. Based on the knowledge of wind tunnel experiments, it is advised to keep the blockage ratio below 3% (Tominaga et al., 2008). In order to satisfy the blockage requirement and to avoid wind speed acceleration outside the explicitly modeled area, $5H_{\max}$ ($= 750$ m) is chosen for the distance between the sides of the domain and the modeled buildings.

Finally, the extensions of the domain in the flow direction should be chosen. For the region between the inlet and the built area, a distance of 750 m is chosen ($5H_{\max}$). To allow for flow re-development behind the wake region, a distance of $15H$ between a single building and the outflow boundary is advised by Franke et al. (2007), but for a model with multiple buildings a smaller distance could be chosen. For security, a distance of 2250 m ($15H_{\max}$) between the urban area and the outlet is applied. These chosen dimensions result in a computational domain with dimensions $l \times w \times h = 5014 \times 3691 \times 900$ m³.

The building area is placed in a circular subdomain. The rectangular domain can be turned around the circular domain, which makes it possible to perform simulations for different wind directions. The explicitly modeled area is divided in 8 subdomains. The dimensions of the ground plane of the domain and the location of the different subdomains are indicated in Figure 4.5.

The subdomain where the care center is located (subdomain 5) is the smallest subdomain. Two versions have been made of this subdomain:

- 1) coarse version: grid without the indoor environment of the care center that will be used for the validation of outdoor air temperatures and surface temperatures;
- 2) detailed version: grid including the indoor environment of the upper floor of the care center. This grid can be used for the evaluation of the UHI effect on indoor temperatures.

By replacing the coarser version of subdomain 5 by the detailed version, model 2 is created which will be explained in more detail in paragraph 4.2.2.

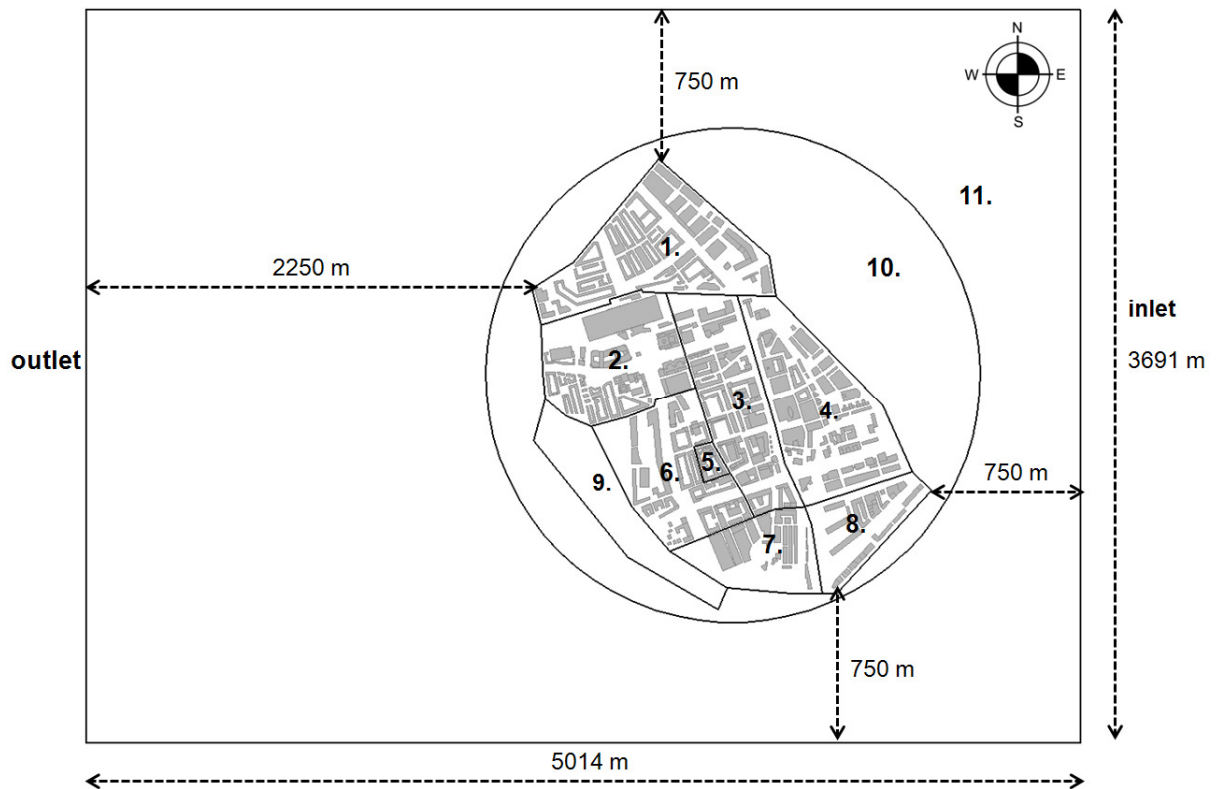


Figure 4.5: Ground plane of the computational domain with its subdomains. The height of the domain is 900 m.

Computational grid

The generation of the computational grid consists of the following steps. First of all, an AutoCAD drawing of Rotterdam is used to create the dimensions of the ground plane of the computational domain with the ground surface of all the buildings. The AutoCAD drawing is being converted in an IGES file, which is a file that can be loaded in the pre-processor software Gambit. For this research, Gambit version 2.4.6 is used. In Gambit, the ground plane is then meshed.

Because of the great size of the ground plane, it would be very time demanding to mesh each edge or face separately. However, a high quality grid is required to reduce the amount of truncation errors. Therefore the following methodology is applied:

- 1) A quad pave mesh with a standard spacing size of 2, 3 or 4 m is applied to a large group of faces (Figure 4.6)
- 2) The mesh of the faces is deleted without removing the mesh of the edges
- 3) A bi-exponent grading type with a ratio of 0.57 is applied to all the edges of the selected faces. In this way smaller cells are obtained at the corners where the highest accuracy is required for determining the flow field (Tominaga et al., 2008).
- 4) Then again a quad pave mesh is applied to the selected faces without spacing

This methodology is applied to three different groups. The further the distance of the group to the care center, the larger the chosen spacing size is. However, this method leads to an unnecessary amount of cells for the larger faces while the smallest faces have a too low amount of cells. Therefore, the mesh of the groups is adjusted manually at the end in order to obtain a high quality mesh. For the area between the different groups, a grid with an exponential ratio is applied. The grid of subdomain 5 including the care

center is not generated according to the above methodology, but is meshed manually. According to the guidelines, at least 10 cells per building edge should be used to resolve the flow near the corners. This criteria is not met everywhere in the model, but stretched cells are avoided by keeping the stretching/compression ratios below 1.3.

It is recommended that the evaluation height is located in the 3rd or higher grid cell from the ground surface (Tominaga et al., 2008). The evaluation height for the air temperature is pedestrian height (± 1.5 m). This requirement is sufficiently met in subdomain 1 - 8. The first cell height varies here between 0.18 and 0.40 m. In subdomain 9 - 11, the first cell height is 2.74 m in order to get the right value for the aerodynamic roughness length z_0 . This will be explained in paragraph 4.3 about the boundary conditions.

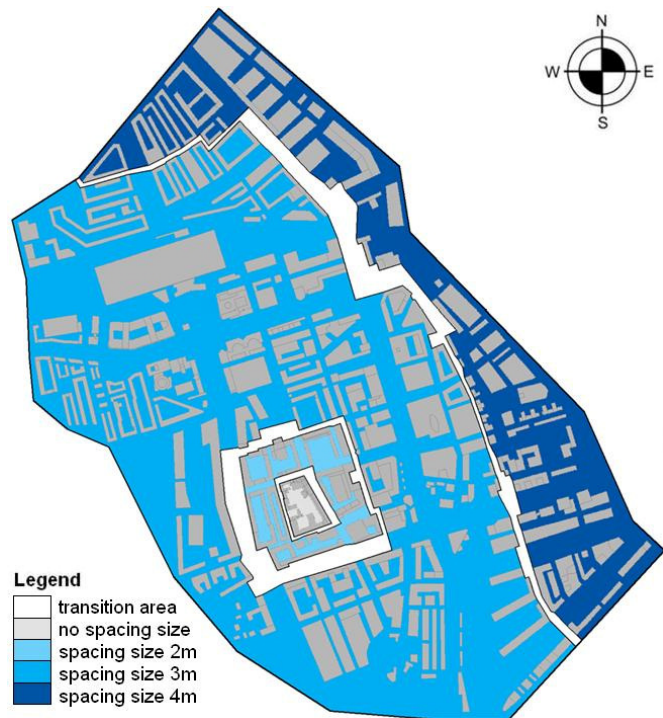


Figure 4.6: Groups with different spacing size

The 3D mesh is created according to the methodology of van Hooff & Blocken (2010). The meshed surfaces of the ground plane of each subdomain are swept along different pre-meshed vertical sweep lines. In this way, hexahedral cells are created instead of pyramidal or tetrahedral cells. The former ones are preferable because they introduce smaller truncation errors and display better iterative convergence (Hirsch et al., 2002). By applying this methodology, the cells are also parallel to the ground surfaces. This in turn improves the accuracy of the simulations. After sweeping the ground mesh, the volumes of the buildings are deleted.

Finally, the boundary types are specified. No-slip conditions are applied to the ground surfaces, walls and roofs. The top of the domain and the sides are modeled as slip walls with zero normal velocity and zero normal gradients of all variables. To the inlet, a logarithmic mean wind speed profile is applied. Zero static pressure is imposed to the outlet. Finally, the connection surfaces between the different subdomains are defined as interfaces which are connected to each other in Fluent.

The entire domain of the care center without the indoor environment in Rotterdam is presented in Figure 4.7. In total, there are 29 million cells in the computational domain. This model will also be used as a basis for model 2 (Care center in Rotterdam including indoor environment of the care center). Because of the high grid resolution needed for the ventilation inlets of the care center in model 2, a higher density grid is applied at 18 m height in the subdomains adjacent to the subdomain of the care center (subdomain 3 and 6). This will be described in more detail in the next paragraph.

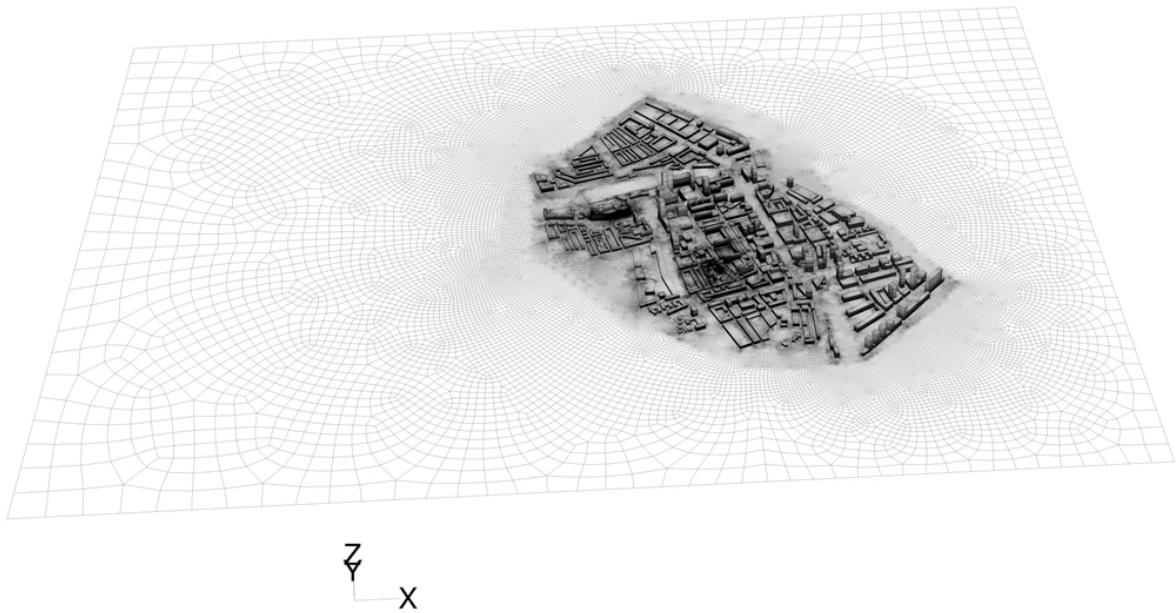


Figure 4.7: Mesh of the entire domain of model 1

Figure 4.8 - 4.11 show the resemblance of the model with reality. Note that not the current entrance building of the train station, but the previous entrance building is included in the model. This, because the current entrance building was not there yet during the heat wave of 2006. The previous entrance building was demolished in 2009. In Figure 4.9, it can be seen that steep roofs are modeled as flat roofs.

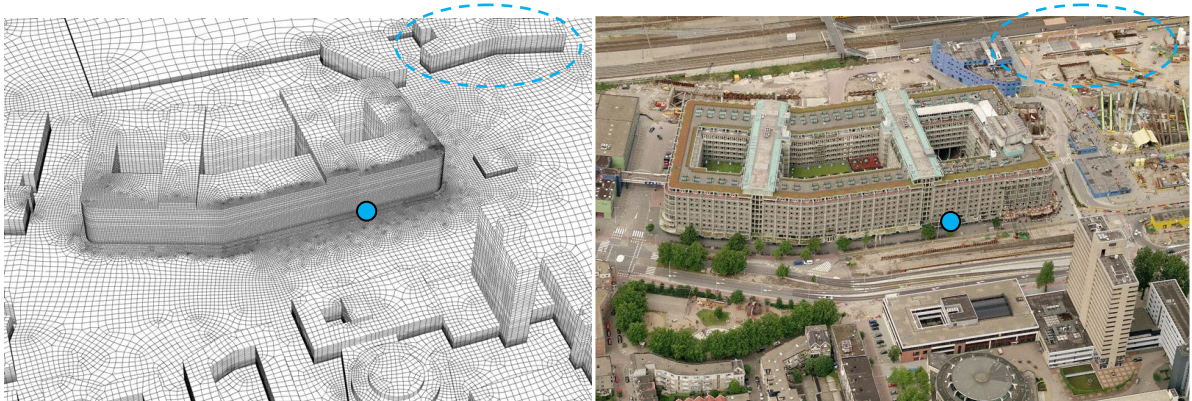


Figure 4.8: Mesh around the weather station (blue dot) and aerial photo. At the photo, the train station is already demolished.

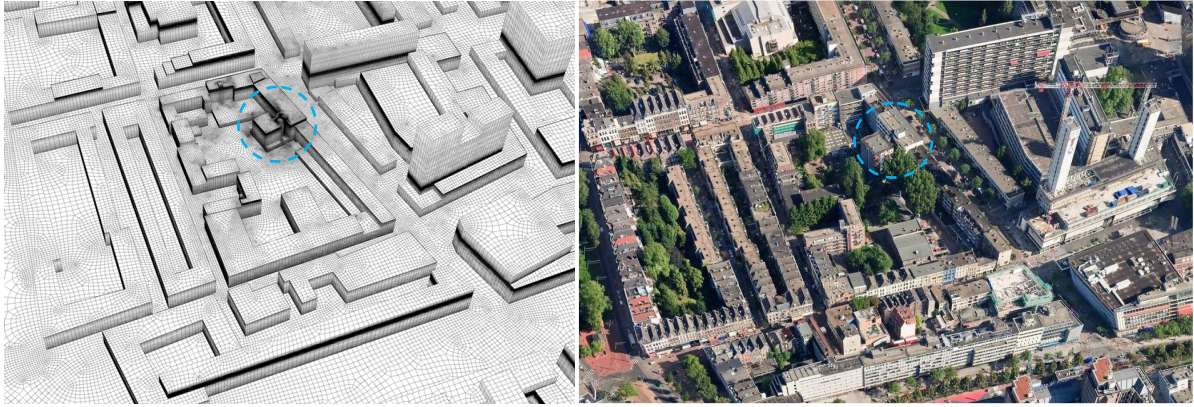


Figure 4.9: Mesh around care center (blue circle) and aerial photo. Steep roofs are modeled as flat roofs.

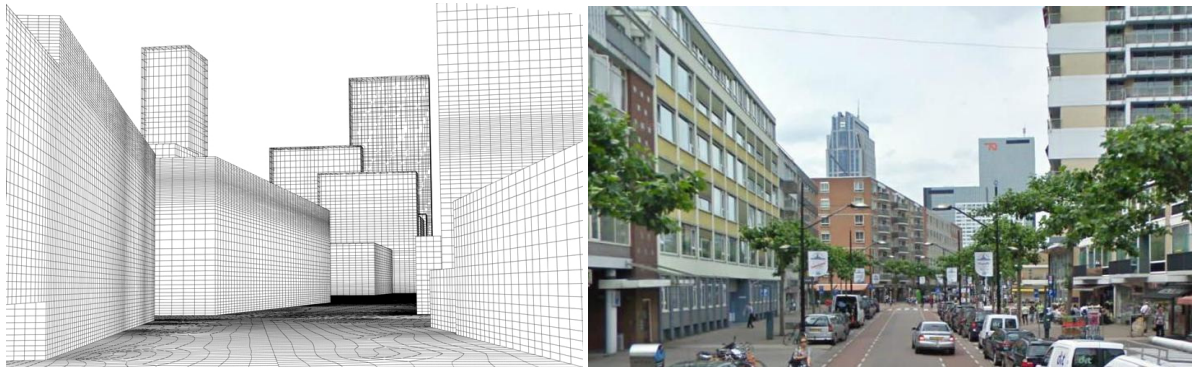


Figure 4.10: Street view of the Karel Doormanstraat. Cars, trees and street lights are not included in the model.

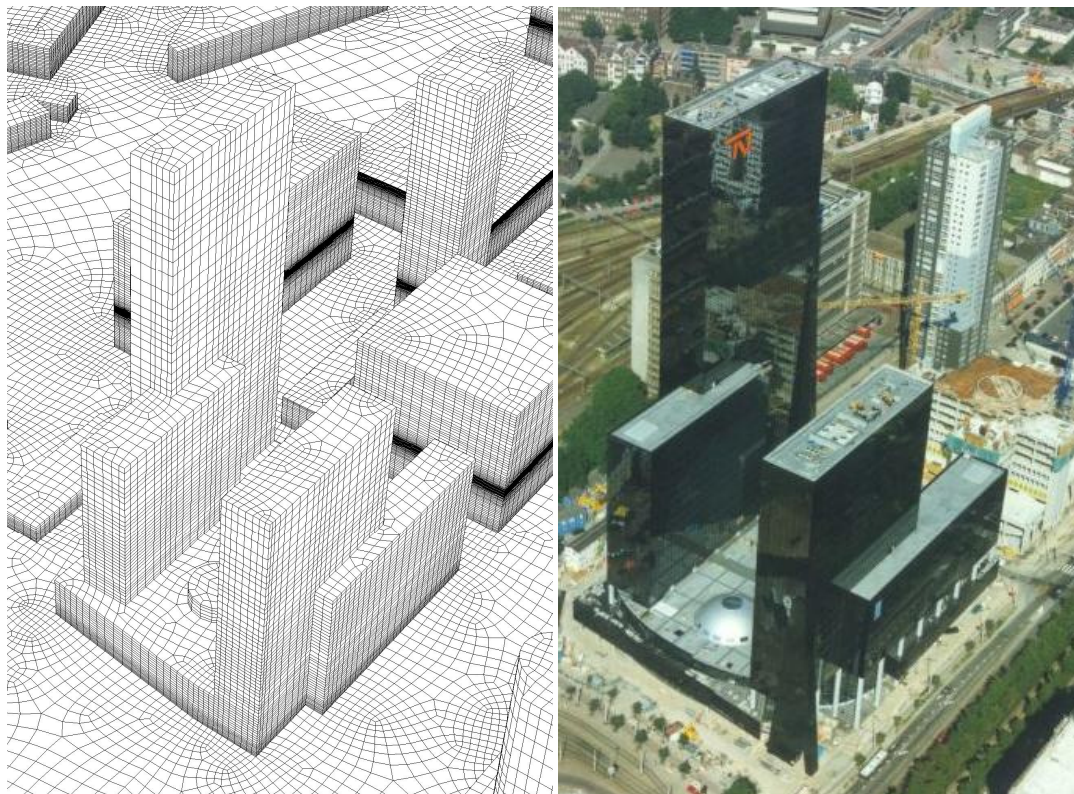


Figure 4.11: Mesh and aerial photo of Delfse Poort building. This is the highest building in the domain.

A picture of the grid of subdomain 1 - 8 and their amount of cells is provided in Figure 4.12. Larger copies of these pictures are included in appendix 1.

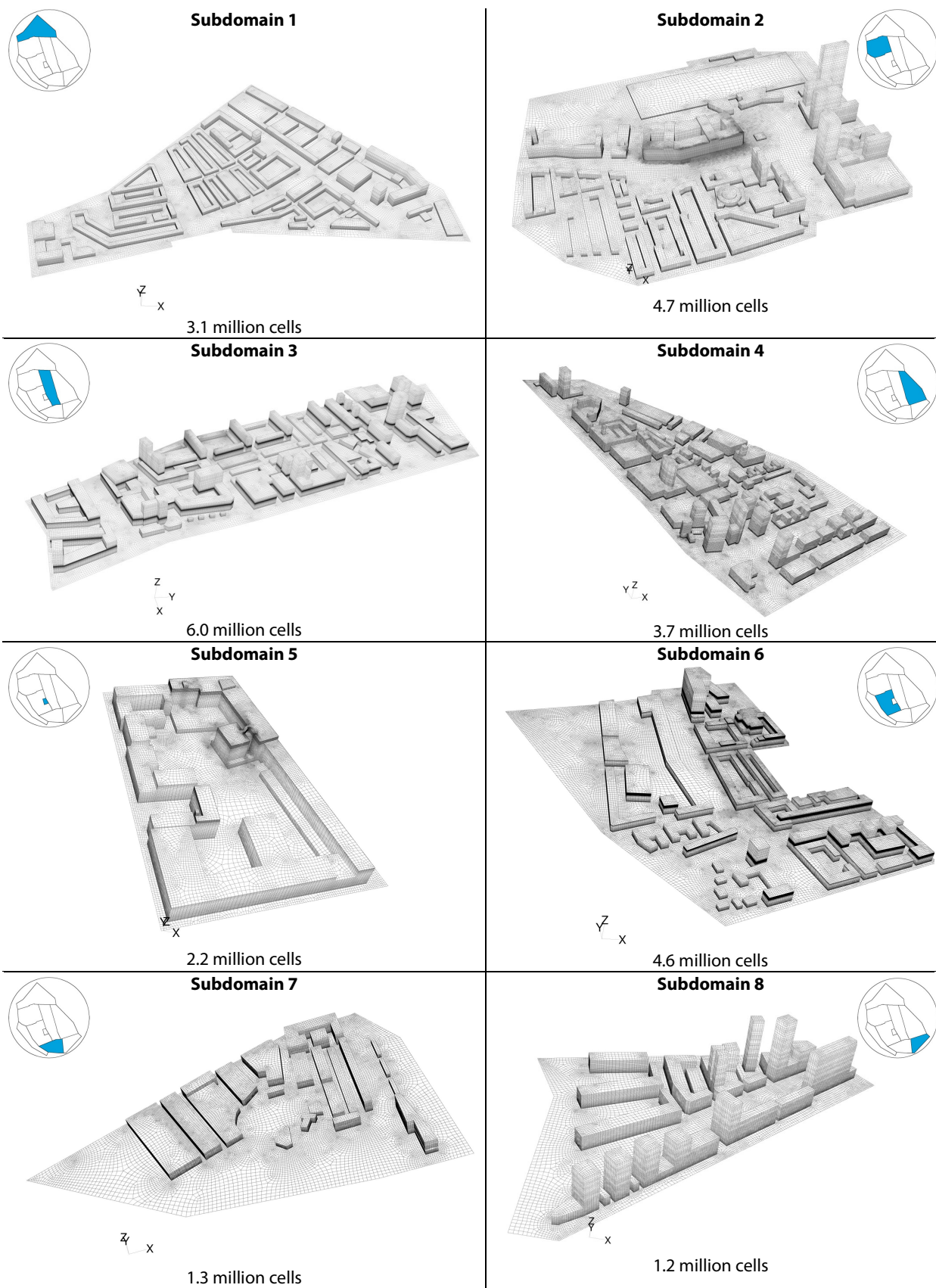


Figure 4.12: 3D grid of the subdomains and the corresponding amount of cells

4.2.2 Model 2: Care center in Rotterdam (indoor environment included)

For the 2nd model, model 1 is used as a basis. Therefore, the explicitly modeled urban area, computational domain and computational grid are as described in the previous paragraph. The only difference is that the coarser version of subdomain 5 is being replaced by a detailed version which includes the indoor environment of the care center. This grid will be described here in more detail.

Computational grid of the care center with indoor environment

First of all, the geometry of the floor plans was simplified. The apartments are modeled as one room instead of separate rooms for the hallway, bathroom and living area as can be seen in Figure 4.13. The furniture and doors are also not taken into account.

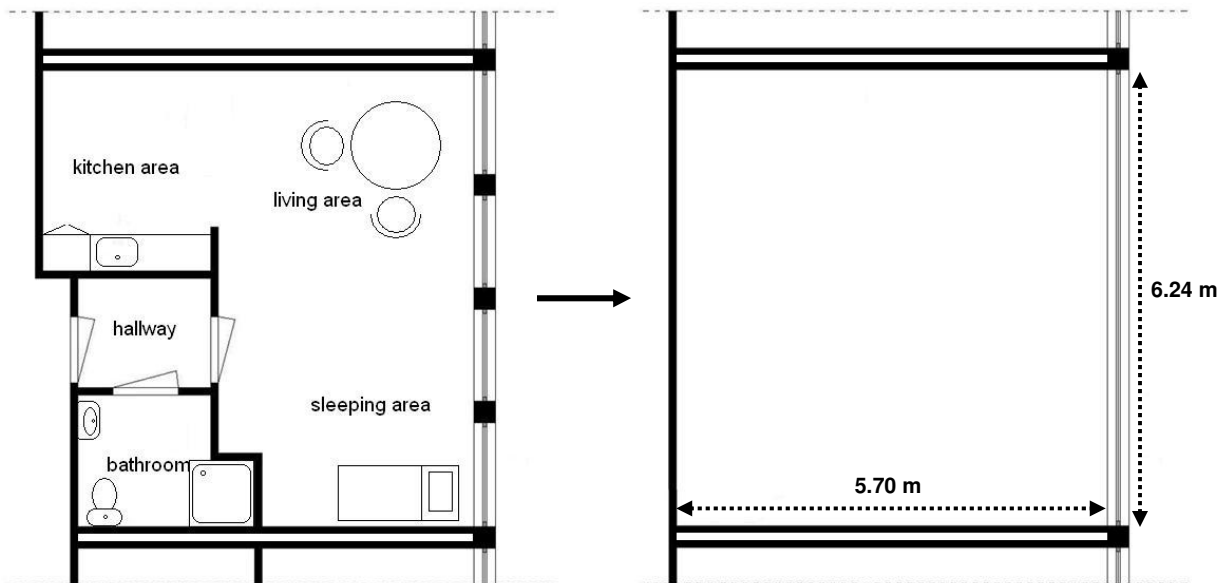


Figure 4.13: Simplification of geometry

There are two possibilities for modeling the building construction. A first possibility is to model the walls as faces without a thickness in Gambit. Subsequently, the walls can be given a thickness in the thermal boundary conditions section of Fluent. This methodology is most suitable for walls such as aluminum sheets, where the wall thickness is small with respect to the overall geometry (ANSYS FLUENT User's guide, 2009). However, this is not the case with the building construction of the care center. Therefore, it is more realistic to model the walls explicitly in Gambit by defining them as separate solid cell zones. Finishing layers with a small thickness, such as plasterwork or bitumen, are modeled implicitly. The wooden frame at the inside of the external walls is not taken into account, because its thermal resistance is negligibly small.

When choosing to model walls explicitly, this will increase the number of cells and in turn computational costs. Because no guidelines were found on the amount of cells that are needed over the thickness of a wall for solving heat transfer problems correctly, it was decided to investigate this with a simple model. A model of a 3D building with an internal volume $3 \times 3 \times 3 \text{ m}^3$ ($l \times w \times h$) was made to investigate the effect of an increasing amount of cells over the wall on the calculated heat transfer rate. The construction (walls and roof) had a thickness of 0.3 m and was made out of concrete with corresponding properties (density $\rho = 2500 \text{ kg/m}^3$; specific heat capacity $c_p = 840 \text{ J/kgK}$; thermal conductivity $\lambda = 2 \text{ W/mK}$). The indoor and outdoor temperature was set to 15°C and respectively 30°C . A structured grid was used and the number of cells was increased from 1, 2, 3, 4, 5, 6 up to 16 cells over the thickness of the walls and roof.

A steady-state CFD simulation was performed, taking only heat transfer by conduction into account. Some of the main results are provided in Figure 4.14.

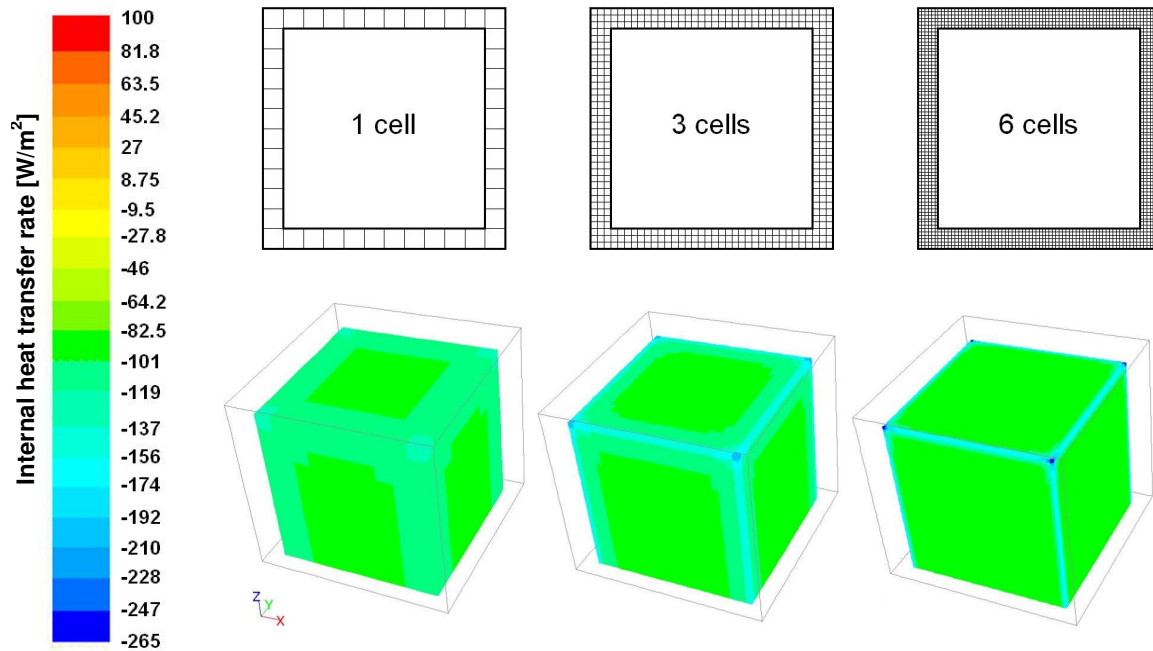


Figure 4.14: Internal heat transfer rate in W/m^2 for a wall with 1, 3 or 6 cells

The heat transfer rate in the middle of the wall can be calculated with the 1D heat transfer formula:

$$Q = (T_e - T_i) \cdot (\lambda / d) \quad (4.1)$$

with heat transfer rate Q [W/m^2], outdoor and indoor temperature T_e [$^{\circ}C$] and T_i [$^{\circ}C$], thermal conductivity λ [W/mK] and thickness of the wall d [m]. According to this formula, the heat transfer rate in the middle of the wall surfaces should be: $(30 - 15) \cdot 2/0.3 = 100 W/m^2$. This value was found for all variants. At the corners and edges, the calculated heat transfer rate differs. The more cells are used, the higher the heat transfer rate is in the corners and edges but the smaller the area with a higher heat transfer rate is.

When looking at the total heat transfer rate, this value slightly increases with increasing number of cells as depicted in Figure 4.15. There is a difference of 2.5% in heat transfer rate between the version with 1 and 16 cells.

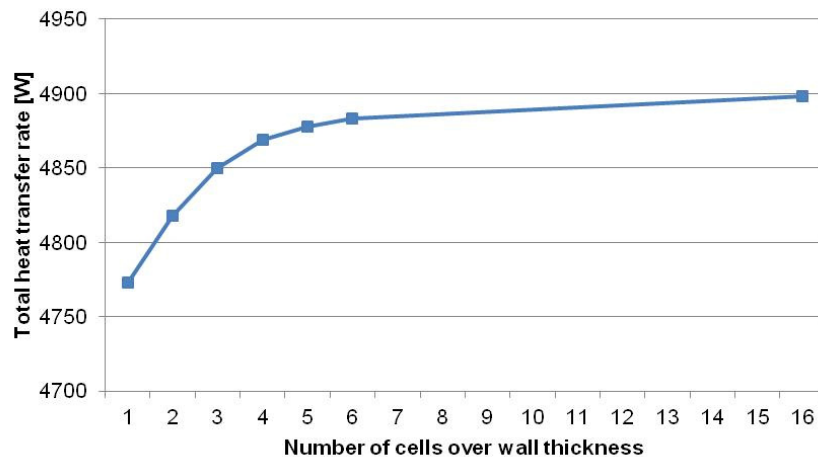


Figure 4.15: Total heat transfer rate [W] compared to the number of cells used over the wall thickness

Because it would be too computationally demanding to use 16 cells and because the target variables are indoor air temperatures instead of surface temperatures or thermal bridges, it is decided to use at least 2 - 5 cells per construction layer, dependent on the thickness of each layer.

The windows are also modeled in a simplified way. The windows of one apartment are modeled as one window with a glass area equivalent to the total glass area of the separate windows (Figure 4.16). Window frames have not been modeled. Because of the small thickness of the windows with respect to the overall geometry, they are implicitly modeled. The double glazed windows with an inner and outer glass pane of 4 and 6 mm respectively are modeled as a single glass pane of 10 mm. This technique was also used in the Fluent tutorial 'Using Solar Load Model for Indoor Ventilation' (Fluent Inc, 2007).

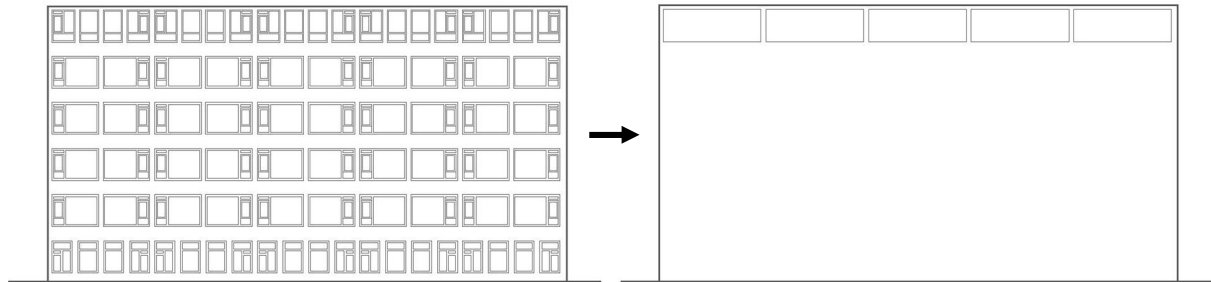


Figure 4.16: Windows of each apartment are combined. Only the upper floor is modeled.

Air is being supplied by two ventilation grilles in the upper corners of the building envelope of the apartments. These inlets are modeled as openings with sizes equivalent to the size of the openings in the inlet and with the center on the same position. According to manufacturer data, the passage surface of the inlets can be varied between 90 - 150 cm². The maximum passage surface is used to define the inlet sizes. The inlets are modeled as openings of 15 x 10 cm² (w x h) with 6 cells over the width and four cells over the height. This results in the smallest cell size in the domain of 0.025 m at 18.5 m height. This level of detail is not needed in the other subdomains. Besides, when this cell size would be adopted in the surrounding subdomains as well, this would lead to an excessive amount of cells in the computational domain. For this reason, the cell size at 18.5 m height is increased from 0.025 m to 0.175 m in the adjacent subdomains (subdomains 3 and 6) and to ± 1.225 m in the subdomains adjacent to subdomain 3 and 6. This leads to a maximum ratio in adjacent cell heights at the interfaces of 1:7.

A fixed velocity is used to model the mechanical exhausts (ANSYS FLUENT User's guide, 2009). The exhausts are modeled as separate cell zones and a fixed velocity magnitude is given to the vertical direction. In this way, air is forced to go through the exhausts with a fixed ventilation rate. The velocity magnitude is based on the surface area of the openings. The applied velocity magnitudes are given in Table 4.1. An example of this method for a fixed velocity rate of 5 m/s is shown in Figure 4.17.

Table 4.1: Applied fixed values for the velocity magnitude of the mechanical exhaust

Mechanical exhaust	Ventilation rate [m ³ /hr]	Dimensions [m ²]	Applied velocity magnitude u [m/s]
Kitchen	75	0.15 x 0.15 = 0.0225	0.926
Bathroom	50	0.15 x 0.15 = 0.0225	0.617
Hallway	25	0.15 x 0.15 = 0.0225	0.309

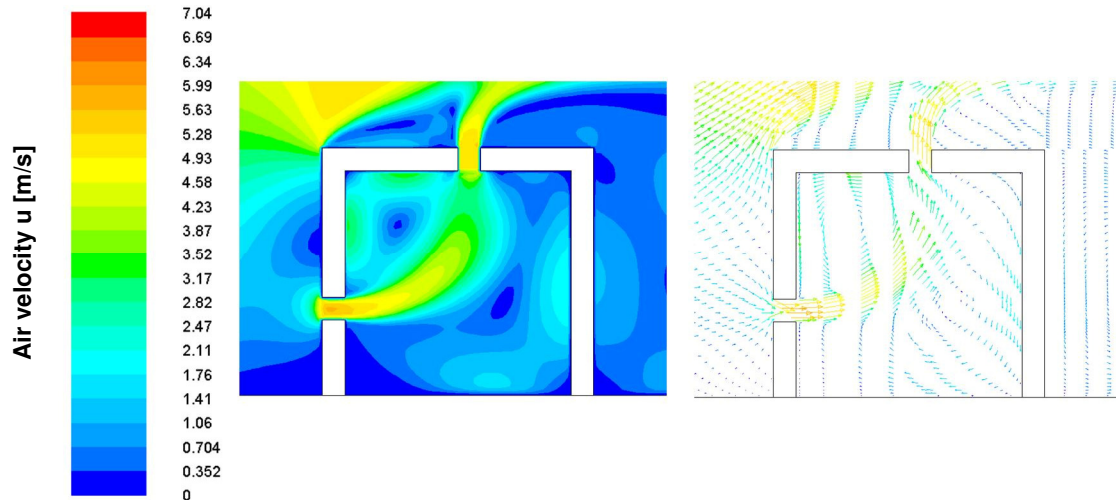
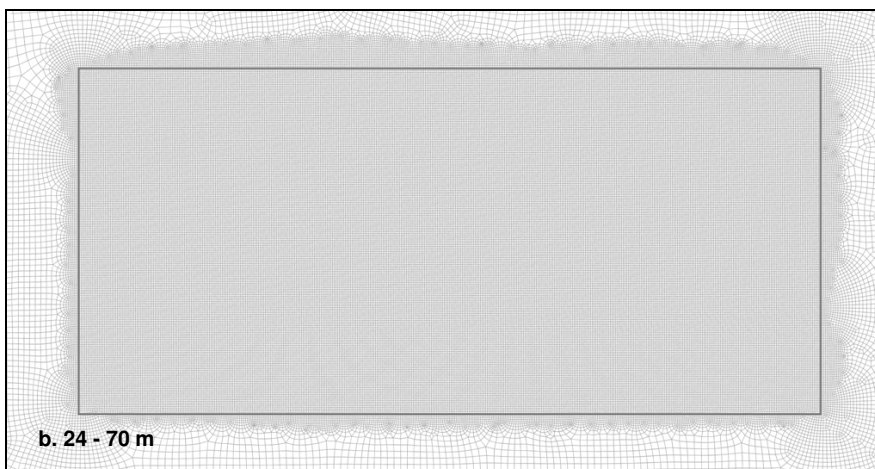
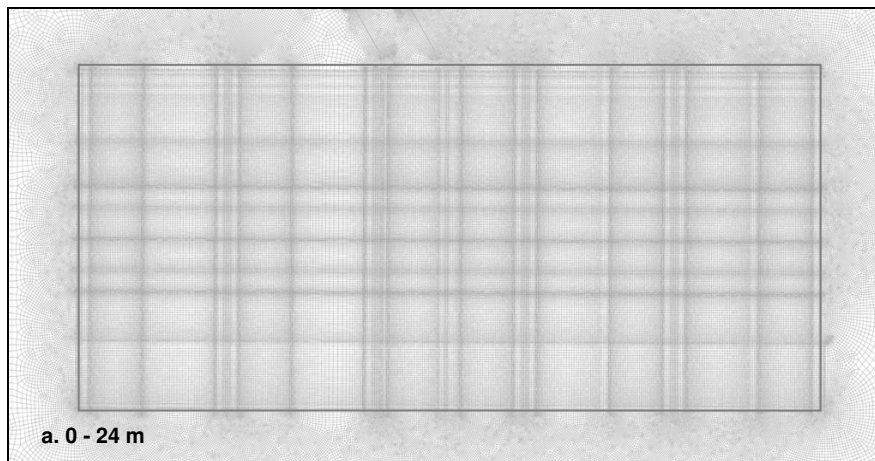


Figure 4.17: Example of the velocity fixing method. A fixed velocity rate of 5 m/s is applied to the outlet in the roof of the building. It can be seen that the air is forced to go through the inlet.

A structured grid is applied to the care center, with smaller cells at the corners and ventilation inlets and outlets. Over the height of the subdomain of the care center with the indoor environment, the subdomain is split in four parts. In order to reduce the total amount of cells, coarser grids are applied to the parts above the care center as can be seen in 4.18.



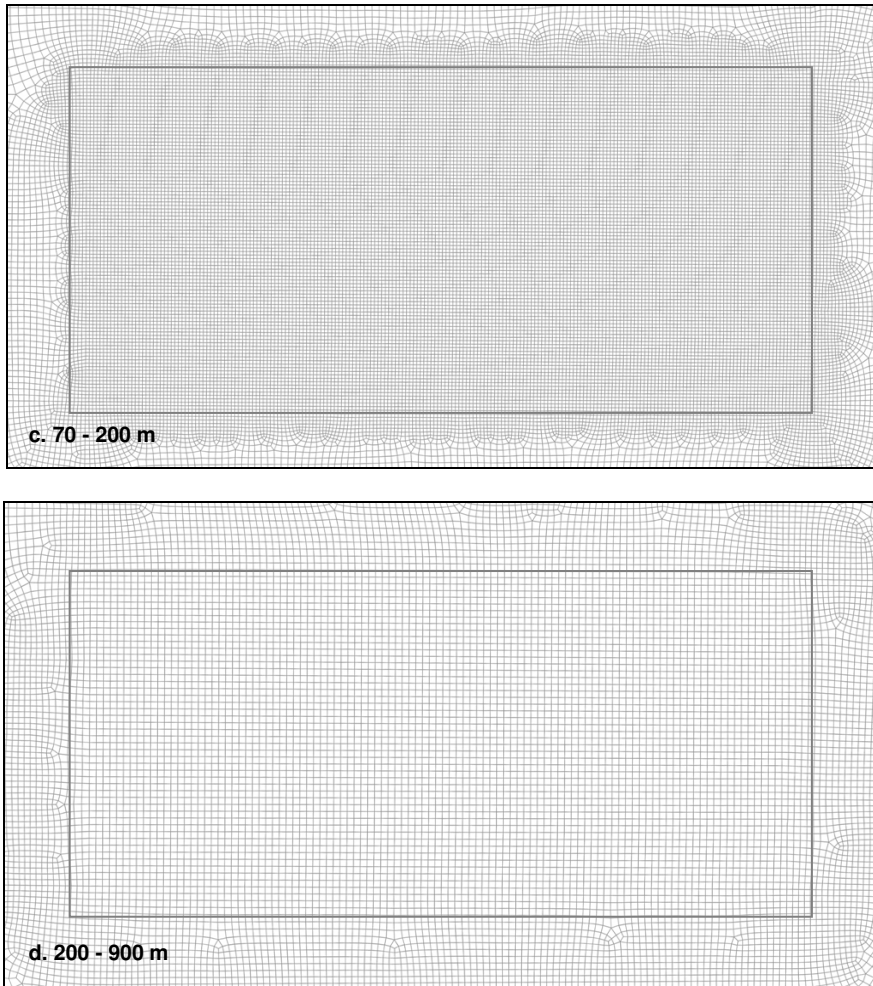


Figure 4.18a-d: Grid at the care center (a) and above the care center (b-d)

The detailed version of subdomain 5 including the indoor environment of the care center, contains 20.8 million cells. Some pictures of the grid of this subdomain and the care center are provided in Figure 4.19 - 4.21. The entire domain of model 2 contains 49.8 million cells.

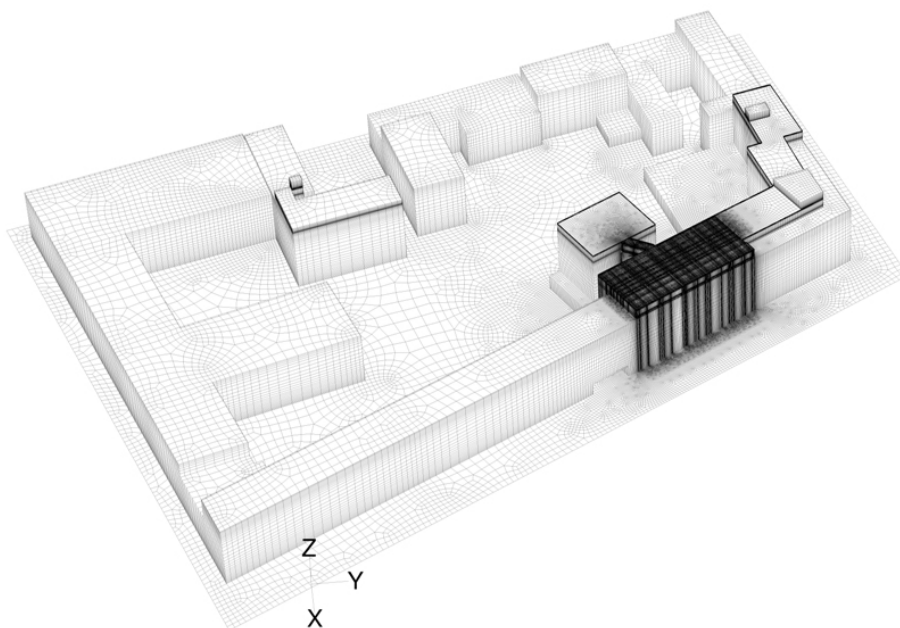


Figure 4.19: Grid of detailed version of subdomain 5 with high density mesh at the care center

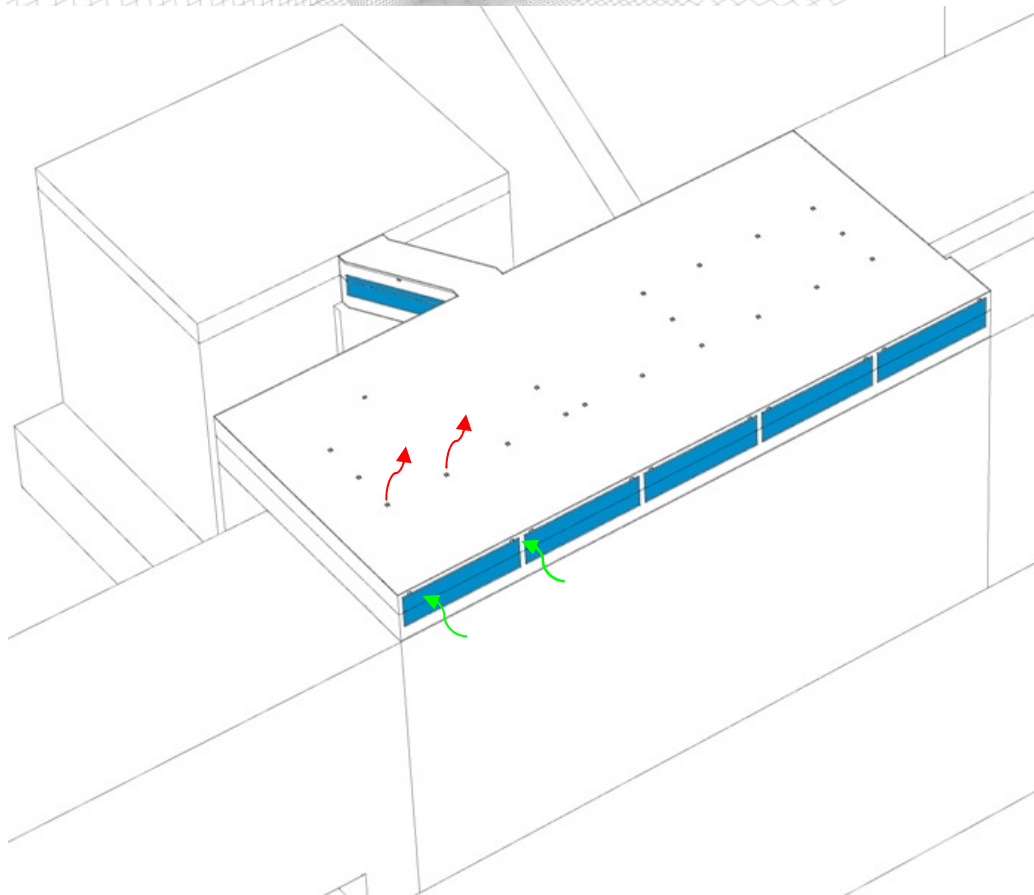
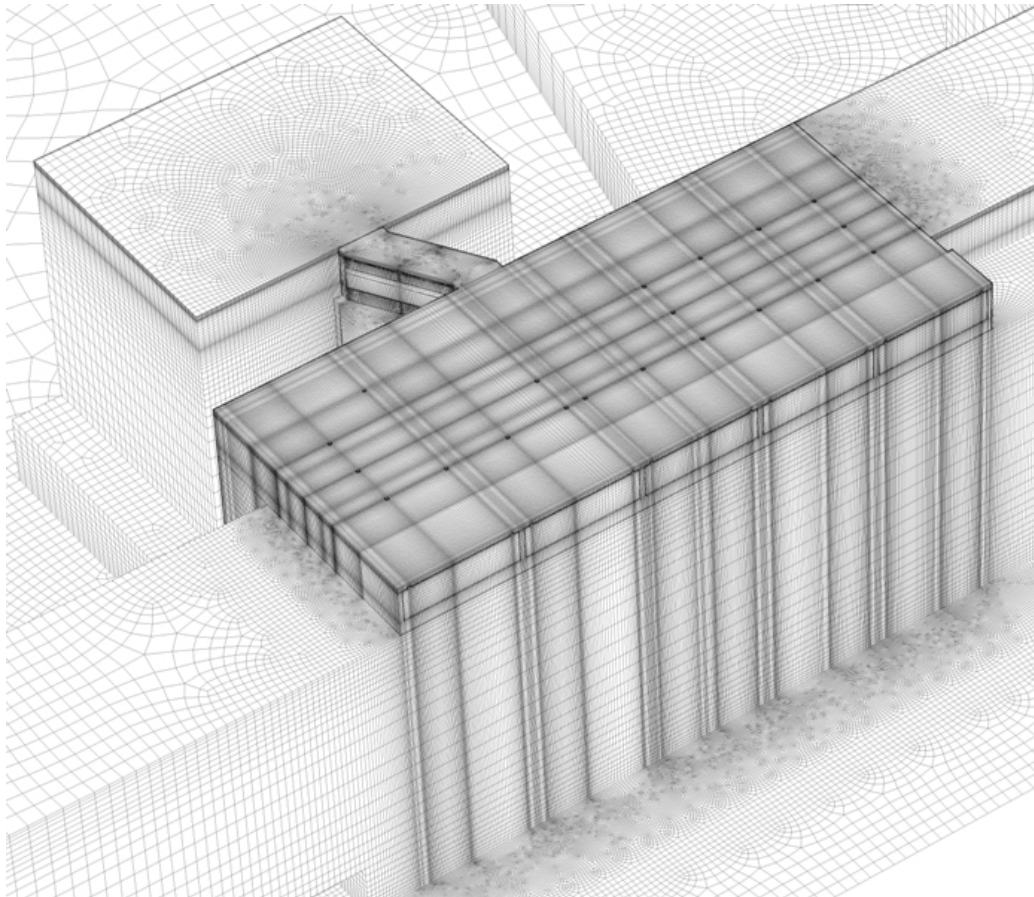


Figure 4.20: Mesh of the care center with windows (blue), ventilation inlets above the windows and ventilation outlets in the roof (indicated with arrows)

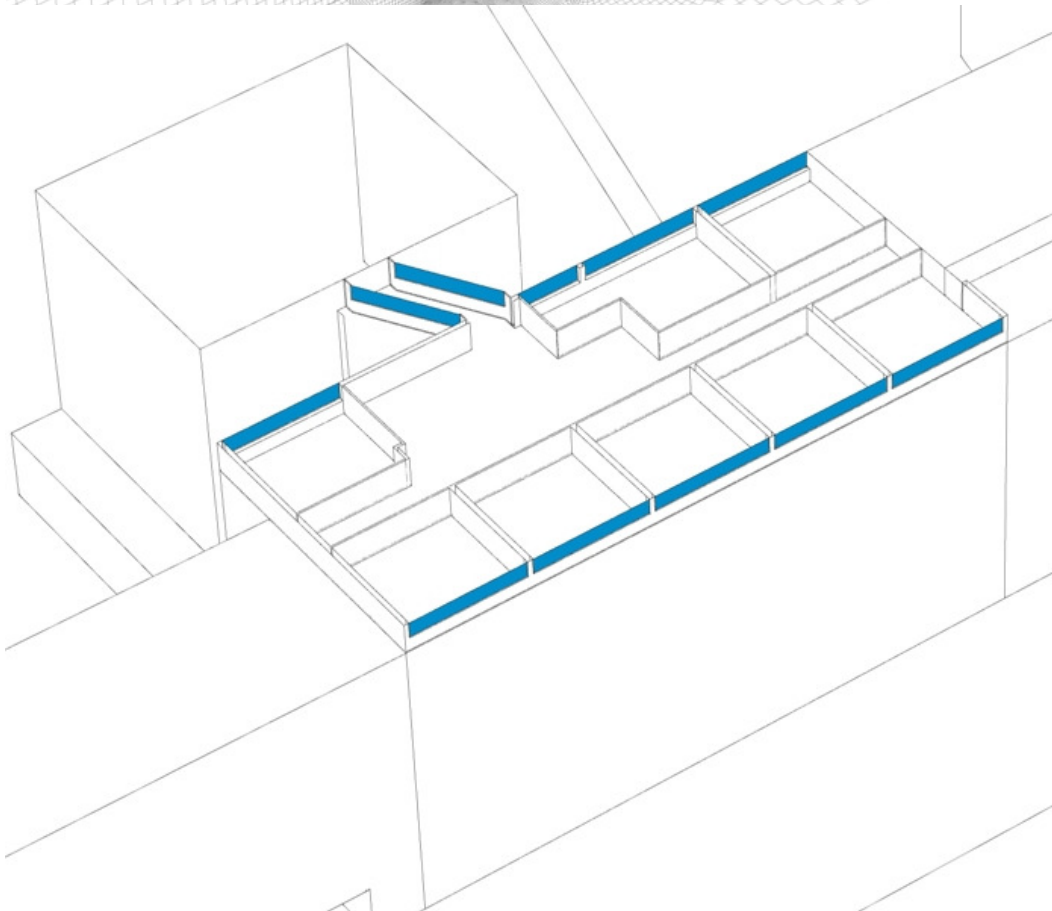
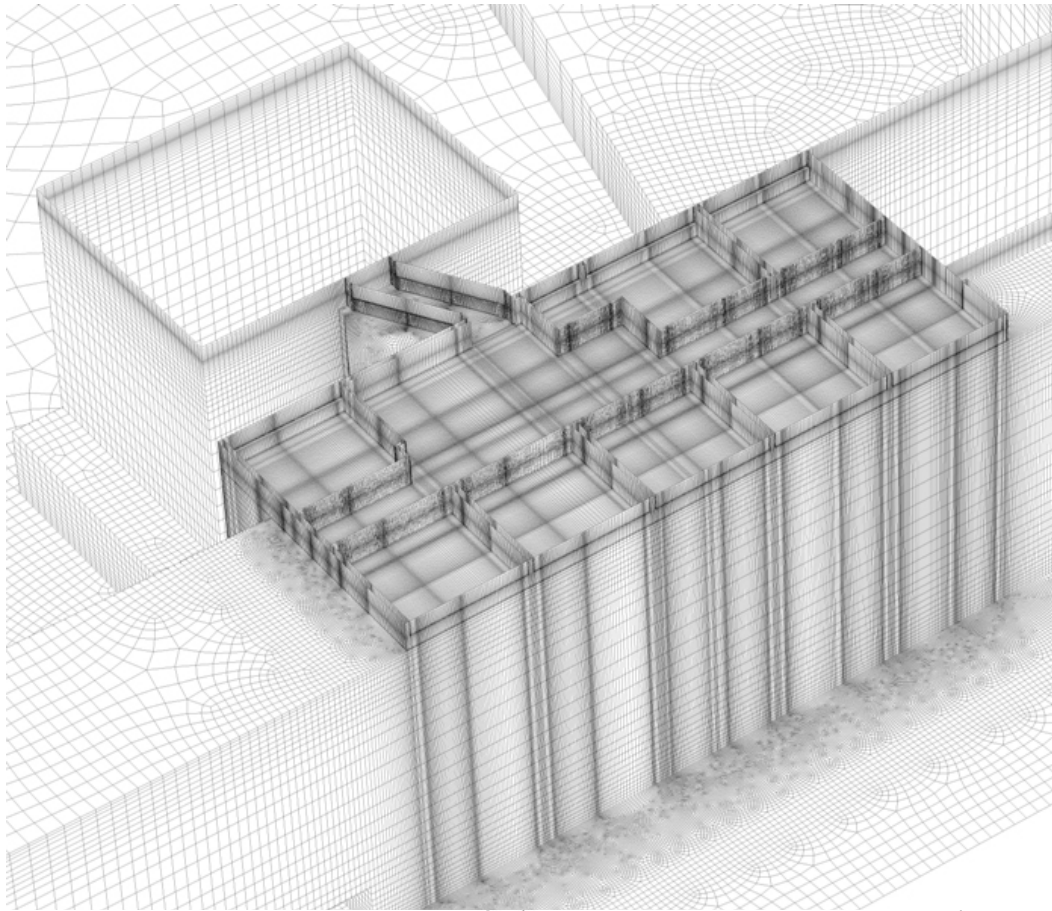


Figure 4.21: Horizontal cross section through the upper floor of the care center. Windows are indicated in blue.

4.2.2 Model 3: Care center in rural area (indoor environment included)

Explicitly modeled area

The 3rd model consists of the care center with indoor environment placed in a rural area. The rural area is assumed to be a grass landscape without any other buildings. So, except for the care center, there are no explicitly modeled buildings or obstacles. The detailed version of subdomain 5 is used as a basis for this model. All the other buildings in this subdomain are deleted by meshing these volumes again down. In this way, a subdomain is created with only the care center.

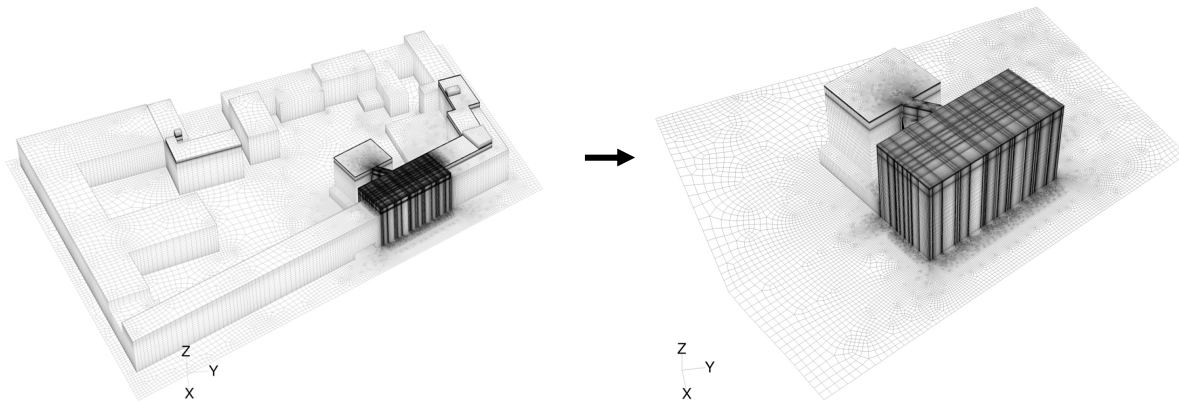


Figure 4.22: Detailed version of subdomain 5 (left) is used as basis for a subdomain with only the care center (right)

Computational domain

The total computational domain consists of a rectangular subdomain placed around the subdomain with the care center. The care center has a building height H of 18.86 m. For a computational model with 1 building, the top of the computational domain should be at least $5H$ above the roof of the building (Franke et al., 2007). With an applied domain height of 120 m, this requirement is sufficiently met.

The distance between the building and the sides of the domain should at least be $5H$ (Tominaga et al., 2008). Furthermore, the blockage ratio should be kept below 3% (Tominaga et al., 2008). A lateral distance of 120 m ($6.4H$) is applied at both sides of the care center resulting in a blockage ratio of 2.5%. According to Franke et al., (2007) (pp 17 - 18), the distance between the outflow boundary and building should at least be $15H$ and for the distance between the inlet and the building a distance of $5H$ is recommended. The distance between the care center and the outlet is set on 300 m ($16H$) and the distance between the inlet and the care center is set on 100 m ($5.3H$). These dimensions result in a computational domain of $461 \times 286 \times 120 \text{ m}^3$ ($l \times w \times h$).

Computational grid

An unstructured mesh is applied to the ground plane of the domain with greater cells at the borders of the domain and smaller cells near the care center. The first cell height is 0.075 m in the entire domain, in order to get the right value for the aerodynamic roughness length z_0 (see equation 4.6 in paragraph 4.3.3).

Again, the boundary types should be specified. No-slip conditions are applied to the ground surfaces, walls and roofs. Slip walls with zero normal velocity and zero normal gradients of all variables are set to the top and the sides of the domain. A logarithmic mean wind speed profile is applied to the inlet. Zero static pressure is imposed to the outlet. The connection surfaces between the inner and outer subdomain are defined as interfaces which are connected to each other in Fluent. The grass is modeled by defining a

separate fluid zone of 0.15 m directly above the ground plane. This will be explained in more detail in the next paragraph.

The dimensions of the computational domain and the applied mesh are presented in Figure 4.24. The total domain contains 25.3 million cells.

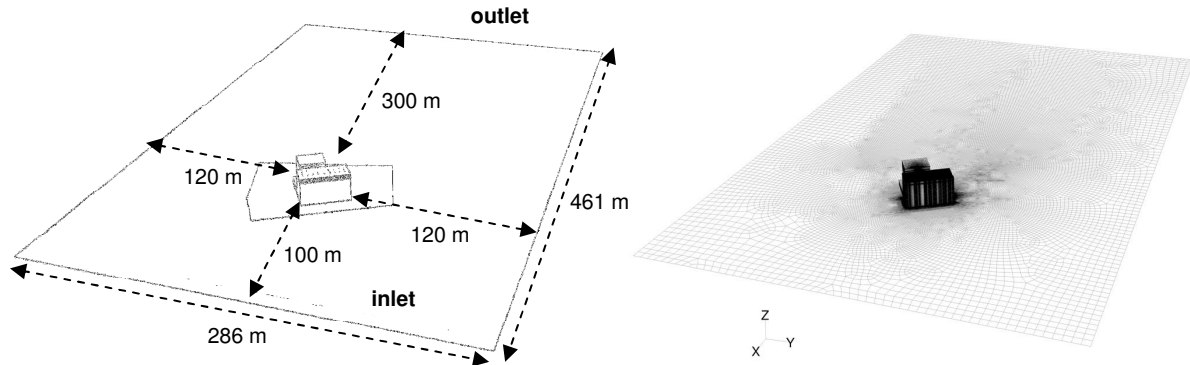


Figure 4.23: Dimensions of the computational domain (left) and applied mesh (right). The domain has a height of 120 m.

4.3 Initial and boundary conditions

4.3.1 Determining aerodynamic roughness length

Because easterly winds are prevailing during heat waves, it was decided to perform the simulations for this wind direction. For the inlet, a logarithmic mean wind speed profile was chosen which represents a neutral atmospheric boundary layer. For the specification of this profile, the aerodynamic roughness length z_0 should be chosen. This is a value for the roughness of the terrain upstream of the computational domain. In Figure 4.24, the roughness of this terrain is given for the models of the care center in Rotterdam for easterly wind.

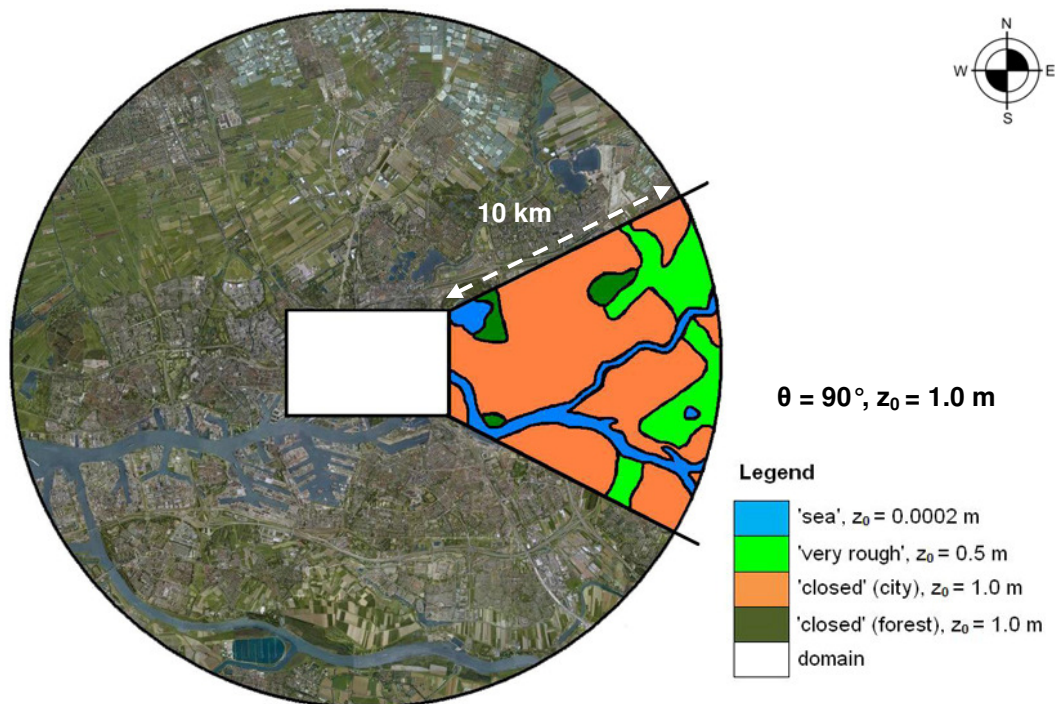


Figure 4.24: Aerodynamic roughness lengths in a radius of 10 km for the terrain upstream of the computational domain according to the revised Davenport roughness classification of Wieringa (1992)

Values are based on the revised Davenport roughness classification (Wieringa, 1992). A radius of 10 km is used for the roughness estimation. The average aerodynamic roughness length is 1.0 m. This value is used for determining the inlet profiles for the simulations of the care center in Rotterdam. For the model of the care center in the rural area, an aerodynamic roughness length of 0.03 m is used, which represents an area with low vegetation (e.g. grass) and isolated obstacles with separation of at least 50 obstacle heights (Wieringa, 1992).

4.3.2 Inlet profiles

Profiles for wind velocity U [m/s], turbulence dissipation rate ϵ [m^2/s^3] and turbulent kinetic energy k [m^2/s^2] as defined by Richards & Hoxey (1993) are applied to the inlet. The profile for the velocity magnitude is given by the following formula:

$$U(z) = \frac{u_{ABL}^*}{\kappa} \cdot \ln\left(\frac{z + z_0}{z_0}\right) \quad (4.2)$$

where z is the height coordinate, κ the von Karman constant ($\kappa = 0.42$), z_0 the aerodynamic roughness length ($z_0 = 1.0$ m) and u_{ABL}^* the atmospheric boundary layer friction velocity which is calculated using:

$$u_{ABL}^* = \frac{\kappa \cdot U_{ref}}{\ln\left(\frac{z_{ref} + z_0}{z_0}\right)} \quad (4.3)$$

with reference mean wind speed U_{ref} at reference height z_{ref} ($z_{ref} = 10$ m). The reference wind speed was taken from KNMI data for weather station Rotterdam Airport, which is located north-west to Rotterdam. During the evaluation period, U_{ref} varied from 1 - 4 m/s.

For the turbulence dissipation rate, the following formula is used:

$$\epsilon(z) = \frac{u_{ABL}^{*3}}{\kappa(z + z_0)} \quad (4.4)$$

The turbulent kinetic energy profile is being calculated by:

$$k(z) = \alpha \cdot (I_u(z) \cdot U(z))^2 \quad (4.5)$$

with the stream-wise turbulent intensity I_u at height z . For α , a value of 1.0 is chosen based on a study performed by Ramponi & Blocken (2012). I_u ranges from 39.4% at pedestrian height to 8.0% at 900 m height for model 1 and 2 (care center in Rotterdam). For model 3 (care center in rural area), I_u ranges from 15.0% at pedestrian height to 3.2% at the top of the domain (120 m). The resulting profiles for the velocity inlet boundary for $U_{10} = 3$ m/s are provided in Figure 4.25 and 4.26. The profiles for the other reference wind speeds can be found in appendix 2.

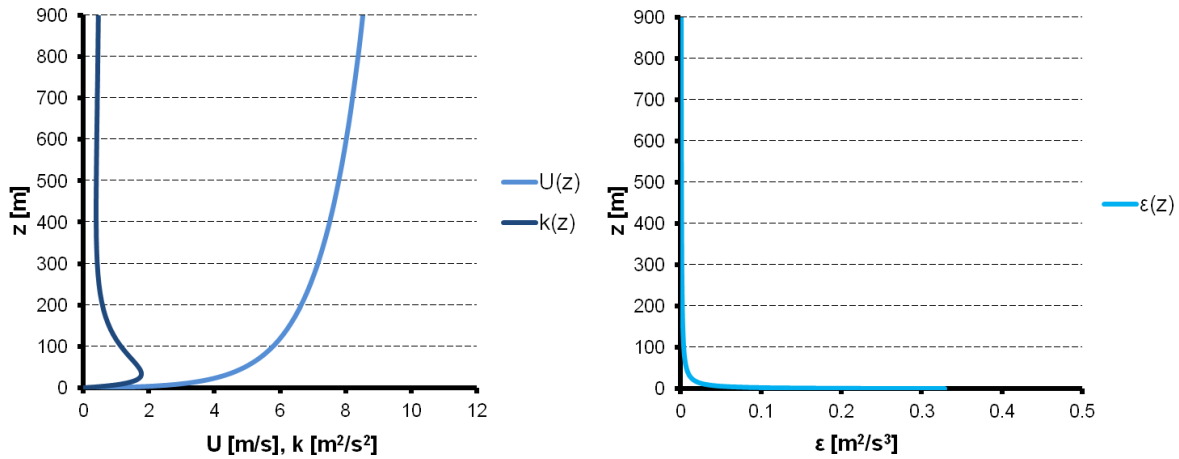


Figure 4.25: Inlet profiles of model 1 and 2 for wind velocity, turbulent kinetic energy and turbulent dissipation rate for $U_{ref} = 3$ m/s and $z_0 = 1.0$ m

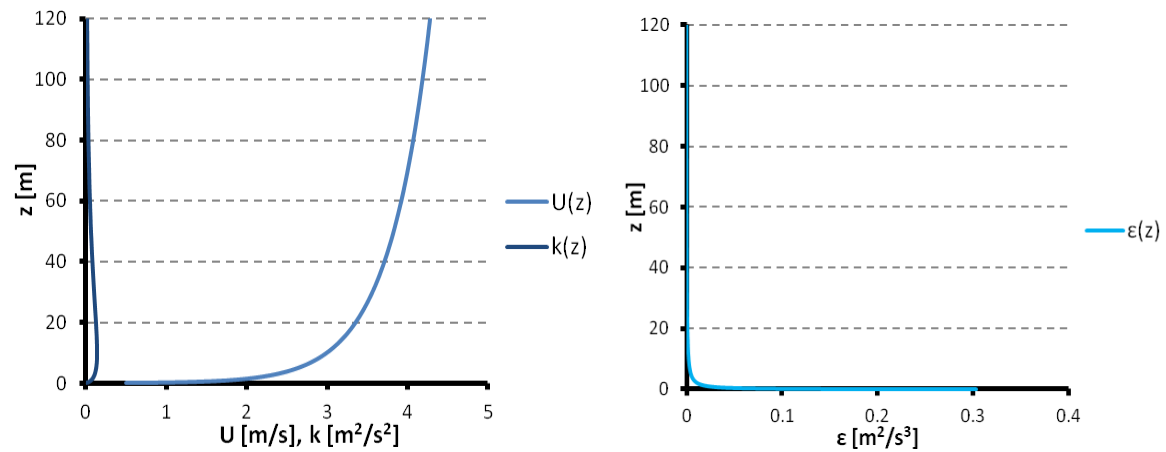


Figure 4.26: Inlet profiles of model 3 for wind velocity, turbulent kinetic energy and turbulent dissipation rate for $U_{ref} = 3$ m/s and $z_0 = 0.03$ m

Besides these profiles, also a temperature should be applied to the inlet. The temperature applied to the inlet is extracted from the weather data of the KNMI weather station at Rotterdam airport. The inlet temperature is changed for different simulations.

4.3.3 Surface roughness parameters

Roughness parameters, thermal parameters and radiation parameters are applied to the wall boundaries which are the building walls, roofs and the ground. Standard wall functions are used which are customized by applying a turbulent Prandtl number of 1.95. This adjustment is recommended by Defraeye et al. (2011) because it increases the accuracy of convective heat transfer predictions. The standard wall functions (Launder & Spalding, 1974) are combined with the sand-grain roughness modification by Cebeci & Bradshaw (1977). z_0 [m] is being described by the equivalent sand-grain roughness height k_s [m] and roughness constant C_s [-] according to the following formula (Blocken et al., 2007):

$$k_s = \frac{9.793 \cdot z_0}{C_s} \quad (4.6)$$

In Ansys Fluent, z_p is the maximum value for k_s , which is the distance between the centre point of the wall-adjacent cell to the ground wall.

For model 1 and 2 (care center in Rotterdam), z_p varies between 0.09 and 0.20 m for subdomain 1 - 8. z_p of subdomain 9 - 11 is 1.05 m. Therefore, k_s values of 0.09 and 1.05 are applied to all the surfaces. C_s is then calculated based on the required aerodynamic roughness length and the equation as derived by Blocken et al. (2007). Different types of rough surfaces have been specified: (1) the building walls and roofs, (2) streets and pavements, (3) surfaces mainly covered with grass, (4) water surface of the river Maas and (5) the surroundings. The applied values are depicted in Figure 4.27. For the buildings, default values are applied ($k_s = 0$ m, $C_s = 0.5$). Text files are used for increasing the roughness constant because by default the highest value for $C_s = 1$ in Fluent. Normally, this constant cannot be set higher than 7 or 9 because at higher values convergence problems might occur. An empty domain was used to test whether the solution converged for $C_s = 9$. No convergence problems occurred. Therefore this value is applied to the surroundings in order to reach a value of z_0 of 1.00 m.

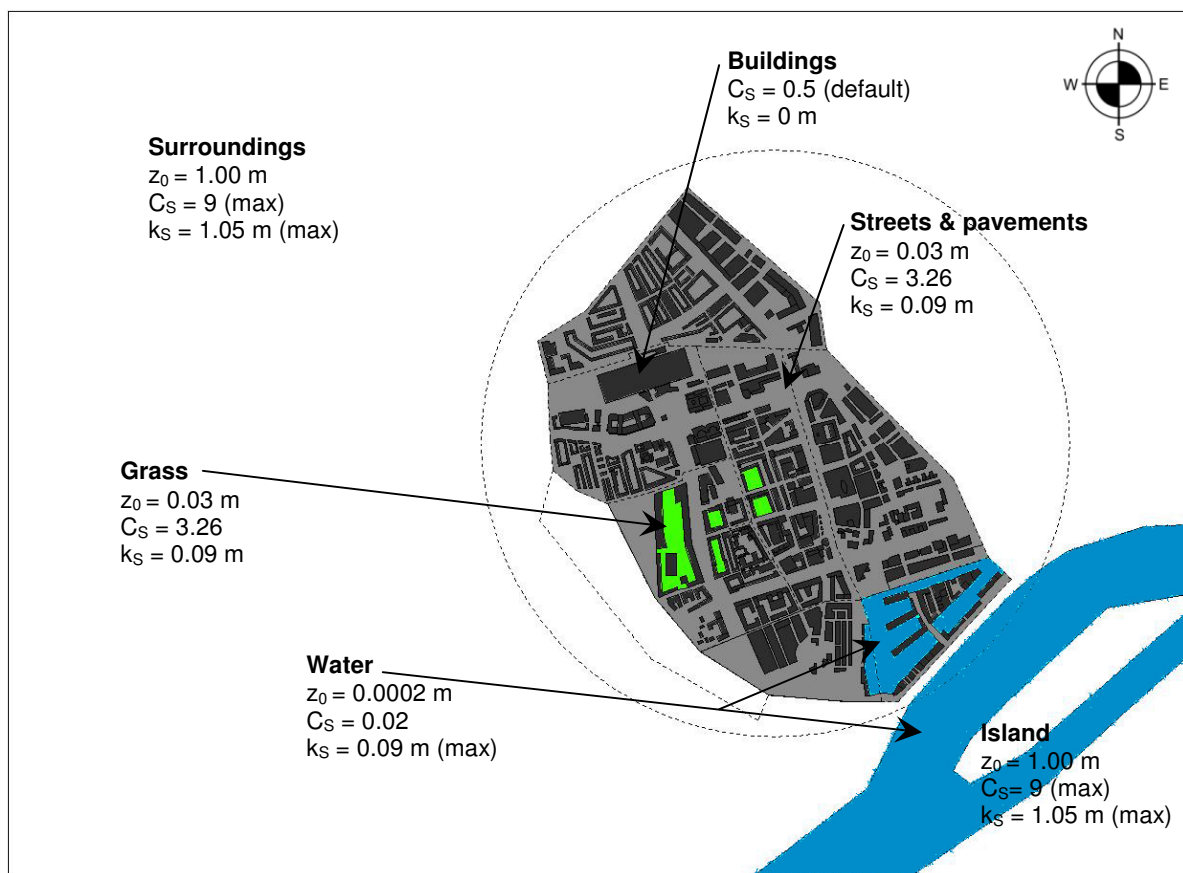


Figure 4.27: Roughness specification for the ground surface and building surfaces of model 1 and 2, based on the required aerodynamic roughness length z_0 and the relationship with the sand-grain roughness height k_s and roughness constant C_s .

The first cell height of model 3 (care center in rural area) is 0.075 m. Therefore, k_s is set on 0.0326 which results in a roughness constant C_s of 9 based on the required aerodynamic roughness length of 0.03 m and equation 4.6.

4.3.4 Thermal and radiation parameters

The thermal and radiation parameters applied to the urban area of model 1 and 2 are given in Table 4.2. All the ground surfaces were assumed to have a dry clay soil underground of 20 m and a free stream temperature of 10°C (Toparlak, 2012). For the pavement and streets and the surroundings an emissivity value

ϵ of 0.9 was used, which is the average value for asphalt and concrete surfaces (van Hove et al., 2011b). Taking into account the effect of shading, the solar absorptivity of these surfaces was decreased from 0.65 to 0.5 (Zulovich, 1993). The absorptivity of green roofs with grass is 0.78 (Onmura, 2001). This value was reduced for the grass surfaces to take into account the effect of shading. Furthermore, the latent heat loss caused by evapotranspiration was simplified by giving the surface a negative heat flux of 20% of the net solar radiation. This value is based on a research performed by Takahashi et al. (2003) on heat flux measurements of urban boundary layers in Kyoto city. The average emissivity of short to long grass is 0.92 (van Hove et al., 2011b).

Close to the care center, most building facades are made out of bricks. Therefore the thermal and radiation properties of bricks are applied to all the surrounding buildings (Fluke Corporation, 2009; ASHRAE fundamentals handbook, 2005). The roofs are assumed to have a concrete construction. To the roof surfaces, the average emissivity and solar absorptivity for various roof finishing layers is used (Buildings department Hong Kong; van Hove et al., 2011b). Both roof and walls are given a thickness of 0.3 m and a standard heat transfer coefficient of 0.5 W/m²K. This heat transfer coefficient describes the thermal conductivity of the walls and is based on the average of the minimal required R_c-value for the building envelope of Dutch dwellings in the period of 1974 - 1991 and 1992 - 2011, respectively 1.3 and 2.5 m²K/W (Haak, 2012). Most of the buildings in the city centre date back from these periods.

The Maas was first modeled as a wall with thermal and radiation characteristics of water. In the end, it was decided to model the Maas as a fluid with a certain thickness which gives much more realistic results. The water was given a fixed temperature based on the average temperature of 20°C of the Maas in July (Air foundation, 2013). This value was lowered to 18°C to take into account the effect of evaporative cooling.

Table 4.2: Applied thermal and radiation properties

Surface type	Material	Heat transfer Coefficient htc [W/m ² K]	Thickness d [m]	Solar emissivity ϵ [-]	Solar absorptivity α [-]
Grass	Dry clay soil	-	20	0.92	0.60
Pavement and streets	Dry clay soil	-	20	0.90	0.50
Building walls	Bricks	0.5	0.3	0.85	0.60
Building roofs	Concrete	0.5	0.3	0.90	0.60
Surroundings	Dry clay soil	-	20	0.90	0.50

The ground surface of model 3 was also assumed to have a dry clay soil underground of 20 m and a free stream temperature of 10°C (Toparlar, 2012). The radiation properties of grass as given in Table 4.3 are also applied to the ground surface.

For model 2 and 3, which include the indoor environment of the care center, the thermal and radiation properties of the different building components and surfaces should be defined. The thermal properties for the different building components are given in Table 4.3.

Table 4.3: Thermal properties of the care center building components

Building component	Material layer	Density ρ [kg/m ³]	Thermal conductivity λ [W/mK]	Specific heat capacity c_p [J/kgK]
Roof	Plasterwork	1600 ^[1]	0.70 (dry) ^[1]	840 ^[1]
	170 x 71 mm wooden beams	550 ^[1]	0.14 ^[1]	1880 ^[1]
	Air (cavity)	1225 ^[4]	1 ^{[2]*}	1006 ^[4]
	Average beams + air (cavity)	1145	0.90	1109
	Expanded PS foam	25 ^[1]	0.035 ^[1]	1470 ^[1]
	Bituminous felt	2100 ^[1]	0.70 ^[1]	840 ^[1]
Floor	Concrete	2400 ^[3]	1.51 ^[3]	880 ^[3]
	Light grey carpet	-	-	-
External walls of hallway	Plasterwork	1600 ^[1]	0.70 (dry) ^[1]	840 ^[1]
	Expanded PS foam	25 ^[1]	0.035 ^[1]	1470 ^[1]
	Aluminum	2719 ^[4]	202.4 ^[4]	871 ^[4]
External walls of apartments	Plasterwork	1600 ^[1]	0.70 (dry) ^[1]	840 ^[1]
	Concrete	2400 ^[3]	1.51 ^[3]	880 ^[3]
	Expanded PS foam	25 ^[1]	0.035 ^[1]	1470 ^[1]
Internal walls between the apartments	Plasterwork	1600 ^[1]	0.70 (dry) ^[1]	840 ^[1]
	Concrete	2400 ^[3]	1.51 ^[3]	880 ^[3]
	Air (cavity)	1225 ^[4]	0.59 ^{[2]*}	1006 ^[4]
	Concrete	2400 ^[3]	1.51 ^[3]	880 ^[3]
	Plasterwork	1600 ^[1]	0.70 (dry) ^[1]	840 ^[1]
Internal walls between hallway and apartments	Plasterwork	1600 ^[1]	0.70 (dry) ^[1]	840 ^[1]
	Concrete bricks	1500 ^[3]	0.68 ^[3]	840 ^[3]
	Plasterwork	1600 ^[1]	0.70 (dry) ^[1]	840 ^[1]

* based on the thickness and given resistance of a cavity of 0.17 m²K/W

^[1] Bone, 2007

^[2] Presentations of ABP master course 'Heat and moisture in the building envelope' at TU/e

^[3] van Hove et al., 2011b

^[4] Fluent Material database

The cavity with the wooden beams in the roof is modeled as one solid layer with the average thermal properties of air and wood together. Also the cavity in the internal walls is modeled as a solid with the properties of an air cavity layer. The wooden frame in front of the external walls is not taken into account. The floor and building separation walls are assumed to be adiabatic.

The surface properties of the building components are provided in Table 4.4. The solar absorptivity of the external plasterwork is slightly lowered and emissivity increased to take the effects of weathering into account. The solar emissivity of carpet could not be found; therefore the value of cotton is used. For the wall covering, the values for different types of wall finishing layers are used.

Table 4.4: Radiation properties of the care center building components

Building component	Surface material	Solar absorptivity α [-]	Solar emissivity ϵ [-]
Roof	Bituminous felt	0.88 ^[2]	0.88 ^[3]
	White plaster	0.10 ^[4]	0.91 ^[1]
Floor	Light grey carpet (top)	0.55 ^[5]	0.77 ^[7]
External walls of apartments	White plaster, weathered (outside)	0.35 ^[4]	0.87 ^[1]
	various (inside)	0.45 ^[6]	0.85 ^[3]
External walls of hallway	Aluminum (outside)	0.3 ^[5]	0.91 ^[1]
	various (inside)	0.45 ^[6]	0.85 ^[3]
Internal walls	various (both sides)	0.45 ^[6]	0.85 ^[3]

^[1] van Hove et al., 2011b

^[2] Buildings department Hong Kong

^[3] ASHRAE fundamentals handbook, 2005

^[4] Protek-USA: Reflectance and emittance of building materials

^[5] Reader Lighting technology, 2010

^[6] NEN-EN 12464, 2011

^[7] engineeringtoolbox

The double glazed windows are modeled as windows with single panes of 10 mm thickness with the thermal and radiation properties of double glazing. The applied values are provided in Table 4.5.

Table 4.5: Glazing properties

Property type	property	value
Glass type	Thickness inner glass pane	6 mm ^[1]
	Thickness cavity	12 mm ^[1]
	Thickness outer glass pane	4 mm ^[1]
Thermal properties	Density ρ	2500 kg/m ³ ^[2]
	Thermal conductivity λ	0.8 W/mK ^[2]
	Specific heat capacity c_p	840 J/kgK ^[2]
	U-value	2.8 W/m ² K ^[2]
Radiant properties	Absorbance α	0.16 ^[3]
	Transmittance τ	0.76 ^[3]

^[1] Construction drawings care center

^[2] Bone, 2007

^[3] Reader Lighting technology, 2010

4.3.5 Cooling power of grass land

In model 3, the grass is modeled more realistically by defining a separate fluid zone of 0.15 m directly above the ground plane and applying a cooling power to it. The height of 0.15 m represents the assumed height of the grass blades. The cooling effect caused by evapotranspiration is allocated to a volume containing vegetation. This technique is also used in a research of Merema (2013) about the cooling effect of different types of vegetation on air temperatures in a street in Arnhem.

The cooling power of grass or a plant depends on the leaf area density (LAD). This is a value for the surface area of leafs or grass blades per unit of volume [m²/m³] (Merema, 2013). The cooling power of plant increases with increasing LAD. In literature, not the LAD but LAI is mostly used, which stands for the leaf area index in m²/m². For different grass types in the Netherlands, LAI range between 1.5 - 15.3 m²/m² (University of Giessen, Germany). The cooling power is not only dependent on the LAI or LAD, but also on meteorological conditions, e.g. the cooling power varies during the day and is often higher after a rain shower.

Relevant information on the cooling capacity of grass surfaces was found in an article of Oke (1988). Oke provides energy balances for hypothetical midlatitude cities at noon during clear summer conditions for rural, suburban and urban areas. Values are also given for the latent heat flux. For the rural area a value of 305 W/m² is given.

Available Energy	Rural		Suburban		Urban	
K↓	800		776		760	
K↑	-160		-116		-106	
L↓	350		357		365	
L↑	-455		-478		-503	
Q*	535		539		516	
Q _F	0		15		30	
Total	535		554		546	

Partitioned Energy	Rural	%	Suburban	%	Urban	%
Q _s	80	15	122	22	148	27
Q _H	150	28	216	39	240	44
Q _E	(305)	57	216	39	158	29
Total	535	100	554	100	546	100

Figure 4.28: Radiation and energy balances for a hypothetical midlatitude city at noon during clear summer conditions. All values are in W/m². Q_e represents the latent heat flux in W/m² (modified from Oke, 1988).

In 1982, Jacobs & Palland estimated the evaporation rate of a grass surface based on direct measurements of the most important energy balance terms (radiative fluxes, sensible heat flux and soil heat flux). The evaporation rate is the rest term from the energy balance. The measurements were performed over a grass surface at Schoonheeten in the Netherlands during 3 consecutive days in July 1978. Results are given in Figure 4.29. At the first day, the sky was cloud free. Around noon an evaporation rate (q_{ev}) of 330 W/m^2 was found. This value is in the same range as the value given in the article of Oke (1988). For the CFD model, a cooling power of 300 W/m^2 is assumed. With a grass height of 0.15 m , this results in a volumetric cooling power P_c of 2000 W/m^3 .

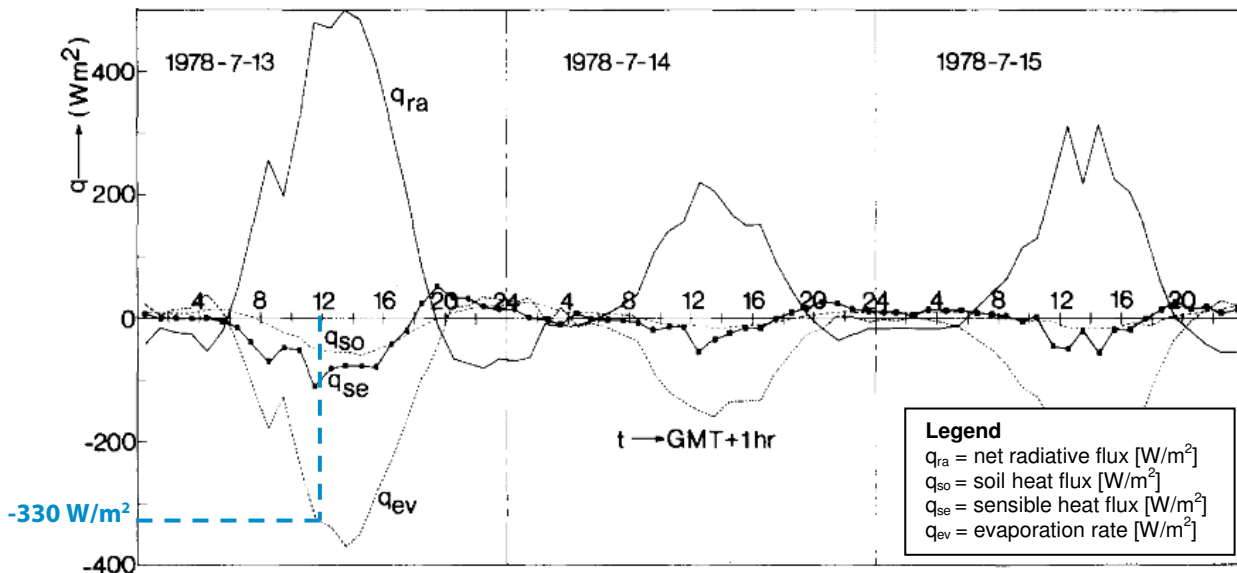


Figure 4.29: Evaporation rate determined from measured energy fluxes for 3 consecutive days in July 1978, Schoonheeten. The evaporation rate at 12.00 a.m. 13 July 1978 is 330 W/m^2 (modified from Jacobs & Palland, 1982).

4.4 Solution parameters

4.4.1 Numerical approximations

For all simulations, 2nd order discretisation schemes are used for momentum, turbulent kinetic energy, turbulence dissipation rate and energy. For the pressure interpolation schemes, body force weighted is chosen because this is the one that should be used in case of buoyancy or natural convection flows (ANSYS FLUENT User's guide, 2009). Because this lead to a floating point exception error, the first order discretisation scheme was used for pressure interpolation for the first iterations and then changed after 150 iterations in body force weighted.

For most flows, the default under-relaxation factors can be used. However, because unstable behavior occurred at the beginning of the simulation the under-relaxation factors for pressure, momentum, k and ϵ and energy were changed from their default values to 0.2, 0.5, 0.5, 0.5 and 0.8 as recommended in the ANSYS FLUENT User's guide, 2009. These values are lower compared to the default under-relaxation values. This leads to an increased stability of the solution. A drawback of reducing the under-relaxation factors is that more iterations are needed to reach the same order of convergence. Therefore, after some time the under-relaxation factors were set back to their default values again.

4.4.2 Iterative convergence criteria

The simulation results are examined when the solution is sufficiently converged. According to Franke et al., (2008), the results can be examined when the residuals dropped four orders of magnitude or when the solution starts to follow a straight line on residuals compared to the number of iterations. This advice is taken into account when the results were being analyzed.

4.5. Thermal model

Airflow is being affected by convection through the following settings. First of all, a gravitational acceleration of 9.80655 m/s^2 is defined for the operational conditions with an operational temperature equal to the inlet temperature. Then the density of the air is set to be calculated according to the Boussinesq approximation (ANSYS FLUENT User's guide, 2009). This approximation is valid when $\beta(T-T_0) \ll 1$, where β is the thermal expansion coefficient ($= 0.0034 \text{ K}^{-1}$) and $T - T_0$ the maximum temperature difference. This means that with a thermal expansion coefficient of 0.0034 K^{-1} the temperature difference should be much lower than 294 K. This requirement is sufficiently met.

Radiation is taken care of by a radiation model. There are several types available: DTRM, DO, P-1, Rosseland and S2S model. When choosing a radiation model, the optical thickness should be considered. The optical thickness or opacity equals $(\alpha + \sigma_s)s$, where α is the absorption coefficient of the medium, σ_s the scattering coefficient and s an appropriate length scale of the domain. For optical thicknesses $\gg 1$, which is the case in this research because of the large size of the domain, the P-1 and Rosseland model are the most appropriate. DTRM and DO could also be used, but are more computationally demanding. For this case, the P-1 radiation model is selected because it takes into account scattering and emissivity while the Rosseland model neglects the emissivity of the wall. The P-1 model was also used in the UHI research as performed by Toparlar (2012). A limitation of the P-1 model is that it assumes all surfaces to be diffuse: the reflection of the incident radiation at the surface is isotropic with respect to the solid angle. Furthermore, the P-1 model assumes gray radiation: the absorption coefficient does not change for different spectral bands (ANSYS FLUENT User's guide, 2006).

Solar load is being calculated by a Solar Calculator which requires the following inputs:

- Longitude, latitude and time zone of the care center being 4.475° , 51.919° and +1 GMT respectively.
- Mesh orientation: The y-axis represents the north direction and the x-axis the east direction.
- Date (month and day) and time (hour and minute): this varies per simulation.

Based on these inputs, the sun direction vector and direct and diffuse solar irradiation are being calculated. The direct solar irradiation is then adjusted to the measured solar irradiation for that moment as measured by KNMI.

The solar load is being calculated by a solar ray tracing algorithm which is not parallelized in FLUENT. This means that solar load data needs to be computed on the serial solver first before a simulation on parallel computing nodes can be started. The data is then read in the parallel solver by an autoread-solar-data command in the text interface (ANSYS FLUENT User's guide, 2009).

4.6. Summary settings

In this chapter, the general settings and parameters of the CFD simulations were described. An overview of the settings and parameters of the 3 models is provided in Table 4.6.

Table 4.6: Overview of CFD settings

	Model 1	Model 2	Model 3
Fluid			
<i>Air, incompressible, viscous</i>			
Density	1.171 kg/m ³ *	1.171 kg/m ³ *	1.168 kg/m ³
Viscosity	1.7894e-05 kg/ms	1.7894e-05 kg/ms	1.7894e-05 kg/ms
Computational domain			
<i>Rectangular domain</i>			
Length	5015 m	5015 m	461 m
Width	3691 m	3691 m	286 m
Height	900 m	900 m	120 m
<i>Circular domain</i>			
Diameter	2500 m	2500 m	n.a.
Height	900 m	900 m	n.a.
<i>Highest building</i>			
Height	150 m	150 m	18.86 m
<i>Distance urban region from boundaries</i>			
Upstream	750 m	750 m	100 m
Downstream	2250 m	2250 m	300 m
Sides	750 m	750 m	120 m
Top	750 m	750 m	111.14 m
<i>Mesh</i>			
Type (X-Y Plane)	unstructured	unstructured	unstructured
Type (z-axis)	structured	structured	structured
Number of cells	29 million	49.8 million	25.3 million
Models			
Turbulence model	Realizable k-ε	Realizable k-ε	Realizable k-ε
Radiation model	P1	P1	P1
Solar load	Solar-ray-tracing	Solar-ray-tracing	Solar-ray-tracing
Von Karman	0.4	0.4	0.4
Gravitational acceleration	9.80655 m/s ²	9.80655 m/s ²	9.80655 m/s ²
Boundary conditions			
<i>Inlet</i>			
Type	Velocity inlet	Velocity inlet	Velocity inlet
Velocity profile	Logarithmic law	Logarithmic law	Logarithmic law
U _{ref} (Wind velocity at 10 m)	1 - 4 m/s	3 m/s	3 m/s
k (m ² /s ²)	$\alpha \cdot (I_u(z) \cdot U(z))^2$ ($\alpha=1$)	$\alpha \cdot (I_u(z) \cdot U(z))^2$ ($\alpha=1$)	$\alpha \cdot (I_u(z) \cdot U(z))^2$ ($\alpha=1$)
ε (m ² /s ³)	$\epsilon(z) = (u_{ABL}^*)^3 / (\kappa(z+z_0))$	$\epsilon(z) = (u_{ABL}^*)^3 / (\kappa(z+z_0))$	$\epsilon(z) = (u_{ABL}^*)^3 / (\kappa(z+z_0))$
<i>Outlet</i>			
Type	Pressure outlet	Pressure outlet	Pressure outlet
<i>Ground surface</i>			
Type	Wall	Wall	Wall
k _s	Varies	Varies	0.0326 m
C _s	Varies	Varies	9
Solver			
<i>Numerical approximations</i>			
Momentum	2 nd order upwind	2 nd order upwind	2 nd order upwind
k, ε	2 nd order upwind	2 nd order upwind	2 nd order upwind
Energy	2 nd order upwind	2 nd order upwind	2 nd order upwind
P1	2 nd order upwind	2 nd order upwind	2 nd order upwind
<i>Interpolation scheme</i>			
Pressure	Body force weighted	Body force weighted	Body force weighted
Pressure-Velocity Coupling	SIMPLEC	SIMPLEC	SIMPLEC

* density varies with inlet temperature

5. CFD simulations: validation study

The topic of this chapter is the validation study. Two validation studies have been performed. In the first validation study, the average surface temperature of the city centre is compared to values described in an article by Klok et al. (2012). In the second validation study, measurement data of the weather station in the city centre is used for validation of the air temperature. For this validation study, model 1 is used.

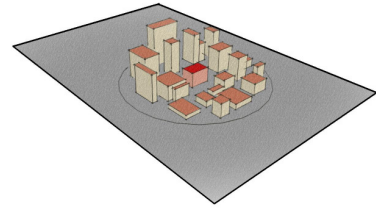


Figure 5.1: model 1 is used for the validation study

5.1 Validation of surface temperatures

5.1.1 Description of validation data

In the study of Klok et al. (2012), as also described in chapter 3, thermal remote sensing data of satellites was used for the quantification of the surface heat island intensity of Rotterdam. These satellites conduct measurements in the thermal infrared spectrum from which surface temperatures can be derived (Klok et al., 2012). One part of the article is about the diurnal variation in average surface temperature of the different districts for the heat wave of 2006, making use of NOAA-AVHRR satellite images. This satellite data was chosen for monitoring the diurnal patterns in the surface temperatures because of its high temporal resolution. However, the spatial resolution of these images is quite low: 1 x 1 km pixels.

The 2nd heat wave of 2006 (15 - 30 July) was chosen for the evaluation of the diurnal pattern in surface temperatures. Because the sky was entirely cloud free for the period of 15 - 19 July 2006, this period was chosen for analysis. 42 images at different times during this period were used. The average surface temperature of each district is calculated based on the average surface temperature of the pixels that are located in the district concerned. For the city centre, the average surface temperature is based on the temperatures of seven pixels. The resulting average surface temperatures for some of the districts in Rotterdam are given in Figure 5.2. The average surface temperatures for district City centre (Stadscentrum) are also given in this graph.

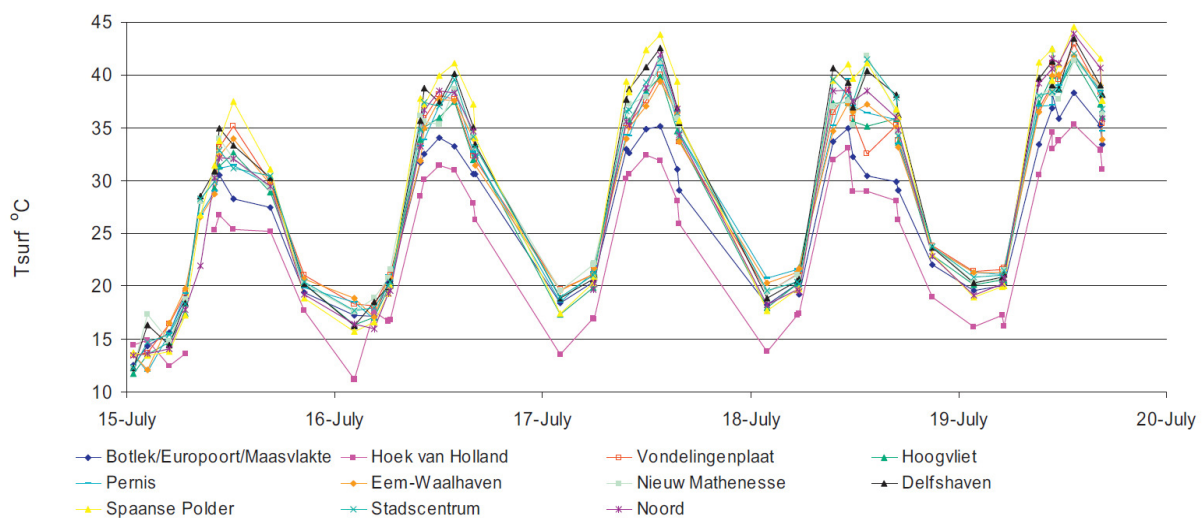


Figure 5.2: The diurnal variation in average surface temperature (T_{surf}) of some of the districts in Rotterdam during the 2nd heat wave of 2006 retrieved from NOAA-AVHRR images as reported in Klok et al. (2012)

5.1.2. Methodology

Because the validation study is about outdoor surface temperatures, the CFD model of Rotterdam without the indoor environment of the care center is used. This is the model containing 29 million cells. The used settings and parameters are already described in the previous chapter.

Because the satellite images are taken from above, the surface temperatures of building walls are not taken into account for determining average surface temperatures of each district. Therefore, by determining the average surface temperature for the city centre as calculated by the CFD model, building wall surfaces will not be included. Subdomains 2 - 8 are located in the city centre, while the largest part of subdomain 1 is located in district North (Figure 5.3). Therefore, subdomain 1 is not taken into account for the determination of the average surface temperature of the CFD model. The average surface temperature of the city centre is being calculated by taking the area-weighted average of the surface temperatures of the ground surfaces (water, grass and stone) and roof surfaces of subdomain 2 - 8. This value is then compared with T_{surf} for the city centre as given by Klok et al. (2012) for the corresponding date and time.

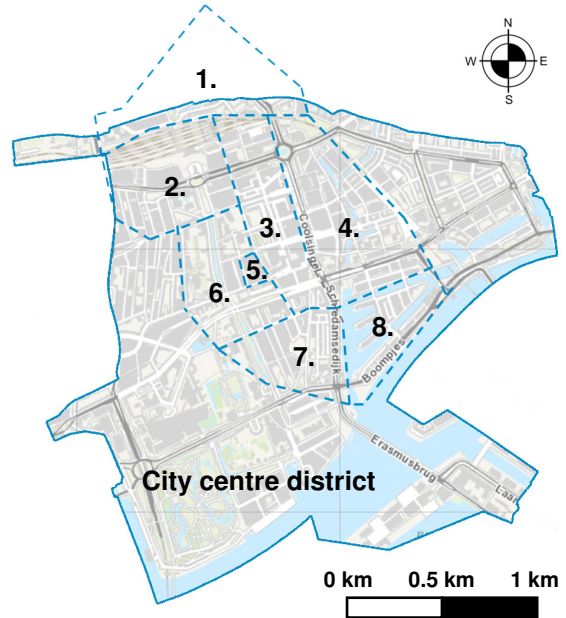


Figure 5.3: Overlap of sub domains with the city centre district

The average surface temperature is being compared for three different moments of the day, (1) the beginning of the day, (2) around noon and (3) at the end of the afternoon. The used moments had to correspond with the acquisition days and times of the NOAA-AVHRR images. Furthermore, at that moment the wind direction should be east because this is the evaluated wind direction for the final case. The chosen dates and times are given in Table 5.1. At the 16th of July, wind direction was east between 11:00 am – 19:00 pm. At the 17th of July, there was easterly wind between 6:00 am – 14:00 pm. From this data, it can be concluded that the wind direction had a constant behavior at the chosen moments during this time slot.

Hourly weather data of the KNMI weather station outside the city near Rotterdam airport is used as input for the simulations. For the first case, the measured air temperatures of 11:00 am and 12:00 am are linearly interpolated to get the inlet temperature at 11:44 am. For the other cases, the hourly values are used. KNMI provides average global radiation values which can be split up in a direct and diffuse part. The diffuse solar radiation as computed by the solar calculator is used. The direct solar radiation is calculated by subtracting the diffuse horizontal solar radiation of the solar calculator from the global radiation as given by KNMI. Besides air temperatures and radiation data, the measured wind speed at 10 m height is used for determining the inlet profile. An overview of the climatic data for the different cases is presented in Table 5.1. The average surface temperatures for the city centre according to Klok et al. (2012) are given as well.

Table 5.1: Climatic conditions for the different cases (KNMI) and the corresponding average surface temperature for the city centre (Klok et al., 2012)

Case	Date and time	Air temperature T_{air} [°C] ^[1]	Global radiation G [W/m ²] ^[1]	U_{ref} at 10m [m/s] ^[1]	Wind direction θ [°] ^[1]	Surface temperature $T_{surf, city centre}$ [°C] ^[2]
1	17-07-2006, 11:44	28.8	811	3.0	90 (east)	40
2	17-07-2006, 7:59	24.0	477	2.0	90 (east)	31
3	16-07-2006, 17:59	28.3	272	4.0	90 (east)	33

[1] KNMI [2] Klok et al., 2012

As a first step, a simulation was performed for case 1 (17th of July at 11:44 am). For this moment, the effect of different parameters such as emissivity and absorptivity values on the average surface temperature is being investigated. Subsequently, the average surface temperatures for case 2 and 3 were being calculated.

5.1.3. Results and comparison

Velocity profile

Before the average surface temperatures were being evaluated, the velocity profile had to be observed. The flow should be completely developed and at the inlet region the flow should be homogeneous. Figure 5.4 shows the velocity magnitude at pedestrian height and 10 m height over the inlet region for $U_{ref} = 3$ m/s. Although there is a slight increase in velocity magnitude at 10 m height and a slight decrease in velocity rate at 1.75 m height, the velocity profile is quite constant over the inlet region. In Figure 5.5, the velocity profile at a point in the inlet region is being compared with the velocity profile applied to the velocity inlet. The velocity profile at the inlet region shows good correspondence with the inlet profile. The vertical cross section in Figure 5.6 shows the flow is also fully developed. In conclusion, no irregularities were found for the velocity profile.

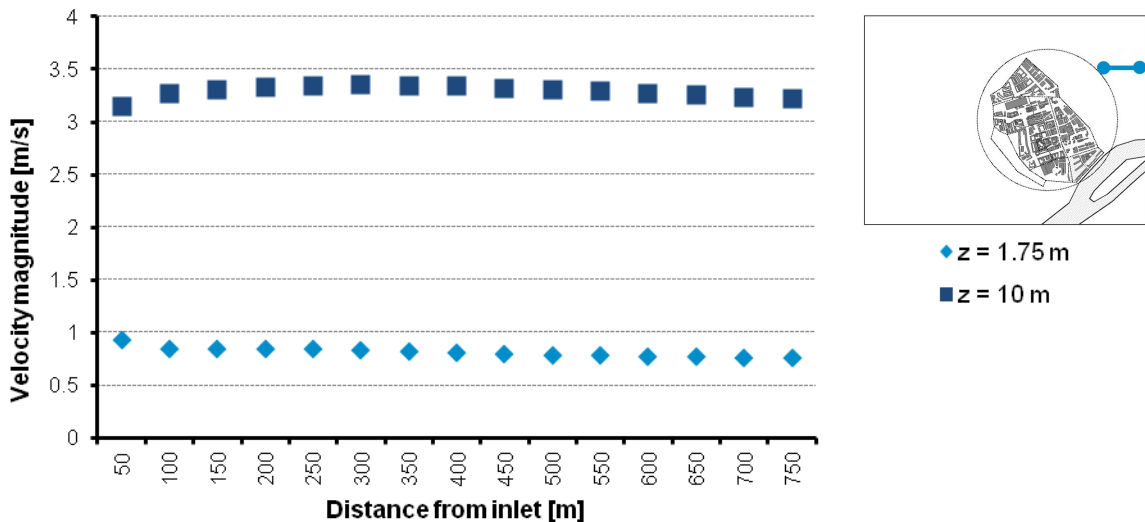


Figure 5.4: Velocity magnitude at inlet region at $z = 1.75$ m and $z = 10$ m. $U_{ref} = 3$ m/s at 10 m height

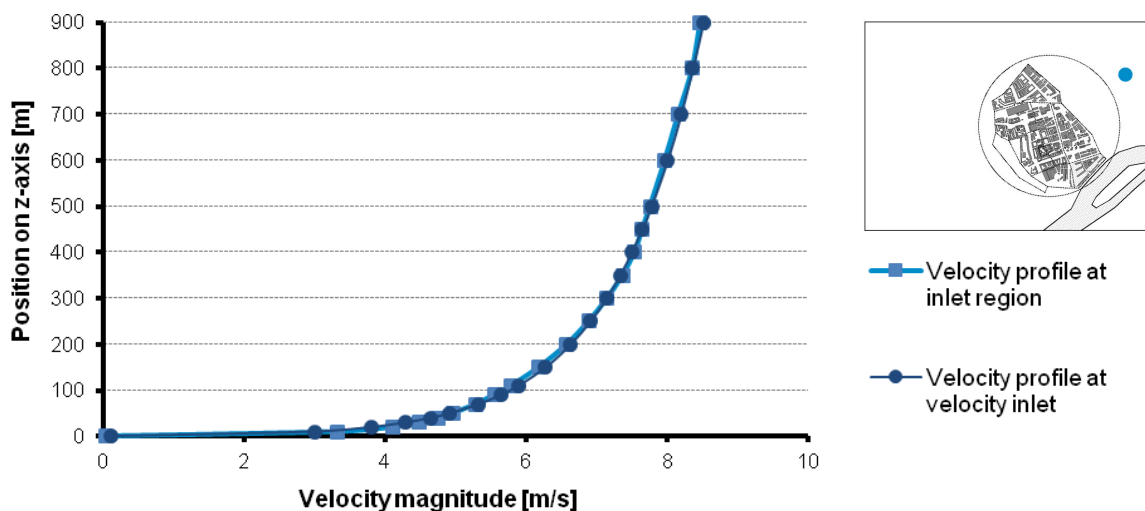


Figure 5.5: Velocity profile at inlet region compared with velocity profile at the velocity inlet. $U_{ref} = 3$ m/s at 10 m height

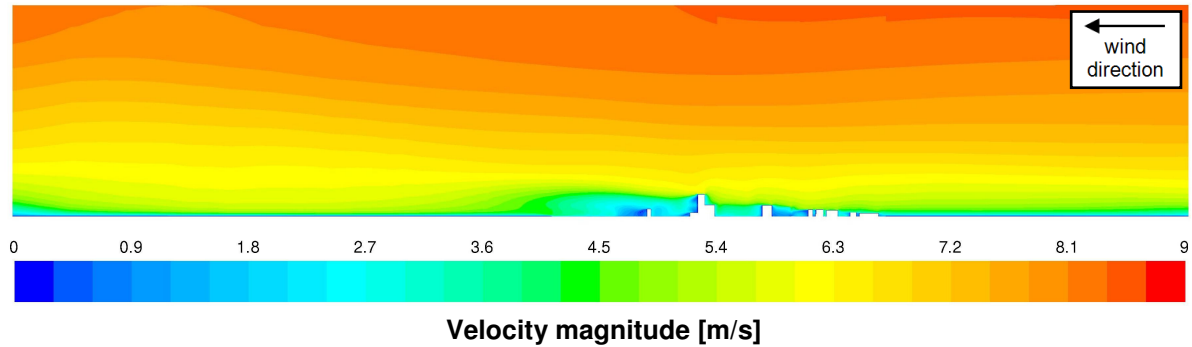


Figure 5.6: Vertical cross section over the domain for the velocity magnitude [m/s]. $U_{ref} = 3$ m/s at 10 m height

Parameter study

The calculated surface temperatures are highly dependent on the climatic conditions, but also on other input parameters such as thermal and radiation properties. Adjustments were made to some parameters to see their effect on the calculated surface temperatures. The adjusted parameters and their values for the different simulations are provided in Table 5.2. The corresponding results are given in Table 5.3.

Table 5.2: Changed parameters for the different simulations

Parameter		Variant 1	Variant 2	Variant 3	Variant 4
Absorptivity values	grass	0.78	0.60	0.60	0.60
	stone	0.55	0.50	0.50	0.50
	surroundings	0.55	0.50	0.50	0.50
	walls	0.65	0.60	0.60	0.60
Emissivity values	stone	0.45	0.45	0.90	0.90
	walls	0.45	0.45	0.85	0.85
	roofs	0.24	0.24	0.90	0.90
Shell conduction		off	on	off	off
Latent heat loss	grass	0 W/m ²	0 W/m ²	0 W/m ²	-8.3 W/m ²
Water		Solid	Solid	Solid	Fluid

Table 5.3: Horizontal surface temperature results for the different variants in °C

		Variant 1	Variant 2	Variant 3	Variant 4
Minimum surface temperature [°C]	CFD	33	34	29	18
Maximum surface temperature [°C]	CFD	102	96	75	75
Average surface temperature [°C]	CFD	62	65	57	56
	Klok et al. (2012)	40	40	40	40
	Difference	22	25	17	16

For variant 1, absorptivity values were applied comparable to the ones used in the UHI study of Toparlar (2012), except for the grass surfaces (grass surfaces were not modeled in the study of Toparlar (2012)). The emissivity of building brick was applied to both walls and stone ground surfaces (van Hove et al., 2011b). For the first case, it was assumed that there is no conduction in the ground shell between shaded surfaces and surfaces in the sun. At first, the effect of evaporative cooling of the grass surfaces was not taken into account. Finally, the water was modeled as a solid surface with thermal and radiation properties of water. This combination of parameters resulted in very high surface temperatures varying from 33 up to 102°C with an average of 62°C. The surface temperatures were highly overestimated.

It was found that the absorptivity value applied to the grass surfaces was too high: the effect of shading was not taken into account. Therefore this value was reduced from 0.78 to 0.60 for variant 2. Also the absorptivity

values of the stone ground surfaces, surroundings and walls were slightly lowered. Furthermore, shell conduction was turned on for this variant. This resulted in a lower temperature range, but an even higher average surface temperature.

For this reason, shell conduction was turned off again in the next simulation (variant 3). After some research, it was found that the emissivity value of aluminum roofing was used instead of the average emissivity of different kinds of roofing types. Therefore this value was changed. Also the emissivity values that were used for the stone ground surfaces and building walls were not realistic. The roads and pavements are not made of building bricks, but asphalt and concrete tiles instead. Hence the average emissivity of asphalt and concrete surfaces is used in variant 3. For the building walls, the emissivity of masonry of building envelopes in particular was used (ASHRAE fundamentals handbook, 2005) instead of the emissivity of common building bricks in general.

The adjustments made in variant 3, lead to a decrease of the average surface temperature of 12°C compared to the previous version. Also the temperature range looks more realistic: surface temperatures varied between 29 - 75°C. However, there was still a temperature difference in average surface temperature of 17°C between the CFD simulation and the results of Klok et al. (2012) for the same date and time.

As a final step, it was decided to apply a fixed heat transfer rate to the grass surfaces, to account for the effect of evaporative cooling. In the previous simulations, the water surfaces were modeled as walls with a fixed temperature of 18°C. However, because the simulations were steady-state, the water surface reached a temperature comparable to the applied inlet temperature. Therefore, it was decided to model the water more realistically by creating fluids of 5 m deep and applying thermal and radiation properties of water to it. It was also given a fixed temperature of 18°C.

In contrast to the other variants, a cooling effect of the water on the air above the water surface was now visible as can be seen in Figure 5.7.

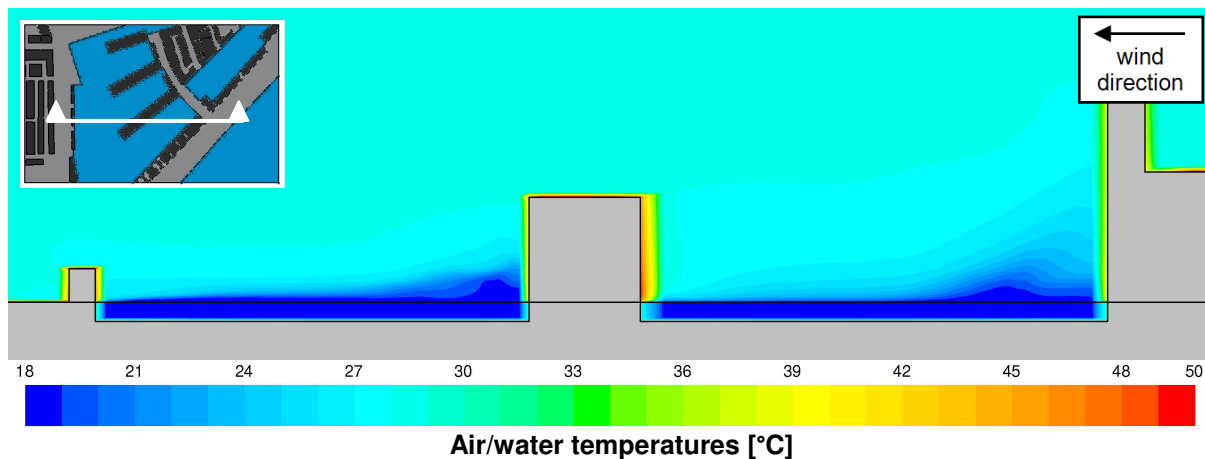


Figure 5.7: Cross section over the water area. It can be seen that the air above the water surface is cooled down by the lower temperature of the water.

Even though the average surface temperature in variant 4 is more comparable to the value found in the research of Klok et al. (2012), there is still a temperature difference of 16°C. This could be explained by the low resolution of the NOAA-AVHRR satellite images. Klok et al. (2012) used these images because of their high temporal resolution. However, their spatial resolution is quite low: 1 x 1 km pixels. Because of this low resolution, water surfaces could not be excluded from the calculation of the average surface temperature. In the CFD simulations, the water surface area was 5% while the water area in the city centre is 22% according to Klok et al. (2012). When assuming 22% of water instead of 5%, the average surface temperature is 49

instead of 56°C. Furthermore, it was found that NOAA-AVHRR satellite images have an error ranging from 0.5 - 1.4°C depending on the satellite viewing angle (Ocean Biogeochemistry Lab). Hence there might be a small error in the value found by Klok et al. (2012). Finally, it should be noted that the technique of Klok et al. (2012) is a good method for deriving average surface temperatures on a large scale but might be too coarse for comparison with the CFD calculation. Nevertheless, it was decided to investigate if the surface temperatures would also be overestimated for the other 2 cases. The parameters of variant 4 are used for the calculation of the surface temperatures of these cases as well.

5.1.3.3 Surface temperatures

In Figure 5.8 - 5.10, the surface temperature distribution around the care center is presented for the different cases. At 7:59 am, surface temperatures around the care center ranged from 26°C in some shaded areas to 46°C at the lower part of sunlit walls. The shaded areas are quite large because of the low sun position. It was expected that the average surface temperature would be underestimated for this moment because the simulation is a steady-state simulation. This means that it is not taken into account that the air temperature and global radiation were lower before 7:59 am. However, the calculated average surface temperature showed good correspondence with the results of Klok et al. (2012). Assuming a water surface area of 22%, the calculated average surface temperature is 30.76°C. Klok et al. (2012) found an average surface temperature of 31°C for this moment.

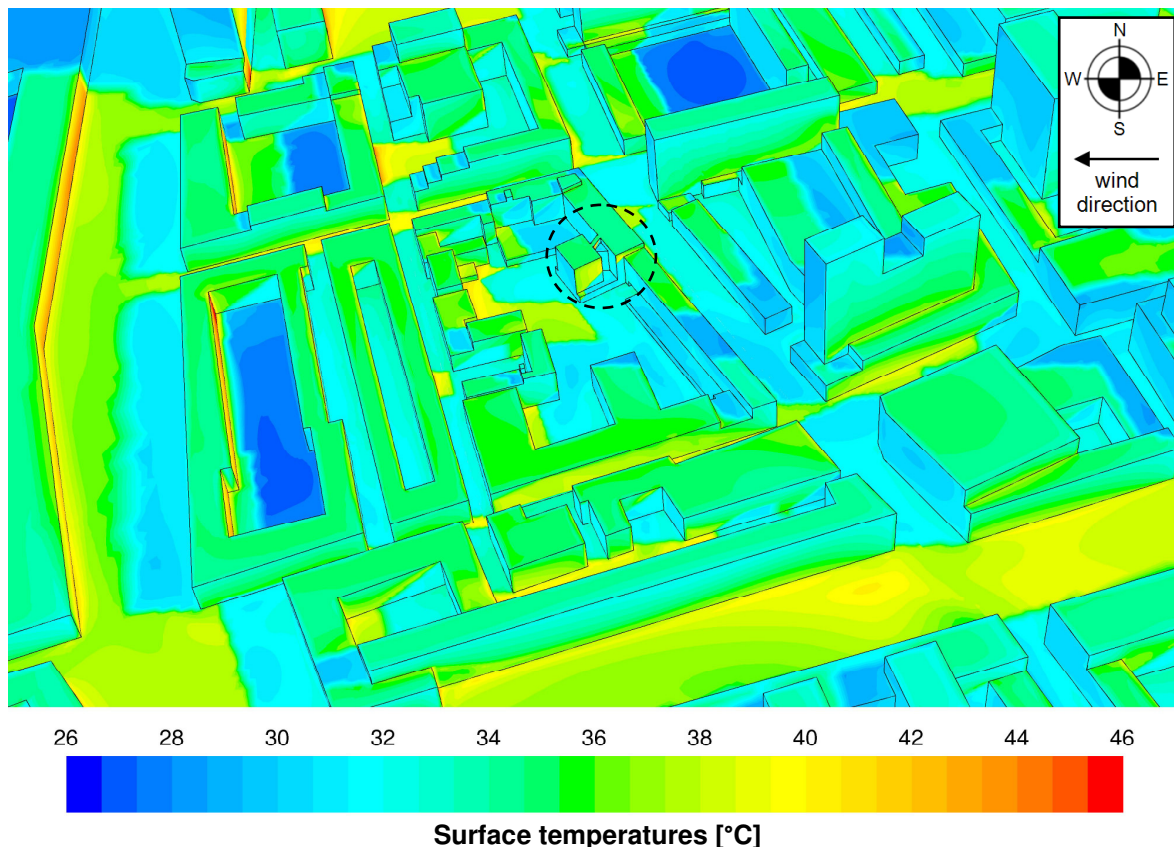


Figure 5.8: Surface temperatures [°C] around the care center at 7:59 am on 17 July 2006

In Figure 5.9, the surface temperature distribution around the care center is shown for 11:44 am. It was already mentioned that the surface temperature varied between 18°C (water surfaces) and 75°C. Around the care center temperatures varied between 35 and 75°C. Low temperatures occurred in shaded areas. The highest surface temperatures were found in sunlit corners of court yards where the velocity magnitude is low. The shadows are short because of the high position of the sun at that time.

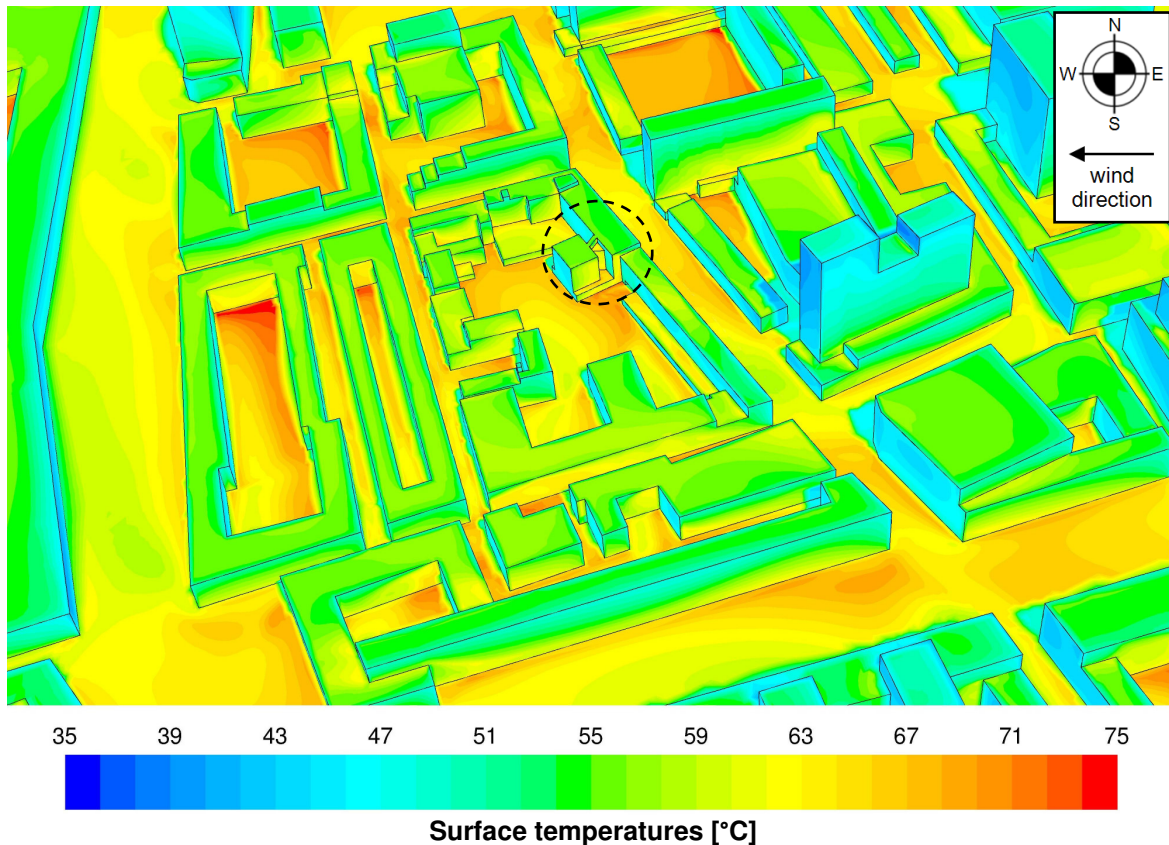


Figure 5.9: Surface temperatures [°C] around the care center at 11:44 am on 17 July 2006. High temperatures occur in court yards where wind speeds are low. Surface temperatures on the roof are lower compared to the ground surface temperatures because of higher wind speeds. Shadows are short because of the high sun position at that time.

Finally, for the case at 17:59 pm, the smallest temperature range and average surface temperature was found. The surface temperatures around the care center varied from 28°C to 38°C. Low surface temperatures occurred in the shaded areas of the court yards. Long shades are visible due to the low position of the sun at this time. Because the simulation is a steady-state simulation, it was expected that the average surface temperature would be underestimated because the air temperatures and global radiation were higher before 17:59 pm. In the steady-state simulation, heat storage is not taken into account. This expectation has been confirmed: an average surface temperature of 28.35°C was found which is 4.65 degrees Celcius lower than the average surface temperature of 33°C as presented in the article of Klok et al. (2012).

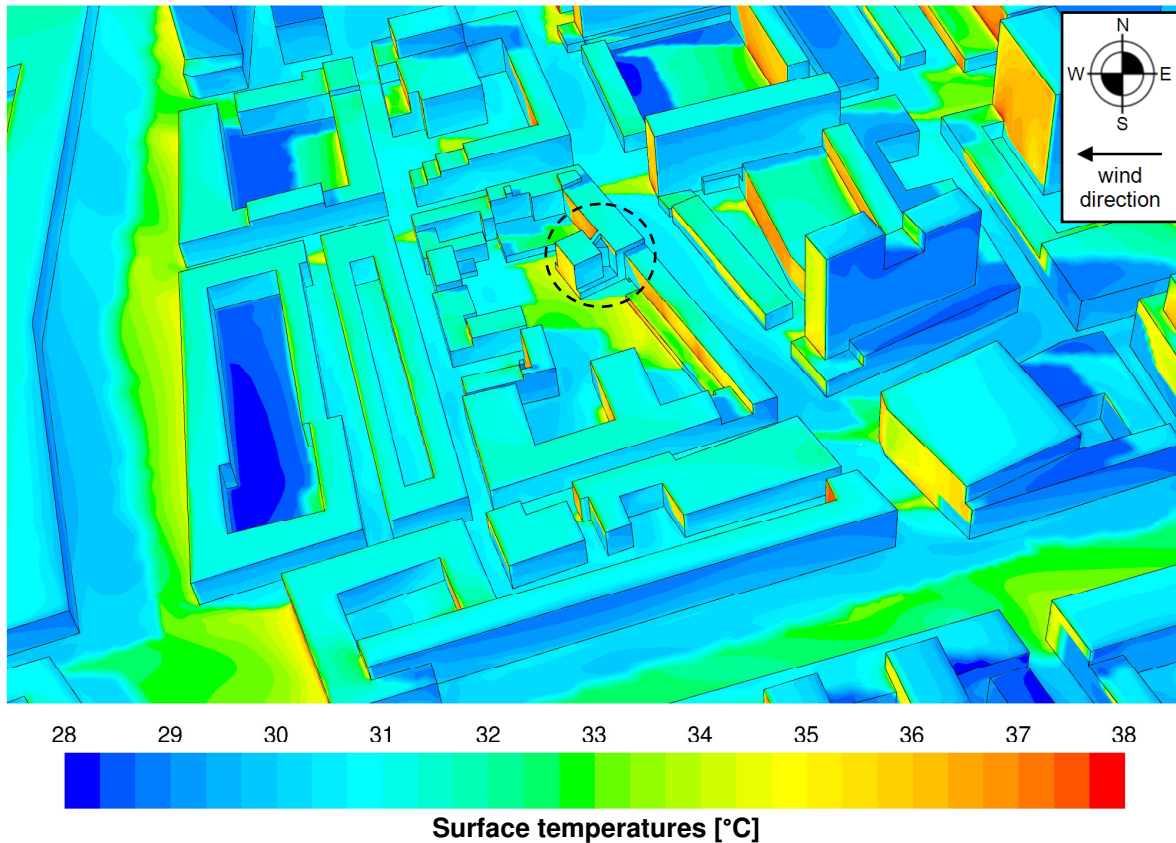


Figure 5.10: Surface temperatures [°C] around the care center at 17:59 pm on 16 July 2006. Long cool shades are visible.

An overview of minimum and maximum surface temperatures in the domain and the average surface temperatures for the different cases is presented in Table 5.4. In this table, the error of max. 1.4°C in the average surface temperature of Klok et al. (2012) caused by an inaccuracy of the satellites is included. Best results are achieved for 7:59 am. The average surface temperature at 11:44 am is overestimated, while the average surface temperature at 17:59 pm is underestimated. In the next paragraph, calculated air temperatures will be compared with measurement data of a weather station in the city centre for the heat wave of July 2013.

Table 5.4: results of the different cases

		Time		
		7:59 am	11:44 am	17:59 pm
Minimum surface temperature [°C]	CFD	18	18	18
Maximum surface temperature [°C]	CFD	48.8	75	40.1
Average surface temperature [°C]	CFD	30.76	49.00	28.35
	Klok et al. (2012)	31 ± 1.4	40 ± 1.4	33 ± 1.4
	Difference	0.24 ± 1.4	9.00 ± 1.4	4.65 ± 1.4

5.2 Validation of air temperatures

5.2.1 Description of validation data

In September 2009, Knowledge for Climate launched a measurement program in Rotterdam with the aim to advance the understanding of the urban climate. Weather stations were placed on several fixed positions in different districts of Rotterdam. One of these weather stations is located in the city centre of Rotterdam. It is placed on an overhang on the south side of the 'Groothandelsgebouw' close to the central train station of Rotterdam (Figure 5.11). The exact location is 4.47°, 51.92° (longitude, latitude) at 6 m height. The weather

station is equipped with sensors performing measurements of air temperature, wind speed, wind direction, relative humidity, precipitation and solar radiation (climateproofcities, 2009).



Figure 5.11: The weather station (blue dot) located on an overhang of the Groothandelsgebouw

Because the weather station only provides air temperatures on one fixed position, it is only possible to compare the air temperature of the CFD simulation at that particular position.

5.2.2. Methodology

Since the weather station was installed in September 2009, no air temperature data is available for the heat wave of 2006. For this reason, the simulations of the validation study of the surface temperatures could not be used for this validation study.

For this validation study, it was also decided to perform CFD simulations for (1) the beginning of the day, (2) around noon and (3) at the end of the afternoon. At the selected moments, wind direction should be east. In addition, the air temperature should be in the same range of a day during a heat wave (25 - 30°C).

The first intention was to select a summer day with easterly wind in the period of 2009 - 2011. During this period, the current train station was not yet constructed and this train station is also not included in the model. The hottest day with easterly wind was not found during summer but in autumn at 1 October 2011 with maximum temperatures at Rotterdam airport of 25.5°C. However, at that time the solar radiation was not so high because of the lower position of the sun. Furthermore, there is some doubt about the exact location of the weather station at that time because a different coordinate position was mentioned in an article of van Hove et al. (2011b) than the current coordinate position of the weather station.

Very recently, during the period of 21 July 2013 - 27 July 2013, a heat wave occurred in the Netherlands. This is the most recent heat wave. At 21st of July 2013, easterly wind was measured between 7:00 am and 18:00 pm at Rotterdam airport. Three moments during this day were chosen for the comparison of the simulated air temperature and the measured air temperature at the position of the weather station. Drawback is that the current train station is not included in the model which might affect the wind velocities and in turn the calculated air temperatures at the position of the weather station. Because the train station is located at the north-eastern side of the Groothandelsgebouw and the evaluated wind direction is east, it is expected that this influence is small.



Figure 5.12: Previous train station as included in the model (left) and the current train station (right). The weather station is positioned on the southern overhang of the Groothandelsgebouw

An overview of the climatic data for the different cases is presented in Table 5.5. The measured air temperatures are given as well.

Table 5.5: Climatic conditions for the different cases (KNMI) and the air temperature measured at the weather station in the city centre (Knowledge for Climate, Climate Proof Cities consortium)

Case	Date and time	Air temperature T_{air} [°C] ^[1]	Global radiation G [W/m ²] ^[1]	U_{ref} at 10m [m/s] ^[1]	Wind direction θ [°] ^[1]	Surface temperature $T_{surf, city centre}$ [°C] ^[2]
1	21-07-2013, 8:00	22.7	467	3.0	90 (east)	21.59
2	21-07-2013, 12:00	28.3	836	4.0	90 (east)	29.36
3	21-07-2013, 17:00	28.8	400	2.0	90 (east)	30.68

[1] KNMI [2] CPC

5.2.3. Results and comparison

In Figure 5.13 - 5.15, the air temperatures around the weather station are presented in a vertical cross section over the measurement position for the different moments. At 8:00 am, the simulated air temperature at the position of the weather station is 24.13°C. This is an overestimation of 2.54°C when comparing this value with the measured air temperature at this position.

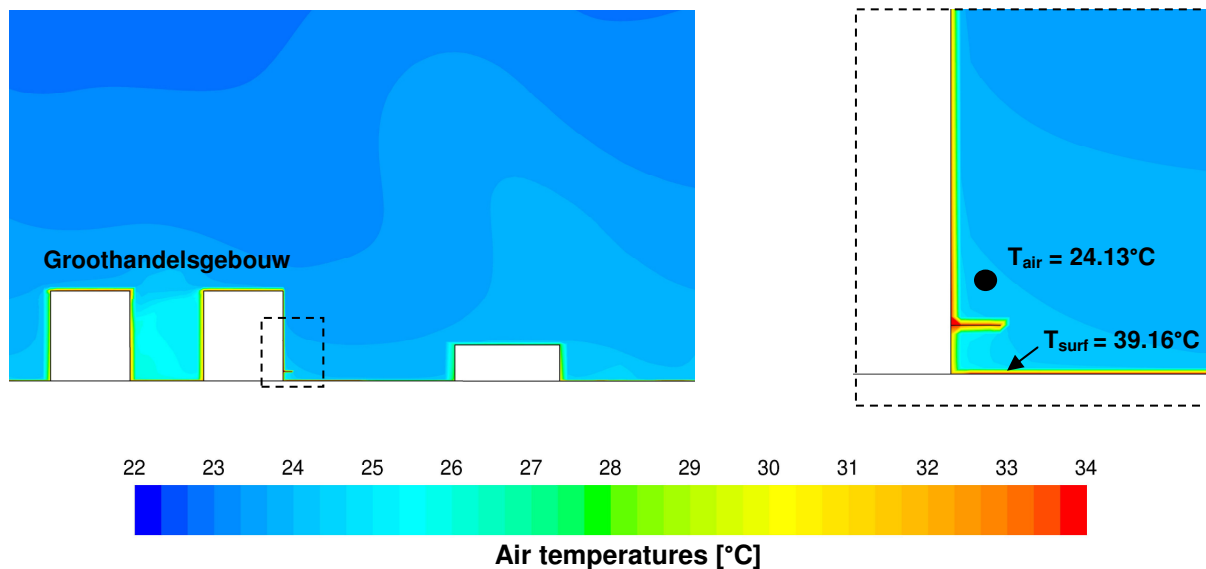


Figure 5.13: Cross section over the 'Groothandelsgebouw' and the weather station at 21 July 2013, 8:00 am. The calculated air temperature at the position of the weather station is 24.13°C.

In the cross section of Figure 5.14 smaller isotherms are visible compared to the cross section of Figure 5.13, which means that there is a higher variation in the air temperature. Air temperatures of 34°C occur in the courtyard of the Groothandelsgebouw. At the position of the weather station, the simulated air temperature is 31.53°C. This is an overestimation of 2.17°C. The overestimation is in the same range as for 8:00 am.

At 17:00 pm, the simulated air temperature is 29.70°C. For this moment, the measured air temperature is 30.68°C. The simulation slightly underestimates the air temperature.

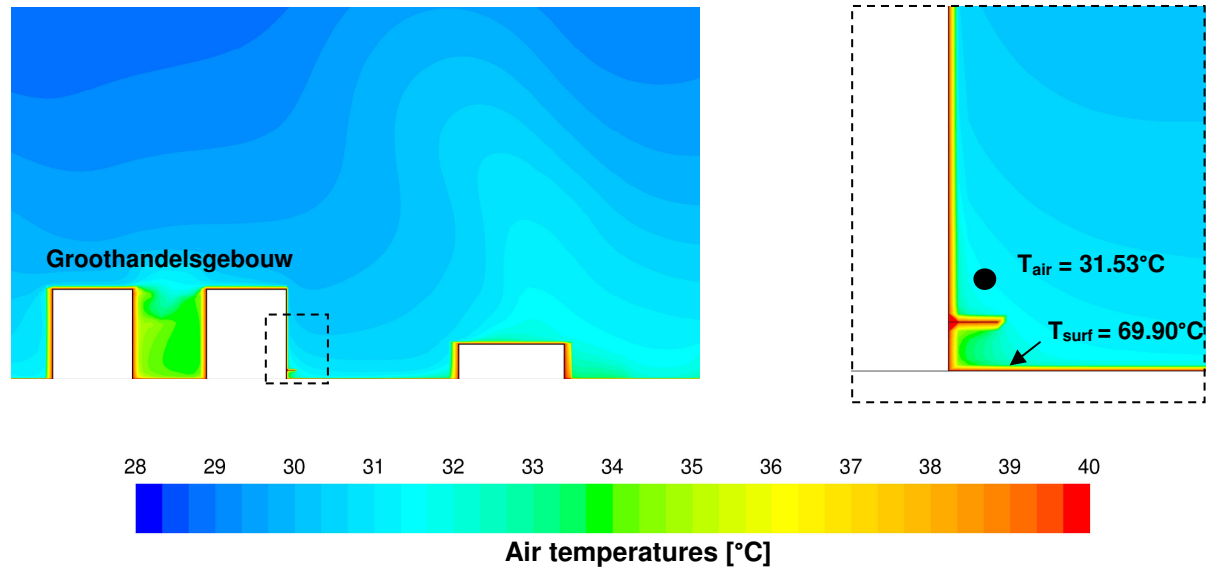


Figure 5.14: Cross section over the 'Groothandelsgebouw' and the weather station at 21 July 2013, 12:00 pm. The calculated air temperature at the position of the weather station is 31.53°C.

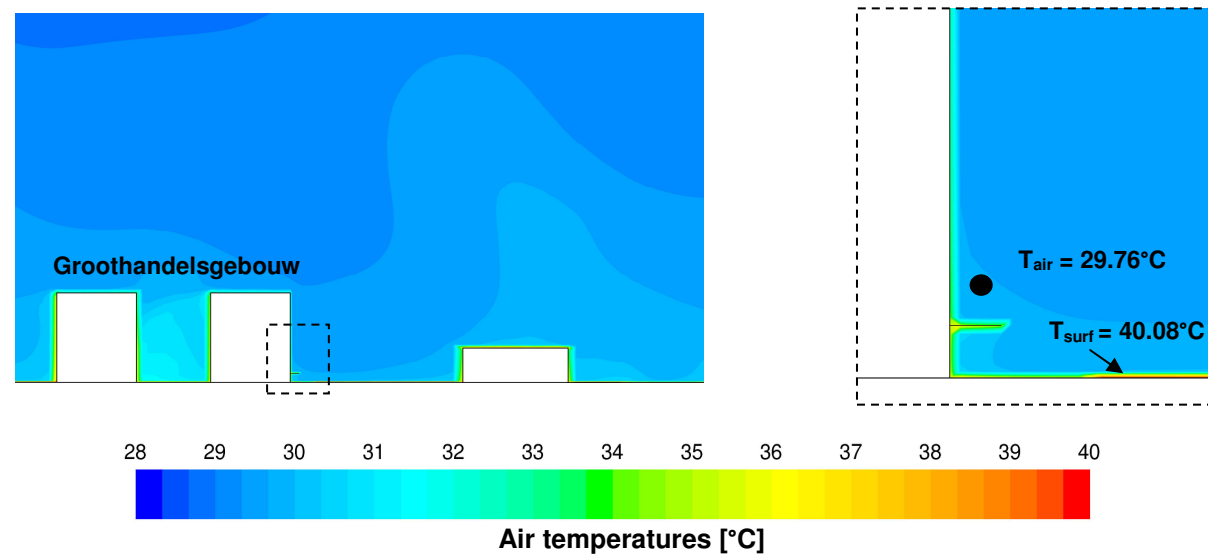


Figure 5.15: Cross section over the 'Groothandelsgebouw' and the weather station at 21 July 2013, 17:00 pm. The calculated air temperature at the position of the weather station is 29.70°C.

The air temperature at Rotterdam airport is used as inlet temperature and represents the air temperature in the rural area. By subtracting this air temperature from the air temperature at the measurement position, the UHI intensity at that particular position is achieved. This can be done for both simulated air temperatures and measured air temperatures. The results are provided in Table 5.6.

Table 5.6: Overview of the UHI intensity [°C] at the position of the weather station for both the CFD simulation and the measured temperatures

		Time		
		8:00 am	12:00 am	17:00 pm
Air temperature at measurement position [°C]	CFD simulation	24.13	31.53	29.70
	Weather station	21.59	29.36	30.68
Air temperature at Rotterdam airport [°C]		22.7	28.3	28.8
UHI intensity at measurement position [°C]	CFD simulation	+1.43	+3.23	+0.90
	Weather station	-1.11	+1.06	+1.88

The UHI-intensity is relatively low or even negative at the position of the weather station. The UHI-intensity ranges between +0.90 and +3.23°C for the simulation and between -1.11 and +1.88°C for the measured air temperature at the position of the weather station. This could be caused by the chosen moments of the simulations: it is found in literature that the UHI effect is most pronounced at summer nights instead of summer days (Steenefeld & van Hove, 2010; van Hove et al., 2011a). Another cause is the location of the weather station. The Groothandelsgebouw is located at a wide main street called Weena. This street is oriented in west-east direction. With easterly wind, hot air is easily being removed from the city by the wind blowing through this street. This is also depicted in Figure 5.16 and 5.17. These figures show the air temperatures and amplification factors at $z = 6$ m (height of the weather station) at 8:00 am. A relationship is found between the air temperature and the velocity magnitude: in the Weena street relatively high amplification factors occur, resulting in lower air temperatures. High temperatures occur at regions with low amplification factors. This is best visible in one of the court yards of the Groothandelsgebouw and small streets perpendicular at the wind direction.

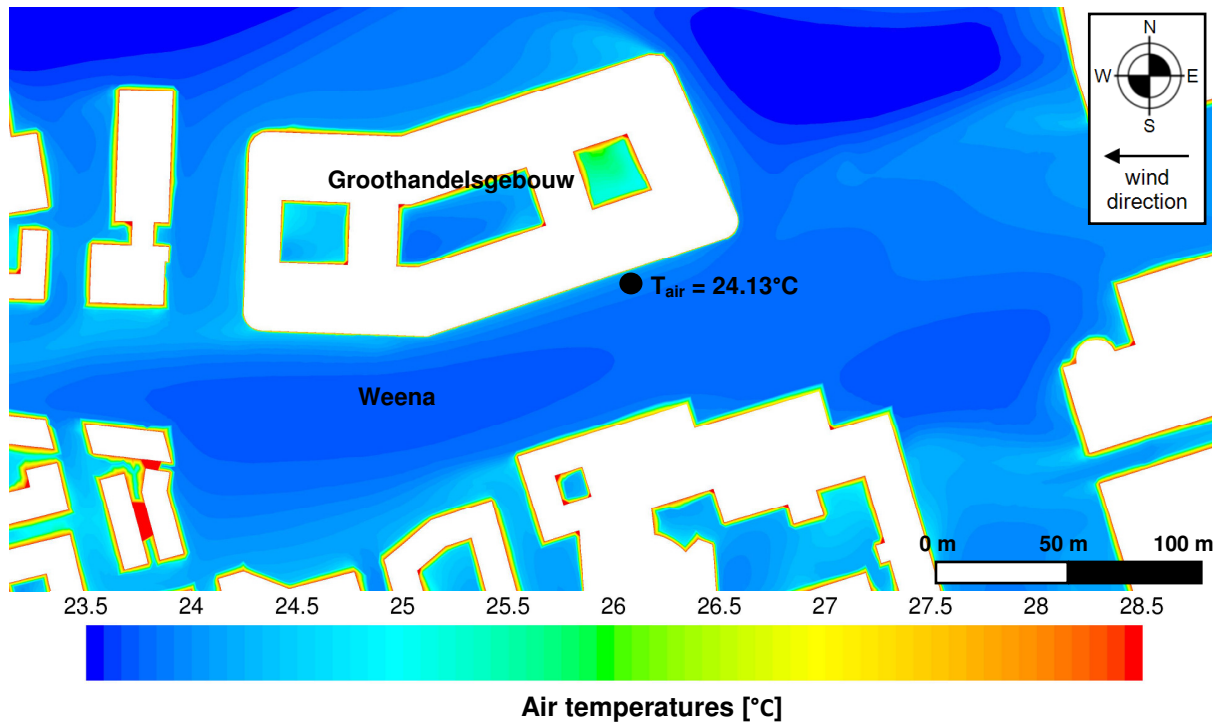


Figure 5.16: Horizontal cross section of the air temperatures [°C] at $z = 6$ m (height of weather station) at 21 July 2013, 8:00 am

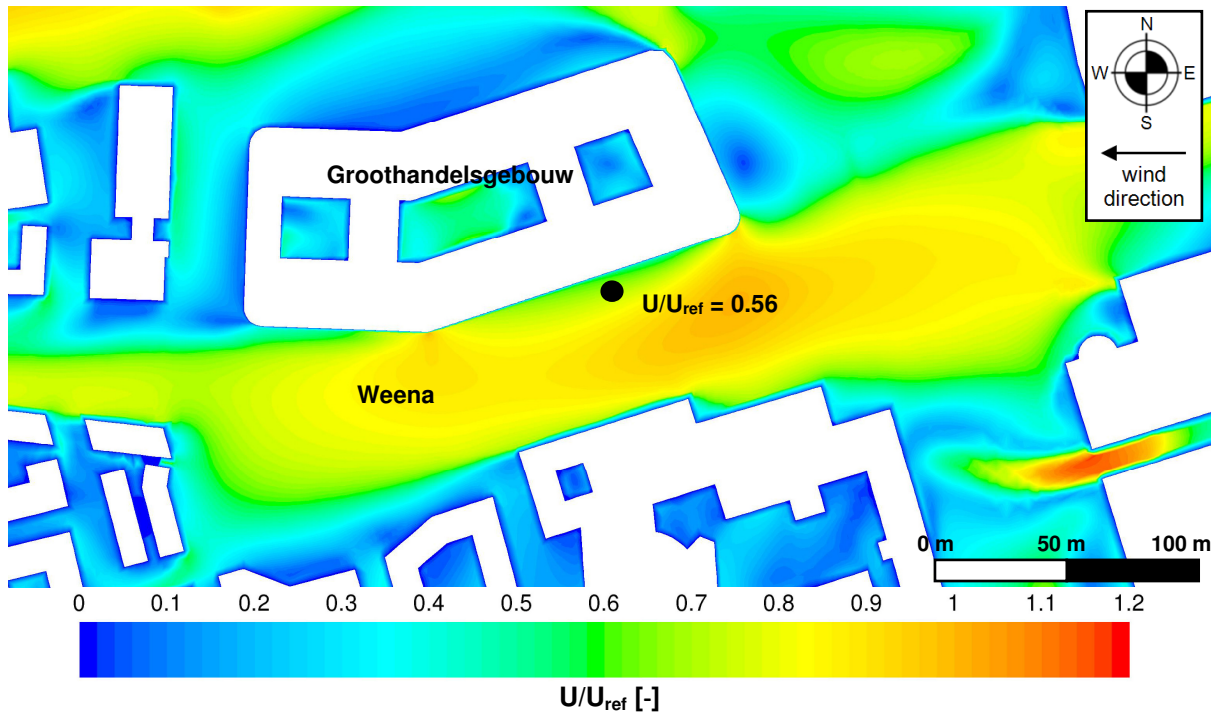


Figure 5.17: Horizontal cross section of the amplification factors [-] at $z = 6\text{ m}$ (height of weather station) at 21 July 2013, 8:00 am with $U_{ref} = 3\text{ m/s}$

A summary of the results of the validation study of the air temperatures is presented in Table 5.7. At 8:00 am and 12:00 am, the CFD simulation slightly overestimates the air temperature. The air temperature is being underestimated at 17:00 pm. It should be noted that the air temperature could only be compared at 1 position. It is possible that the air temperature on other positions in the domain is in better correspondence with reality.

In the validation study of the surface temperatures, the average surface temperature was also overestimated at noon, but in good correspondence with the validation data in the early morning. In the validation study of the surface temperatures, the average surface temperature in the late afternoon was also being underestimated. These over and underestimations should be taken into account when observing the UHI intensity in and around the care center and the effects of it on thermal comfort of the elderly.

Table 5.7: Overview of the air temperatures at the position of the weather station [$^{\circ}\text{C}$] as calculated by the CFD simulations compared with the measured air temperatures at the weather station

Average air temperature [$^{\circ}\text{C}$]	Time		
	8:00 am	12:00 am	17:00 pm
CFD simulation	24.13	31.53	29.76
Weather station	21.59	29.36	30.68
Difference	2.54	2.17	0.92

Difference with validation data [$^{\circ}\text{C}$]	Time		
	morning	noon	afternoon
Average surface temperatures	-0.24 (± 1.4)	+9 (± 1.4)	-4.65 (± 1.4)
Air temperature	+2.54	+2.17	-0.92

6. Results: outdoor environment

In this chapter, the outdoor thermal environment around the care center will be evaluated for the heat wave of 2006. Based on the results of the simulations performed for the validation study, UHI intensities and SHI intensities can be calculated. Finally, the UTCI index will be used as a performance indicator for the outdoor thermal comfort of the elderly.

6.1 UHI intensity

The UHI intensity can be calculated by subtracting the inlet temperature (which represents the rural temperature) from the air temperature at pedestrian height ($z = 1.50$ m). In Figure 6.1, the UHI intensity distribution around the care center is given for the morning case. The UHI intensity varies from approximately 0.5 to 3.5°C. The values can only be compared with UHI intensities found in literature based on local air temperature measurements. For the period of 27 June 2010 until 4 July 2010, calculated UHI intensities at 8:00 am varied between 1 - 4°C for the position of the CPC weather station (CPC, 2009).

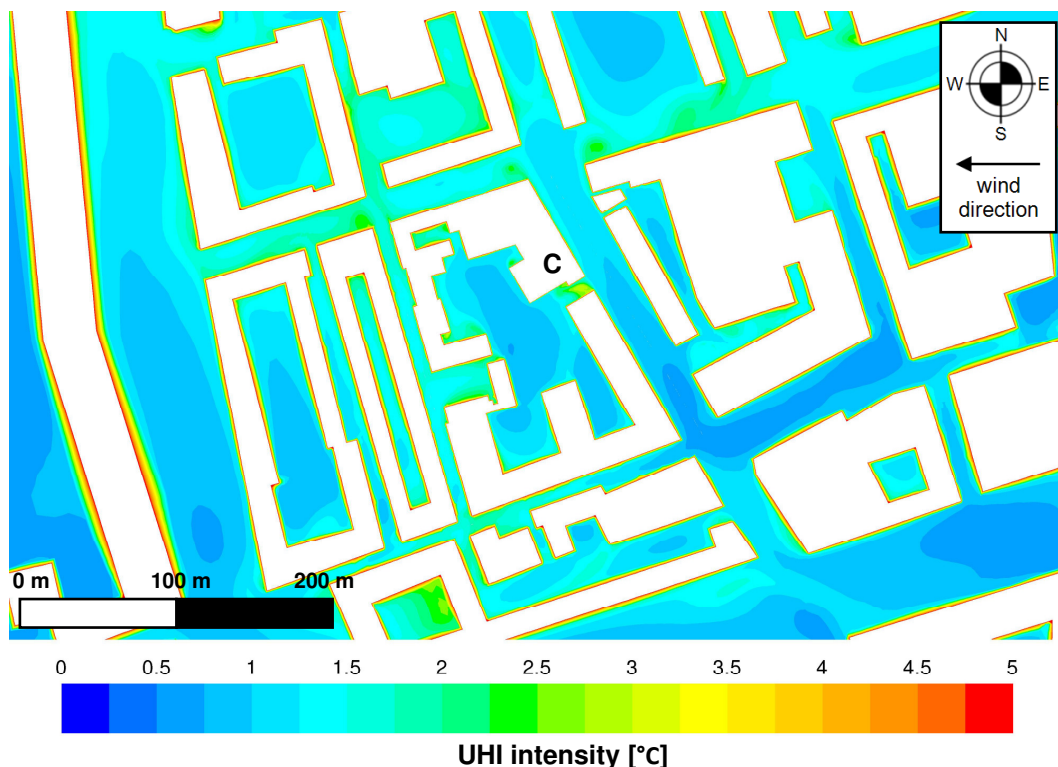


Figure 6.1: UHI intensity at pedestrian height ($z = 1.5$ m) around the care center at 17 July 2006, in the morning at 7:59 am. T_{rural} at that time is 24.0°C. The care center is indicated with a C.

The effect of building facades on the UHI intensity is clearly visible: in the middle of wide street canyons, the UHI intensity is lower compared to the regions near the facades. Close to the facades, air temperatures are higher because of lower air velocities and the effect of the facades' high surface temperatures. In smaller street canyons, higher UHI intensities occur. Because mixing of air occurs, the effect of shading is not clearly visible. From Figure 6.1 and 6.2, it can be concluded that local air temperatures are more dependent on local air velocities than whether that point is located in the shadings or in the sun. The highest air

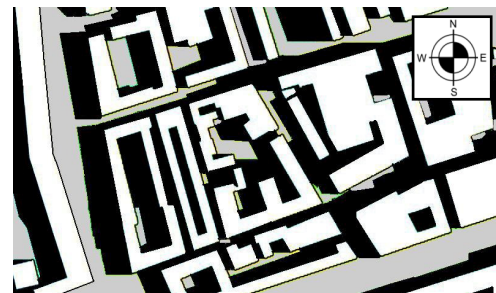


Figure 6.2: Shadings at 17 July 2006, 7:59 am

temperatures and corresponding UHI intensities are found on positions with low air velocities at the corners of some of the buildings.

In Figure 6.3, the UHI intensity distribution is given for 11:44 am at 17 July 2006. The UHI intensity is higher in most regions compared to the morning case. The range is also larger: UHI intensities vary between 1 and 6.5°C. For comparison: the UHI intensities calculated from the CPC weather station for 27 June 2010 - 4 July 2010 are in the range of 1.8 - 4°C (CPC, 2009).

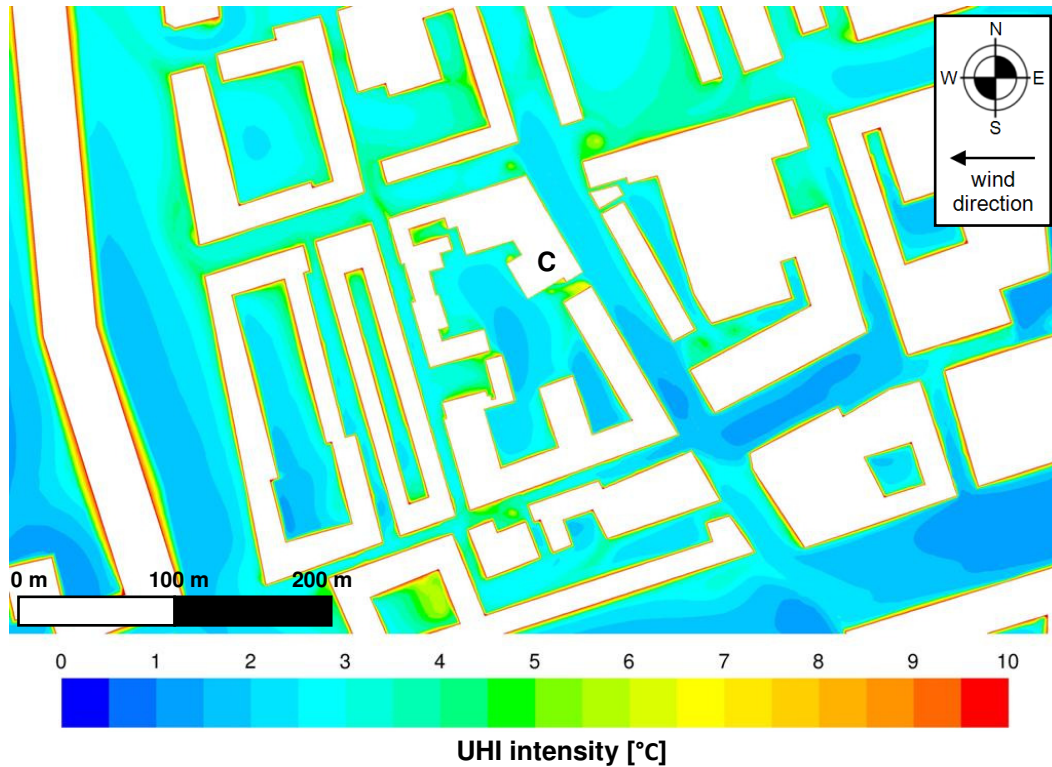


Figure 6.3: UHI intensity at pedestrian height ($z = 1.5$ m) around the care center at 17 July 2006, 11:44 am. $T_{\text{rural}} = 28.8^\circ\text{C}$. The care center is indicated with a C.

The UHI intensities close to building facades are higher, as the air temperatures approach the surface temperatures. Furthermore, highest UHI intensities are found at positions with low wind velocities. Again, the effect of direct sunlight on the air temperature is not visible (Figure 6.3 and Figure 6.4). In the middle of the wider streets and court yards, the lowest UHI intensities are found.

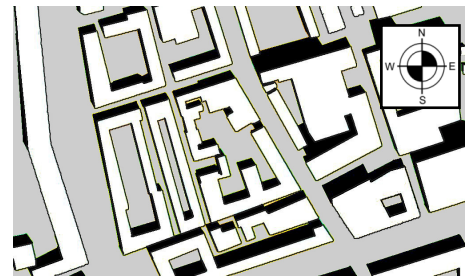


Figure 6.4: Shadings at 17 July 2006, 11:44 am

In Figure 6.6, the UHI intensity at pedestrian height is given for the late afternoon case. At this time, the UHI effect is not significant and sometimes even negative. The UHI intensity varies from -1.5 to $+0.5^\circ\text{C}$. These values are slightly lower than the UHI intensities found for 27 June 2010 - 4 July 2010 at the CPC weather station at 18:00 pm: the UHI intensity at this time varied between 1.8°C and 2.5°C . Air temperatures appear not to be lower for shaded areas compared to sunlit areas. However, close to sunlit building facades the air temperature and UHI intensity is higher.

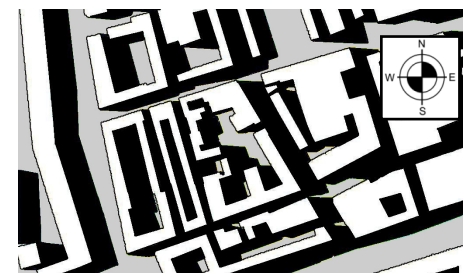


Figure 6.5: Shadings at 16 July 2006, 17:59 am

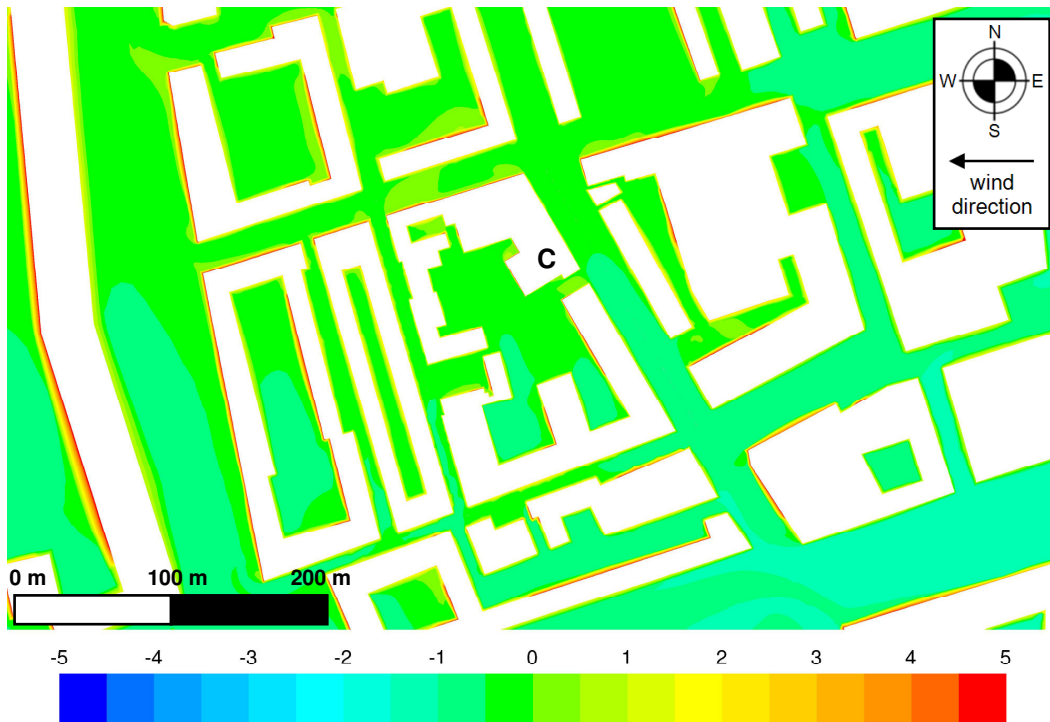


Figure 6.6: UHI intensity at pedestrian height ($z = 1.5$ m) around the care center at 16 July 2006, 17:59 pm. $T_{rural} = 28.3^{\circ}\text{C}$. The care center is indicated with a C.

Although the inlet temperature is almost equal to the case at 11:44 am (0.5°C temperature difference), global radiation values are 3 times lower (272 instead of 811 W/m^2). Therefore, UHI intensities are low at this time. Furthermore, UHI intensities are low because of the cooling effect of the water surfaces (see Figure 6.7 and 6.8). The cooling effect is more visible compared to the other 2 cases because of higher wind speeds. Because of this cooling effect, UHI intensities are negative in some regions.

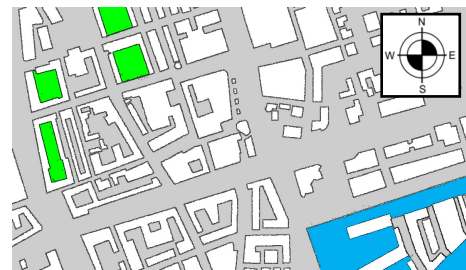


Figure 6.7: Location of nearby water surfaces

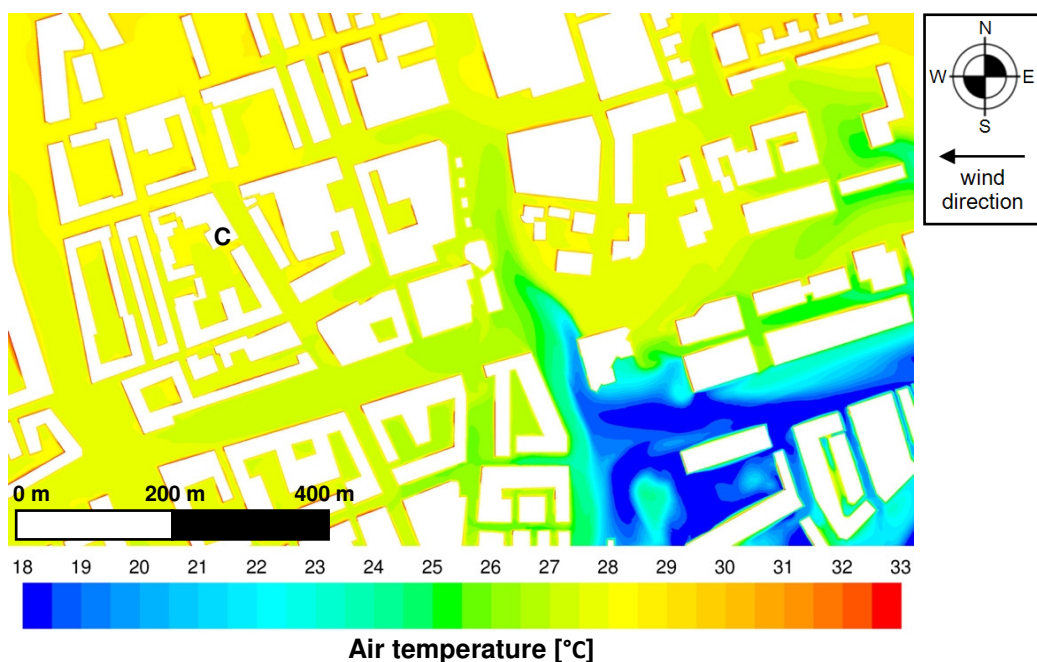


Figure 6.8: Air temperature at pedestrian height ($z = 1.5$ m) at July 2006, 17:59 pm. The care center is indicated with a C.

6.2 SHI intensity

The surface heat island intensity (SHI intensity) can be calculated by subtracting the average surface temperature of rural surroundings from the ground temperatures around the care centre. For the average surface temperature of the rural surroundings, the average surface temperature is used of district 'Industrial area Schieveen' as given in the study of Klok et al. (2012). The name of this district is misleading: the intention of the municipality of Rotterdam was to turn this area into an industrial terrain, but this idea is never implemented. Until now, this district mainly consists of grassland. It is located north-west to the airport of Rotterdam. The average surface temperature of this district for the evaluated dates and times are provided in Table 6.1 (Klok et al., 2012).



Figure 6.9: Location of district 'Industrial area Schieveen'

Table 6.1: Average surface temperatures of industrial area Schieveen for the evaluated dates and times (Klok et al., 2012)

Date	Time	$T_{surf, industrial\ area\ Schieveen}$ [°C] (Klok et al., 2012)
17-07-2006	7:59 am	26
17-07-2006	11:44 am	37
16-07-2006	17:59 pm	27

In Figure 6.11, the SHI intensity is presented for 17 July 2006, 7:59 am. The SHI intensities in shadow regions vary between 0 and 7°C. The lowest temperatures occur in the shades of courtyards with the properties of grass applied to the ground. Sharp temperature gradients are visible between shaded and unshaded ground surfaces. The SHI intensities of the grounds in sunlit areas are in the range of 10 to 15°C. Close to sunlit building walls, even higher SHI intensities occur. The effect of higher wind velocities on surface temperatures and SHI intensities is present but not as clearly visible as for the UHI intensities for this date and time.

It is difficult to compare the results with other SHI studies, because only average surface temperatures from satellite data are found in literature. No values were found in literature for the spatial distribution of the SHI intensity. For example, in the study of Klok et al. (2012), the calculated average surface temperature at 8:00 am varies between 25°C and 35°C for the heat wave of 2006. The simulated surface temperatures at 17 July 2006, 7:59 am are in the range of 26°C and 41°C. The calculated SHI intensities seem to be realistic.

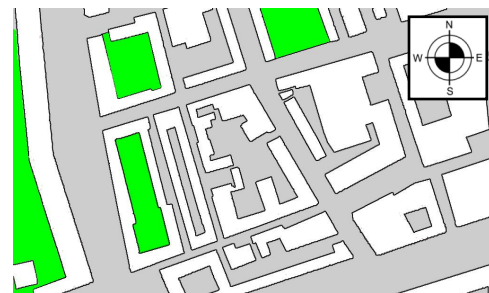


Figure 6.10: The properties of grass are applied to the green colored areas

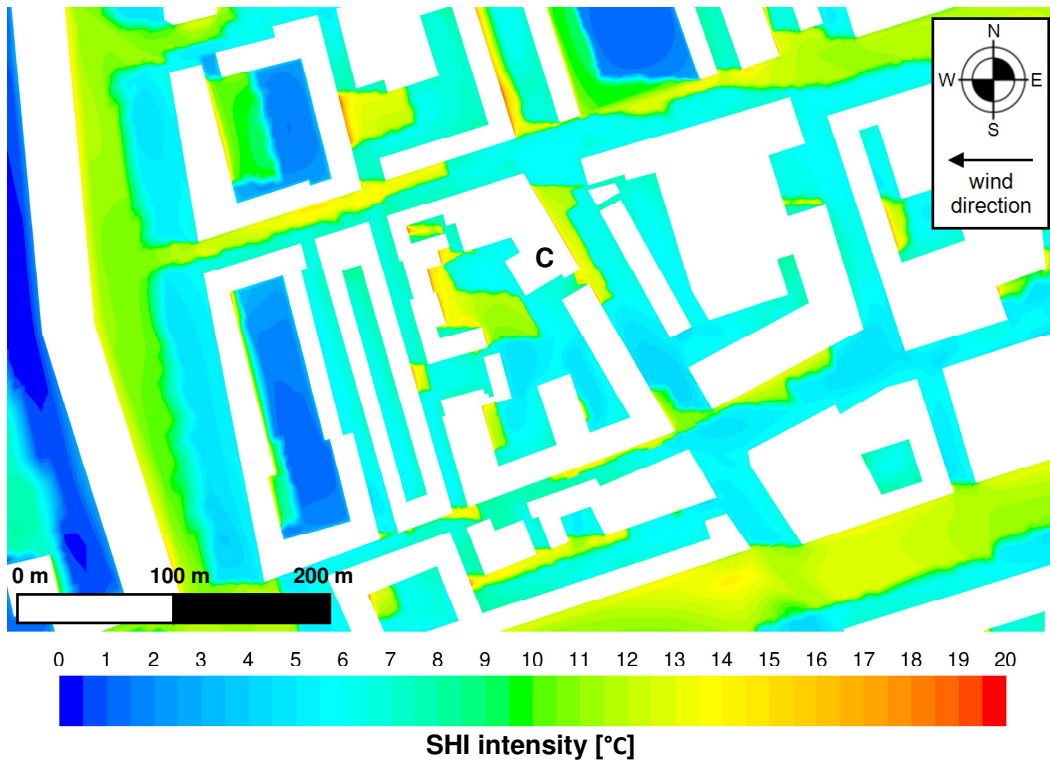


Figure 6.11: SHI intensity at ground level around the care center at 17 July 2006, 7:59 am. $T_{surf,rural} = 26^{\circ}\text{C}$.

Figure 6.12 shows the SHI intensity distribution around the care center at 17 July at 11:44 am. First of all, it should be noted, that according to the validation study, surface temperatures are overestimated for this moment. In reality, the surface temperatures might be lower.

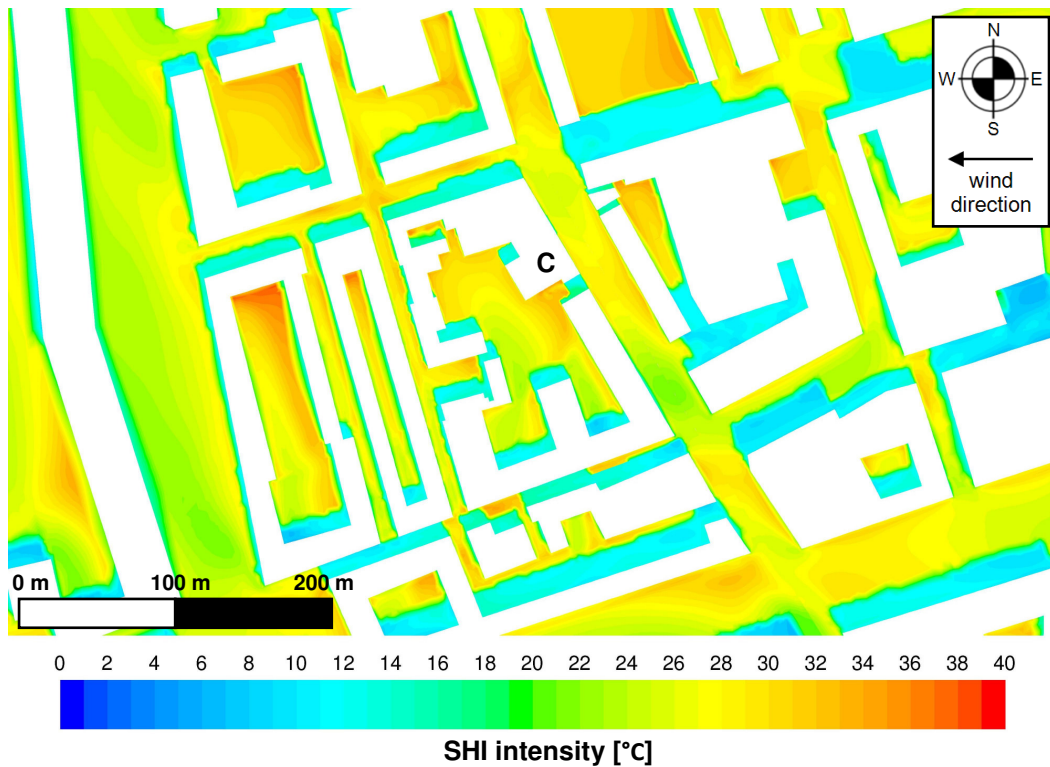


Figure 6.12: SHI intensity at ground level around the care center at 17 July 2006, 11:44 am. $T_{surf,rural} = 37^{\circ}\text{C}$.

Because of the large global radiation for this moment, the cooling effect of the grass surfaces is negligible and therefore not visible in the graph. Large surface temperature differences are found for this moment. The

SHI intensity varies between 4 and 16°C in shaded areas. In sunlit areas, the SHI intensities are high and vary between 20 and 38°C (surface temperatures between 57 and 75°C). The highest SHI intensities are present close to northern building walls and corners which are exposed to direct sunlight and where air velocities are low. When not taking the shaded areas in account, lowest surface temperatures can be found in the middle of wider street canyons.

Klok et al. (2012) found average surface temperatures for the City centre district of 32 - 42°C at 12:00 pm for the 2nd heat wave of 2006. The calculated surface temperatures at 17 July 2006, 11:44 am are higher: 41 - 75°C. However, at tropical days asphalt surfaces can reach temperatures of 65°C at noon and concrete surfaces can reach temperatures of 52°C at noon (KemTek Thermal Solutions, 2013). The simulated surface temperatures and corresponding SHI intensities seem to be slightly overestimated as also concluded from the validation study.

Finally, in Figure 6.13, the SHI intensity distribution of the ground surface around the care center is given for 17:59 pm at 16 July 2006. Similar to the morning case, lowest surface temperatures and corresponding SHI intensities appear in the shaded areas of courtyards with grass properties applied to the ground surface. The range in SHI intensity is smaller compared to the other 2 cases because of the lower global radiation for that time. SHI intensities in the shaded areas are in the range of 1 - 4°C. In most shaded areas, the SHI intensity is approximately 3.5°C. In the sun SHI intensities vary between 5 - 8.5°C. Differences in surface temperatures in the sunlit areas are more clearly visible. These differences are caused by differences in local wind velocities.

Klok et al. (2012) found average surface temperatures in the range of 27 - 33°C for 18.00 pm during the 2nd heat wave of July 2006. The surface temperatures around the care center as calculated by the CFD simulation for 16 July 2006, 17:59 pm are in the range of 28 - 34.5°C and are therefore assumed to be reliable.

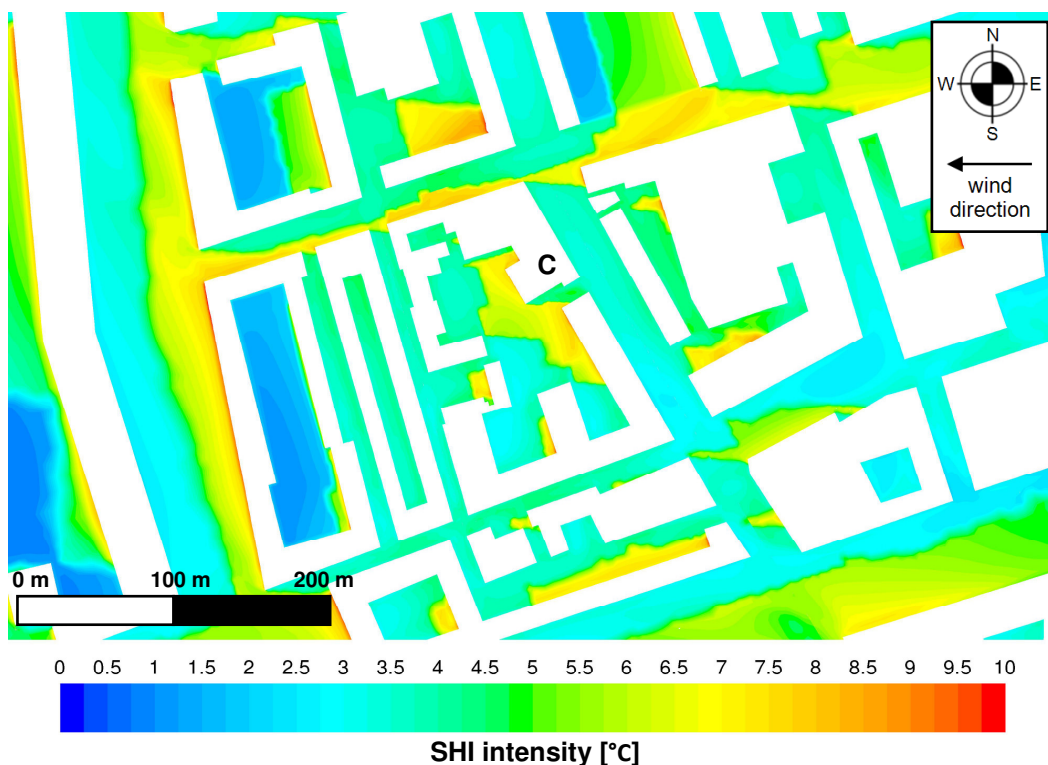


Figure 6.13: SHI intensity at ground level around the care center at 16 July 2006, 17:59 pm. $T_{surf,rural} = 27^{\circ}\text{C}$.

6.3 Outdoor thermal comfort

For the thermal comfort assessment of the outdoor environment around the care center, the Universal Thermal Climate Index is used. This index is expressed as an equivalent air temperature of a reference environment that produces the same strain index of a reference person as the actual environment (Blazejczyk et al., 2011). As mentioned in the literature study, the characteristics of the reference person correspond with the characteristics of Dutch elderly > 65 years old (DINED anthropometric database). The calculation of the UTCI equivalent temperature is based on the thermophysiological model of Fiala and an adaptive clothing model.

The use of simulation software implementing the coupled UTCI-Fiala and clothing models is quite complex. Furthermore, the processing time of these software types is quite high because of the complex calculations behind the model. Because of this reason, simplified procedures have been developed for a faster computation of the UTCI equivalent temperature (Bröde et al., 2011a). On the UTCI website (<http://www.utci.org>) a UTCI calculator is available which calculates UTCI values in less than 4 seconds. The UTCI calculator is based on a grid dataset (created with complex UTCI simulation software) of UTCI for different meteorological conditions (Bröde et al., 2011a). The required input parameters and their range of validity are given in Table 6.2. Within the validity range, the root mean squared error of the UTCI calculator is 1.1°C (Bröde et al., 2011a). Out of the validity range, calculated UTCI values are less reliable.

Table 6.2: Input parameters for the UTCI-calculator and validity ranges (UTCI)

Inputparameter	Range of validity
1. Wind speed u_{10} at 10m height	0.5 to 17 m/s (\approx 0.3 to 11.6 m/s at 1.1 m height)
2. Relative Humidity RH or water vapor pressure p_a	< 100% or < 50 hPa
3. Air temperature T_{air}	-50 to +50°C
4. Difference in mean radiant temperature T_{mrt} and air temperature T_{air} ($\Delta T_{mrt} = T_{mrt} - T_{air}$)	30 below to 70°C above T_{air}

Not the wind speed at 10 m height, but local air velocities around the body are important for the prediction of the thermoregulatory reactions of the human body. However, these local air velocities are not always known. For this reason, the wind speed at 10 m height is used in the complex UTCI simulation software and online UTCI calculator. This data can easily be extracted from weather data. Based on this wind speed, the Fiala model calculates the local air velocity u_a according to the following formula of Oke (1987):

$$u_a = u_{ref} \frac{\log(z / z_0)}{\log(z_{ref} / z_0)} \quad (6.1)$$

With local air velocity u_a [m/s], meteorological wind speed at 10 m height above the ground u_{ref} [m/s], the height of the body centre above the ground z [m], reference height of the meteorological measurement z_{ref} [m] and roughness length z_0 [m]. For UTCI purposes, the roughness length is assumed to be 0.01 m (Fiala et al., 2011). The average height of the body centre is 1.1 m.

Because the CFD simulation already provides the air velocities at 1.1 m height, it would be more accurate to use these values instead of the wind speed at 10 m height from the weather station at Rotterdam airport. Because the UTCI-calculator needs u_{10} as input, formula 6.1 is rewritten into formula 6.2:

$$u_a = u_{10} \frac{\log(1.1 / 0.01)}{\log(10 / 0.01)} \quad \rightarrow \quad u_a = u_{10} \cdot 0.68 \quad \rightarrow \quad u_{10} = u_a \cdot 1.47 \quad (6.2)$$

For the relative humidity, the measured value at the Rotterdam airport weather station for the corresponding dates and times is used. For the air temperature, the air temperature at 1.1 m height as calculated by the CFD is used. Finally, the mean radiant temperature T_{mrt} should be implemented. This parameter sums up all the short and long wave radiation fluxes to which the human body is exposed. In an outdoor environment this includes both solar radiation, as well as radiation from surrounding surfaces. For the mean radiant temperature, the radiation temperature T_r at 1.1 m height as calculated by CFD is used, which is the sum of all radiation fluxes entering a point. It should be noted that T_r does not take into account the emissivity and absorptivity values of the human body (ANSYS FLUENT Theory guide, 2009). Therefore there might be a slight difference between T_r and T_{mrt} which will be discussed in more detail in chapter 8. However, because no T_{mrt} measurement data is available, T_r of Fluent is used.

For this research, the UTCI equivalent temperature should be calculated for the entire area surrounding the care center. It would be a very time-consuming task to calculate the UTCI equivalent temperature for this amount of positions one by one with the UTCI-calculator. For this reason, a MATLAB script is created being able to read an array of x,y,z-coordinates with corresponding values for air temperature, radiation temperature, air velocity and relative humidity. As a result, the MATLAB script writes an output file with x- and y-coordinates and corresponding UTCI equivalent temperatures. The script of the online UTCI calculator (available on the UTCI-website) was used as a basis for this MATLAB file. The original script was written in Fortran. Therefore, it first had to be adjusted to be readable by MATLAB. For this research, MATLAB version R2011a is used. The final MATLAB script can be found in appendix 3.

Based on the x,y-coordinates and their UTCI equivalent temperatures, contour plots are created in MATLAB for the morning case (17 July 2006, 7:59 am), noon case (17 July 2006, 11:44 am) and late afternoon case (16 July 2006, 17:59 am).

In Figure 6.14, the required input information from the CFD simulation is given for the morning case. According to KNMI, the relative humidity at that time was 50%. Air temperatures around the care center at 1.1 m height varied from approximately 24.5 up to 27°C. Near sunlit walls higher air temperatures occur. In the contour plot of the radiation temperature a clear difference can be seen in temperature between shaded areas and areas in the sun. It should be noted that air velocities smaller than 0.3 m/s occur, especially close to building walls and in corners. In these regions, calculated UTCI equivalent temperatures are less reliable. The calculated UTCI equivalent temperatures are given in Figure 6.15. In Figure 6.16, the UTCI stress category is calculated based on the UTCI equivalent temperature distribution.

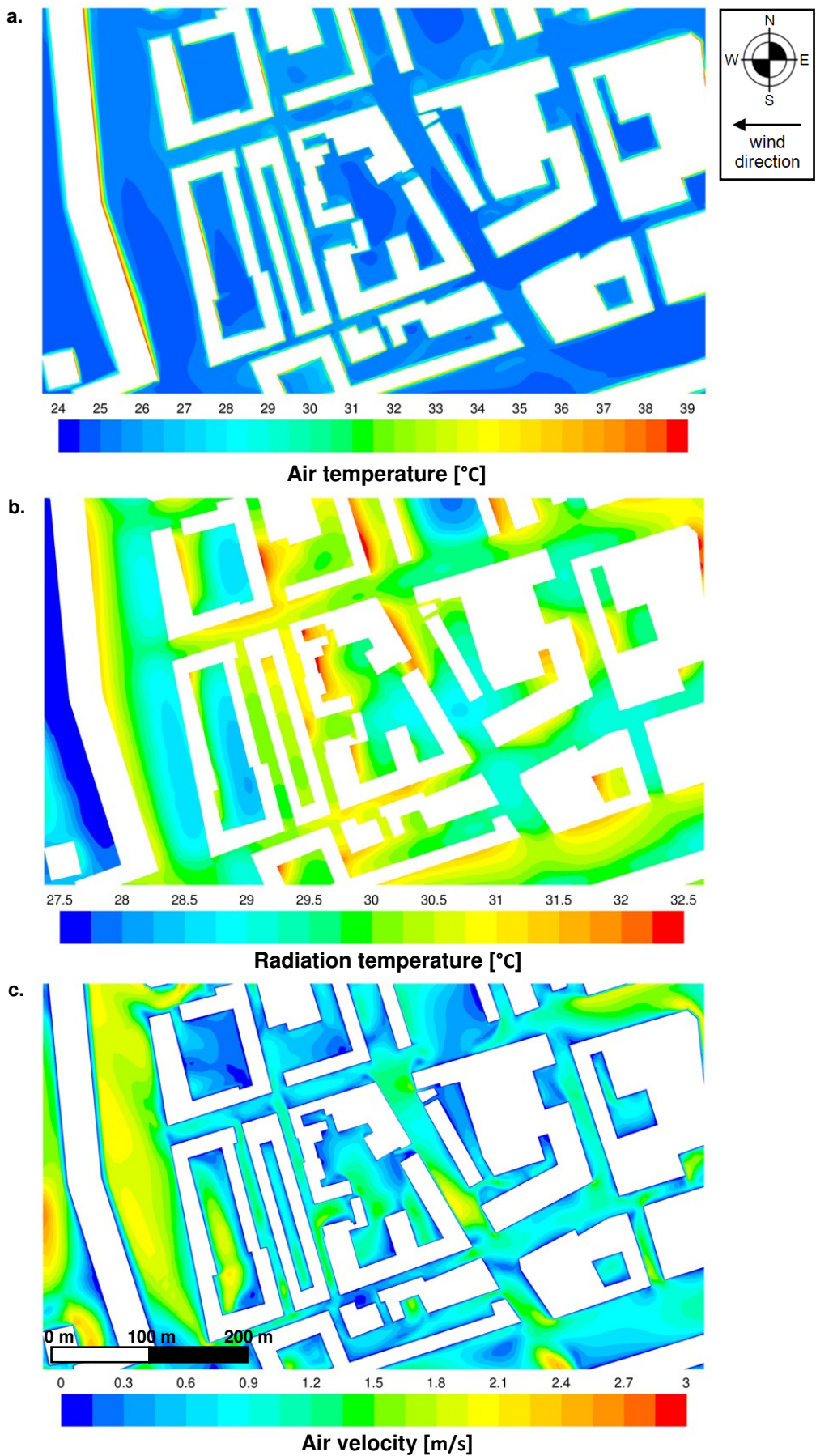


Figure 6.14: Air temperatures [°C], radiation temperatures [°C] and air velocities [m/s] at 1.1 m height around the care center at 17 July 2006, 7:59 am. The relative humidity at that time was 50% (KNMI).

It is remarkable to see that heat stress areas are already visible in the early morning while the average air temperature in the city is approximately 25°C. No thermal stress appears in regions with high wind velocities and shaded areas where radiation temperatures are low. Moderate heat stress occurs in regions with lower wind velocities. Physiological responses corresponding to moderate heat stress are the occurrence of sweating after 30 minutes and a steep increase in skin wittedness (Blazejczyk et al., 2013). Strong to very strong heat stress occurs close to the east walls of the buildings which are exposed directly to the sun. Physiological responses are an increase of the core temperature at exposure times of > 30 minutes, change in skin temperature, increase of sweat rate and latent heat loss.

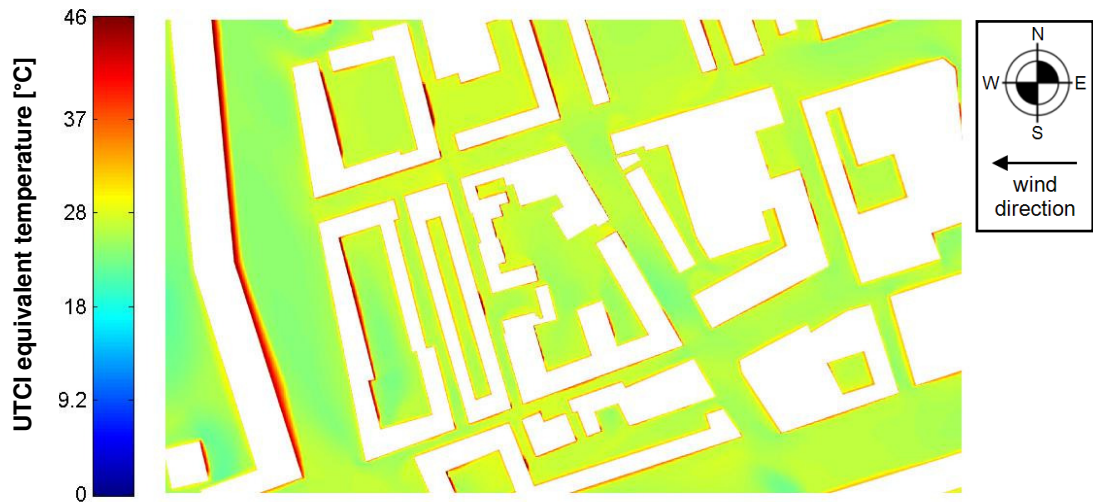


Figure 6.15: UTCl equivalent temperature [°C] around the care center at 17 July 2006, 7:59 am

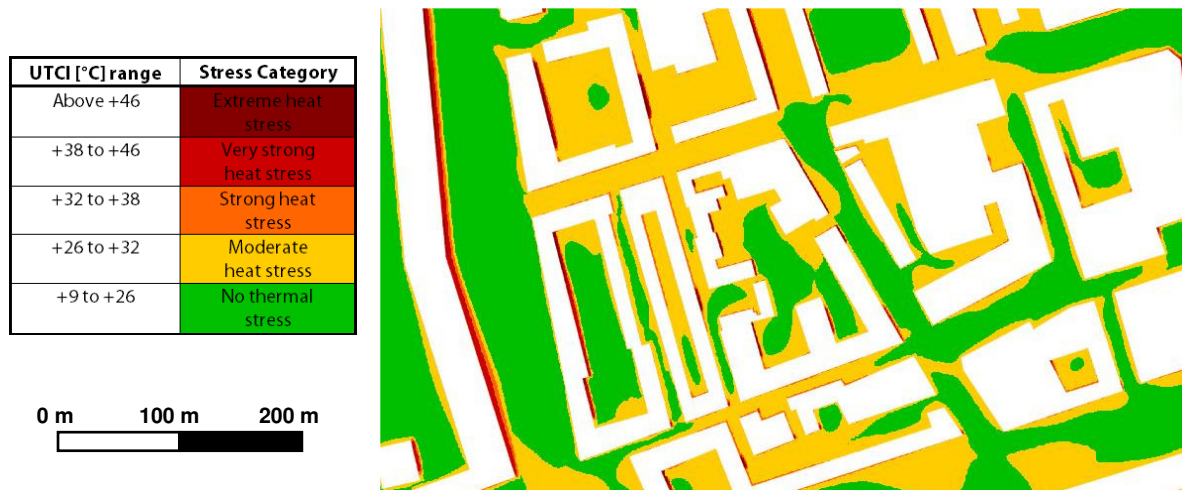


Figure 6.16: UTCl Stress category around the care center at 17 July 2006, 7:59 am based on the UTCl equivalent temperature [°C]

In Figure 6.17, the input information from Fluent is provided for the case at 11:44 am (17 July 2006). For this date and time, a relative humidity of 34% was measured at Rotterdam airport. The air temperature at 1.1 m height is in the range of 30 - 35°C. Near building facades, higher temperatures occur. The radiation temperatures are higher than the air temperatures and vary from 41°C in shaded areas to 51°C close to sunlit facades. The air velocities are slightly higher compared to the morning case. Therefore, a smaller area with air velocities < 0.3 m/s occurs. The calculated UTCl equivalent temperatures are given in Figure 6.18. In Figure 6.19, the UTCl-stress category is calculated based on the UTCl equivalent temperature distribution.

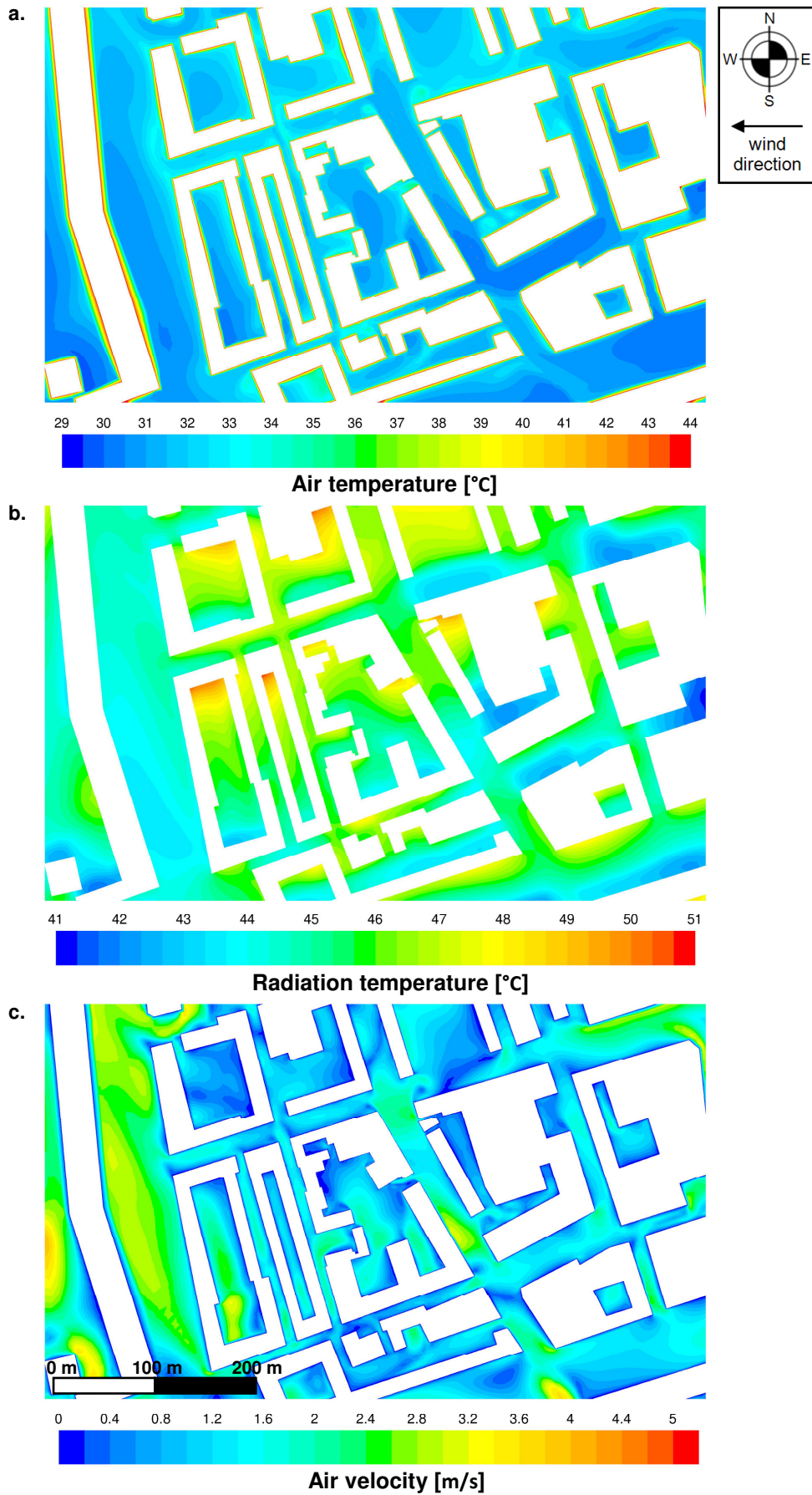


Figure 6.17: Air temperatures [°C], radiation temperatures [°C] and air velocities [m/s] at 1.1 m height around the care center at 17 July 2006, 11:44 am. The relative humidity at that time was 34% (KNMI).

For the noon case, there are no areas visible around the care center without heat stress. In most regions around the care center, strong heat stress is experienced. The least heat stress (moderate heat stress category) appears in regions with local air velocities of > 2.5 m/s. Only close to the southern part of sunlit walls, very strong to extreme heat stress is being experienced because of the high surface temperatures, radiation temperatures and low wind velocities.



Figure 6.18: UTCI equivalent temperature [°C] around the care center at 17 July 2006, 11:44 am

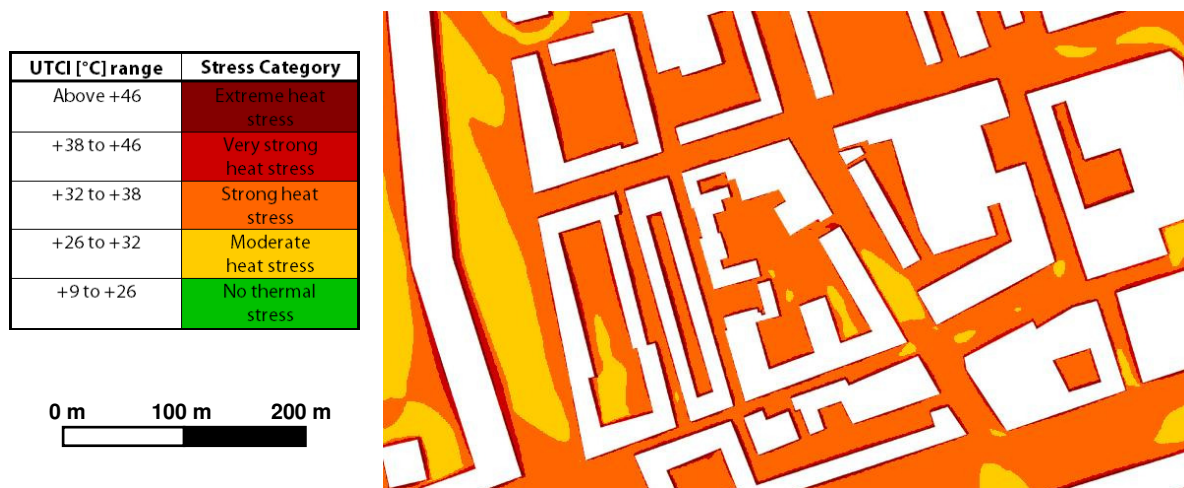


Figure 6.19: UTCI Stress category around the care center at 17 July 2006, 11:44 am based on the UTCI equivalent temperature [°C]

In Figure 6.20, input information from the CFD simulation is given for 17:59 pm. For this case, the relative humidity measured at Rotterdam airport is 36% (KNMI). Air temperatures around the care center vary between approximately 26.5 and 29°C. Radiation temperatures are slightly higher: they vary between 28 and 32°C. The air velocities vary between 0 and 3.6 m/s. The area with velocities < 0.3 m/s is relatively small. In Figure 6.21, the UTCI equivalent temperatures are presented. In Figure 6.22, the UTCI-stress category is calculated based on the UTCI equivalent temperature distribution.

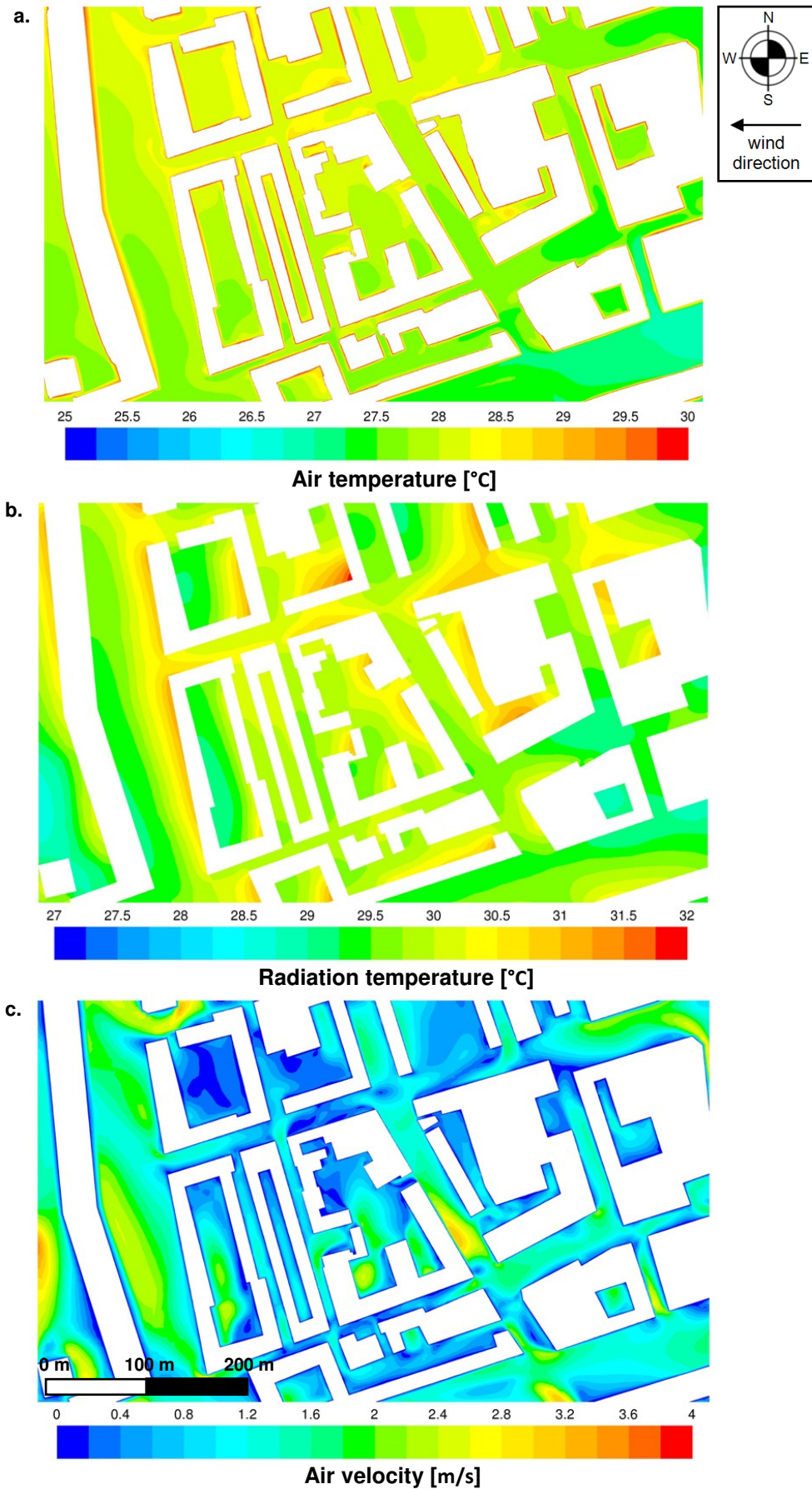


Figure 6.20: Air temperatures [°C], radiation temperatures [°C] and air velocities [m/s] at 1.1 m height around the care center at 16 July 2006, 17:59 pm. The relative humidity at that time was 36% (KNMI).

Compared to the morning case, a larger area with moderate heat stress occurs at 17:59 pm. This is caused by the higher air temperatures around the care center. No areas are visible with strong, very strong or extreme heat stress. The relation between air velocities and stress category is clearly visible: the areas with no thermal stress are the areas with the highest wind velocities.

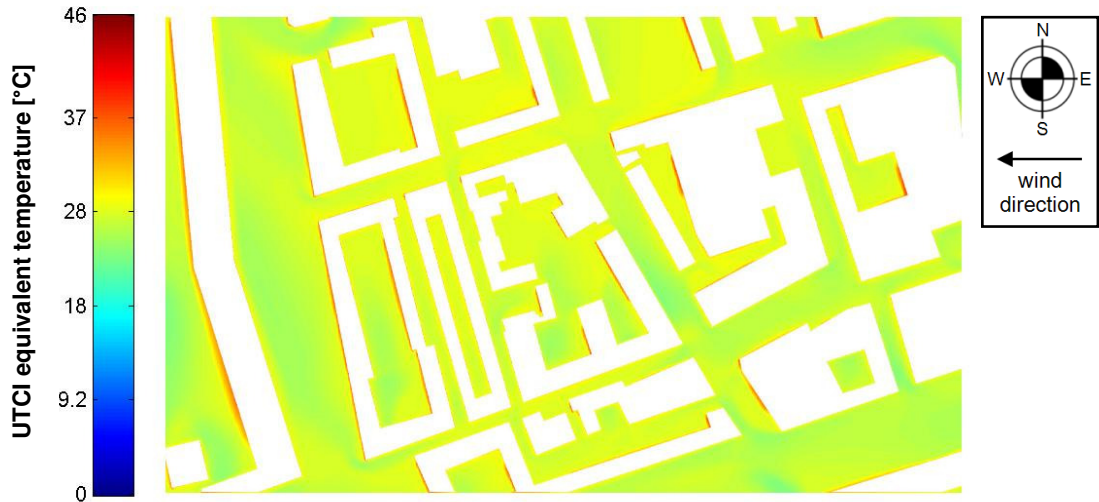


Figure 6.21: UTCI equivalent temperature [°C] around the care center at 16 July 2006, 17:59 pm

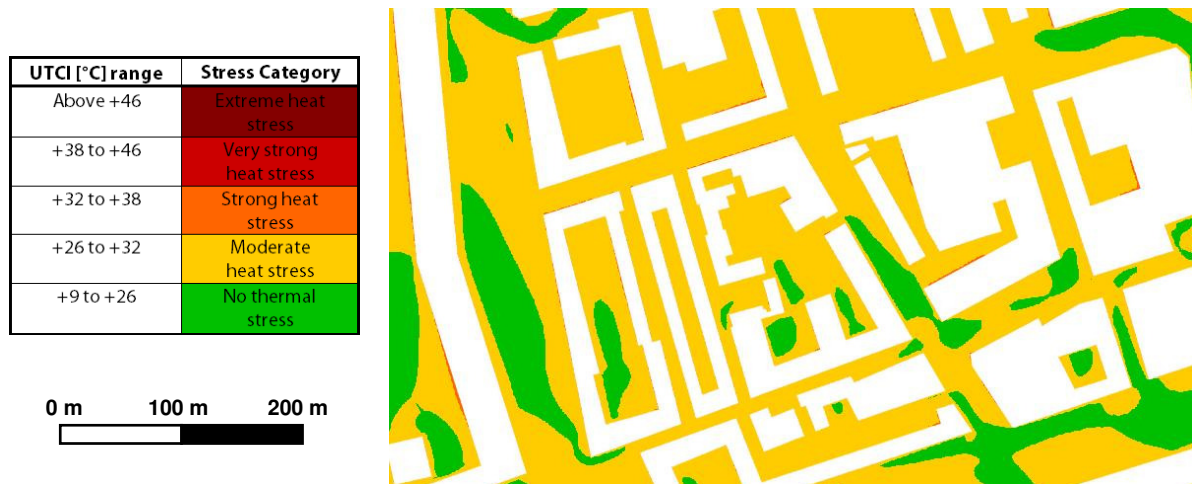


Figure 6.22: UTCI Stress category around the care center at 16 July 2006, 17:59 pm based on the UTCI equivalent temperature [°C]

As mentioned before, the relative humidity values measured at Rotterdam airport are used as input for the UTCI-calculation. However, the relative humidity in the city might deviate from the relative humidity at Rotterdam airport. According to Bröde et al. (2011a), the effect of humidity on UTCI is small at low air temperatures. At moderate temperatures, UTCI is slightly increased for RH-values above the reference of 50% and negligibly reduced for lower RH-values. The relation between UTCI and relative humidity is different for high temperatures (above 20°C). In Figure 6.23, UTCI equivalent temperatures and heat stress categories are given for the late afternoon case for varying RH values of 15, 36, 55 and 75%.

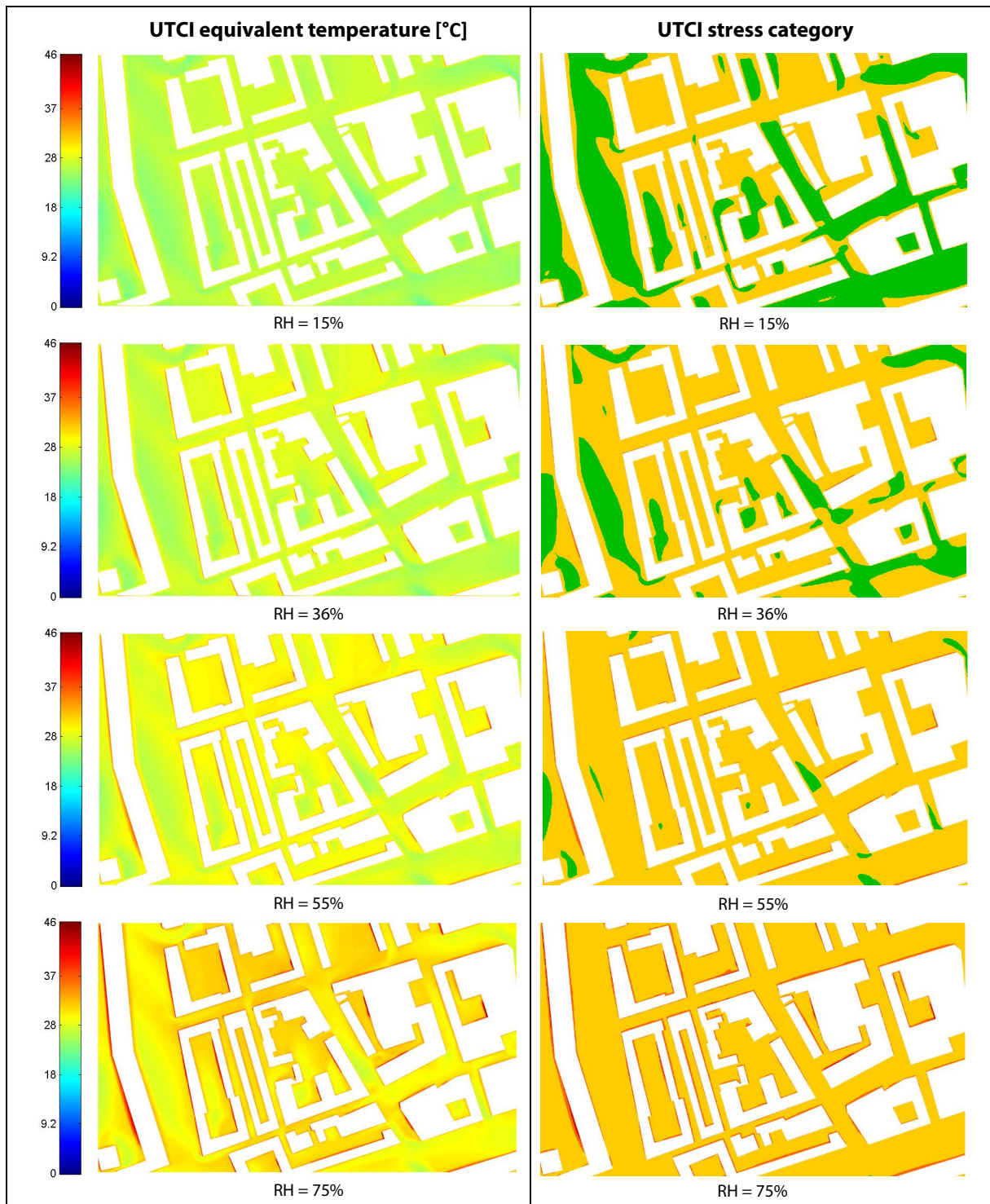


Figure 6.23: Effect of the relative humidity [%] on the UTCI equivalent temperature [°C] and UTCI Stress category for 16 July 2006, 17:59 pm

The area with moderate heat stress increases with increasing relative humidity. At an RH of 75%, the areas with no thermal stress have completely vanished. The relationship between UTCI, air temperature and humidity is also presented in Figure 6.24 for $T_r = T_{air}$ and $u_{10} = 0.5$ m/s.

Especially at high temperature and humidity levels, there is a stronger influence of humidity on UTCI (Bröde et al., 2011a). The category of heat stress that occurs during a heat wave is therefore highly dependent on the ambient relative humidity.

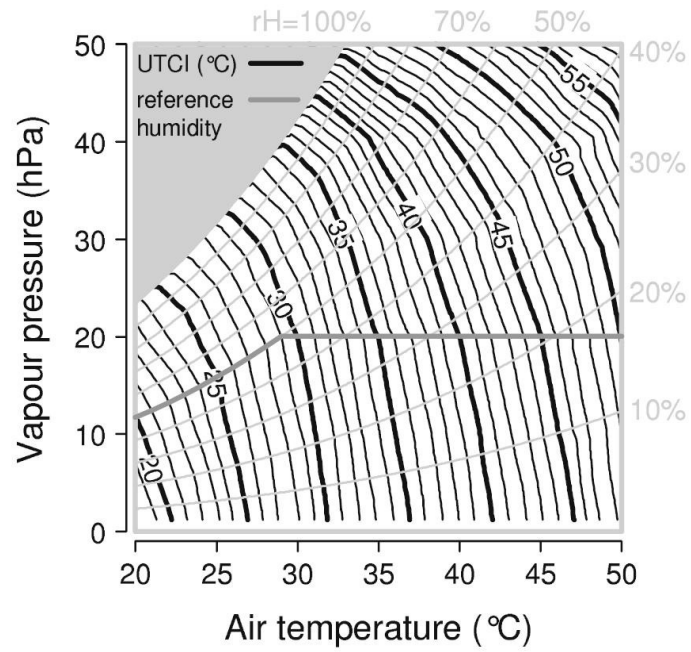


Figure 6.24: relationship between air temperature, vapor pressure (or relative humidity) and the UTCI equivalent temperature (Bröde et al., 2011a)

7. Results: indoor environment

In order to give an answer on the initial 2nd research question about the UHI effect on the temperature rise and thermal comfort in the care center for the 2nd heat wave of 2006, 2 simulations had to be performed. First, a simulation with the model of the care center in Rotterdam including the indoor environment (model 2) and second, a simulation with the model of the care center in the rural environment (model 3). By comparing the calculated temperatures inside the care center of both models, the effect of the city on the indoor temperatures in the care center could be investigated.

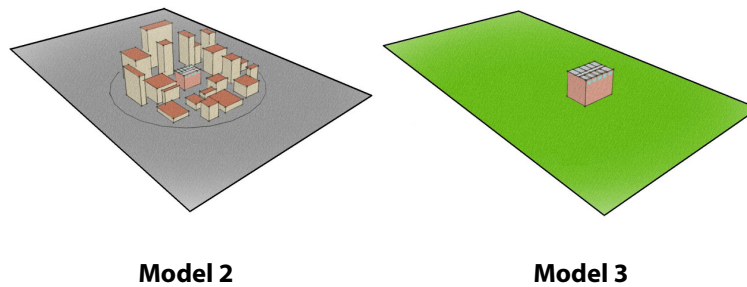


Figure 7.1: Model 2 and 3 are used for the investigation of indoor temperatures and indoor thermal comfort

Unfortunately, during the progress of this project the problem occurred that the initialization time can be extremely long when using the solar load model with large CFD models. This made it impossible to answer the initial research question within the time frame of this research. Nevertheless, the initialization problem has been investigated and several solutions are found for decreasing the initialization time. Subsequently, this chapter will discuss a research on the effect of different parameters on the initialization time and possible solutions to the problem.

7.1 Calculation procedure and initialization problem

The intention was to perform an unsteady RANS simulation in order to calculate the indoor temperatures of the care center. In this way, the thermal buffering effect of the building envelope could be taken into account which results in a more accurate prediction of the indoor temperatures. The procedure for performing a transient simulation with the solar load model is described in the Fluent User guide (ANSYS FLUENT User's guide, 2009). For a transient simulation, the number of time steps per Solar Load Update should be specified. With this specified frequency, the sun position and irradiation will be re-computed and solar loads will be updated. Solar loads are computed on initialization. For a transient simulation, the initialization time equals the amount of Solar Load Updates times the initialization time for a steady-state simulation. For example: when the initialization time of a model with solar load is 15 minutes for a steady-state simulation, the initialization time for a transient simulation with 20 Solar Load Updates equals 20×15 minutes = 300 minutes (5 hours).

Because the solar ray tracing algorithm is not parallelized in FLUENT, solar data should be generated in the serial mode first. This data can then be used in the parallel simulation.

The initialization time of the validation cases was about 2 hours for each case. This is quite high when comparing this with the initialization time of CFD simulations of urban wind flow with initialization times of a few seconds. Because the cell size of model 2 and 3 is much larger than model 1 that is used for the validation study, it was expected that the initialization time would also be larger. For this reason, it was decided to perform a steady RANS simulation instead of an unsteady RANS simulation.

In the literature study, it was mentioned that the UHI effect is most pronounced at summer nights (Steenefeld & van Hove, 2010; van Hove et al., 2011a). However, because steady-state simulations were performed it was not possible to perform a simulation for the night. It was chosen to perform a simulation with model 2 and 3 for 17th of July 2006 at 12:00 am, because highest UHI and SHI intensities around the care center were found around noon. For this moment U_{10} at the inlet is 3 m/s, the inlet temperature is 29.1°C, global radiation 811 W/m² and the wind is coming from the easterly direction (KNMI). The location of the shadings of the care center in the grassland for this time is given in Figure 7.2.

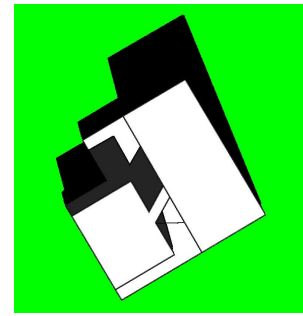


Figure 7.2: Shadings at 17 July 2006, 12:00 am

At the fastest servers of the unit Building Physics and Services (server at 2.66 Mhz with in total 96 GB of memory and 12 nodes), the initialization time of the model with the care center in the rural environment was 4 days. In Figure 7.3, a horizontal cross section at 18 m across the upper floor of the care center is given for the air temperature and amplification factors with $U_{ref} = 3$ m/s.

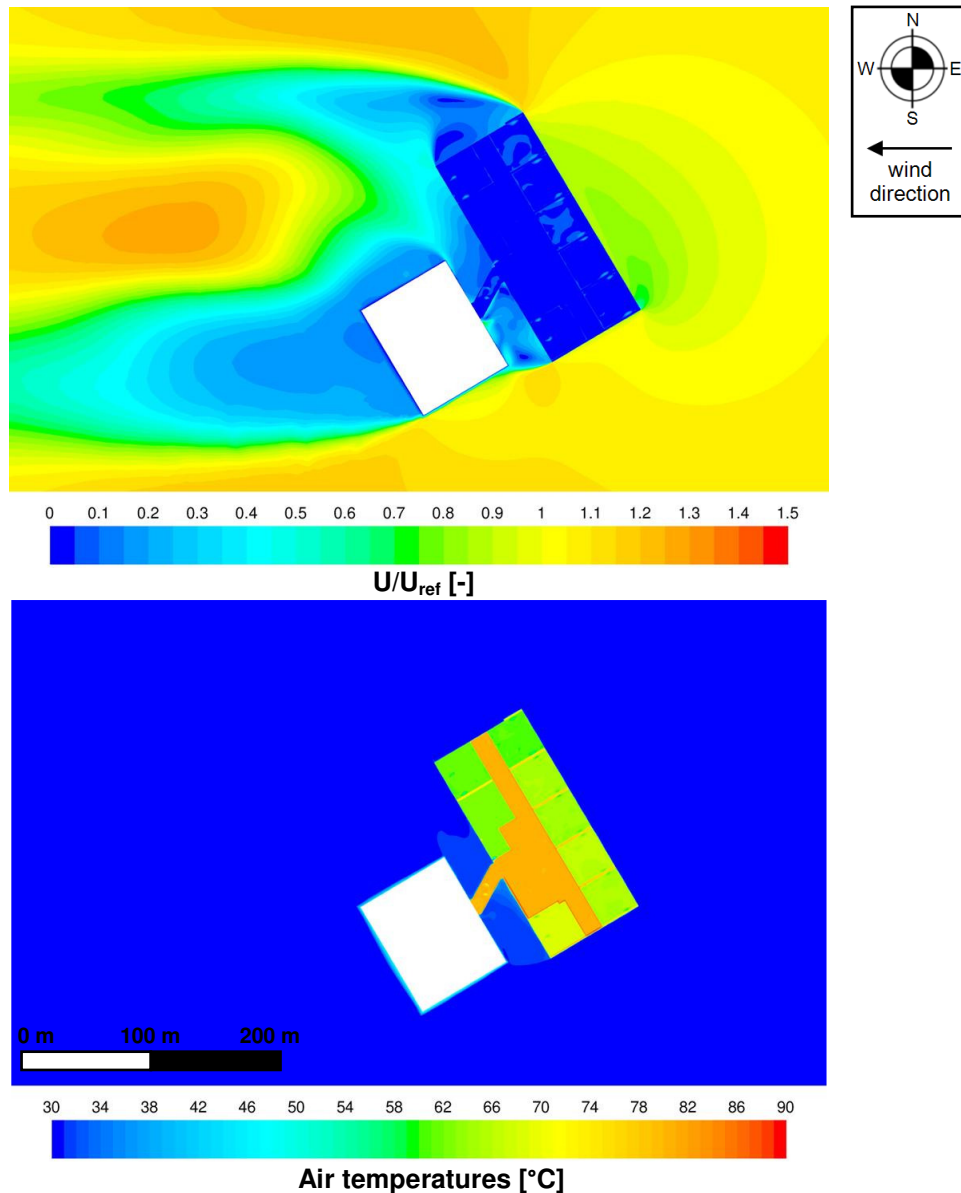


Figure 7.3: Horizontal cross section at $z = 18$ m of the amplification factors [-] and air temperatures [°C] for the care center in the rural area

The air temperatures vary between 60 and 80°C in the care center. It is very unlikely that this is correct. A reason for these high temperatures could be the fact that it is a steady-state simulation instead of a transient situation. It is not taken into account, that solar radiation and air temperature values are lower before 12:00 pm. Furthermore, the thermal conductivity value of the aluminum surface panels of the connection bridge is probably set too high, resulting in extreme temperatures in the hallway of the care center. The most northern apartments show lower air temperatures than the most southern apartments because of the southern position of the sun at that time. In the wake region at the west side of the care center, slightly higher air temperatures are visible caused by the lower air velocities in this region. In Figure 7.4, a vertical cross section over the 2 northern apartments is given of the air temperature. A vertical temperature stratification is visible, especially for the hallway.

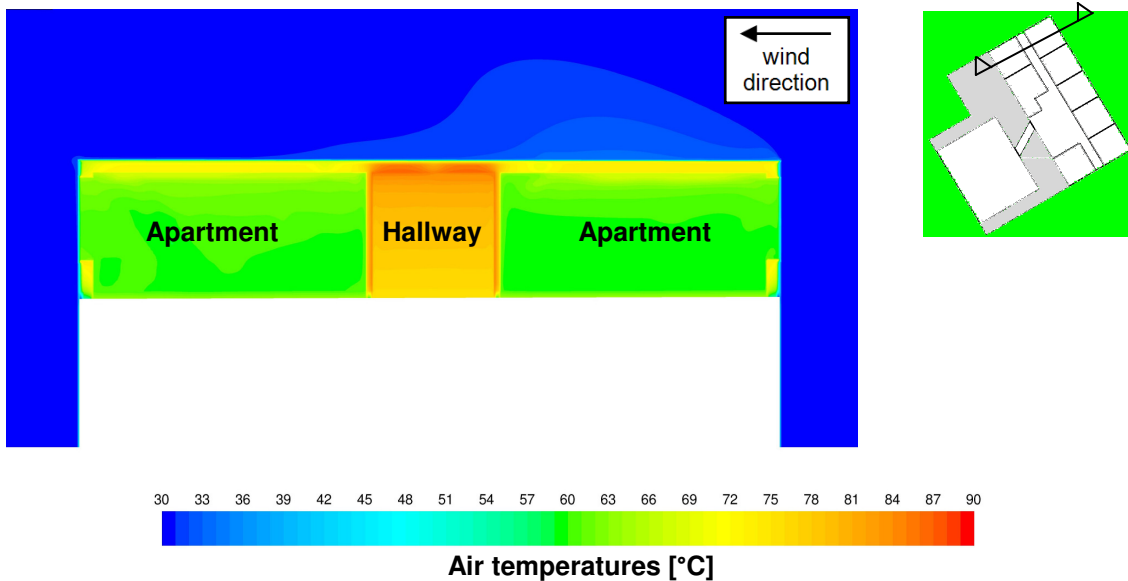


Figure 7.4: Vertical cross section over the most northern apartments and hallway of the air temperatures [°C] of the care center in the rural area.

Finally, the cooling effect of the grass on the air temperature is clearly visible (Figure 7.5). However, this does not affect the air temperature at the upper floor of the care center.

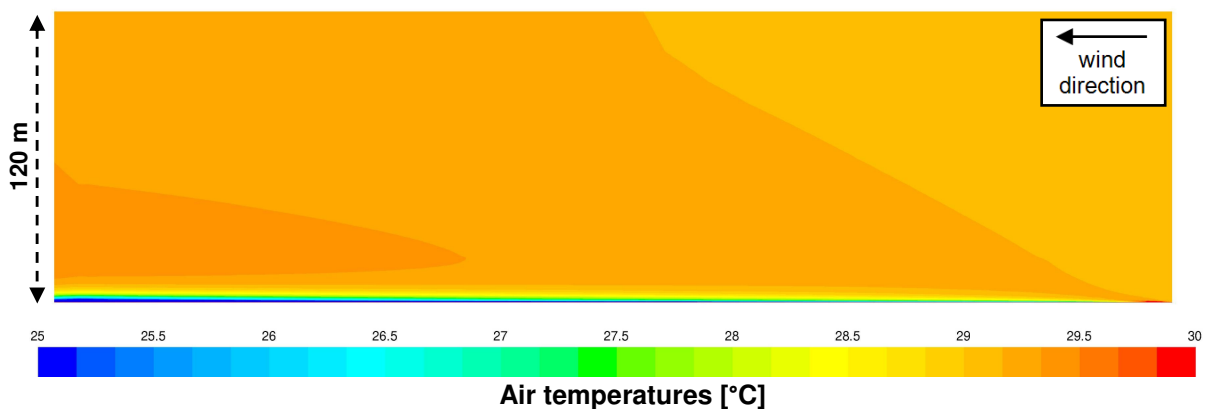


Figure 7.5: Vertical cross section over the domain of the air temperatures [°C]. The inlet air temperature is 29.1°C. The cooling effect of the grass is clearly visible.

The initialization process of the model of the care center in the city took about a month (30 days). Unfortunately, the model of the care center in the city immediately crashed after 10 iterations due to a floating point exception error. Floating point exception errors occur due to a limitation of machine or because of wrong input parameters (CFD Online forum). Because, the simulation was the only simulation

running on the server and only 72 GB of memory was used, the error probably occurred due to an incorrect input parameter instead of a limitation of machine. However, because of the large initialization time, it would be too time-consuming to investigate what parameter caused the error. Therefore, it was decided to perform a CFD research on the influence of different parameters on the initialization time of a model with solar load. This will be described in more detail in the next paragraph.

7.2 Parameter study

The solar load model was also used in a research of Toparlar (2012). In his research, a CFD model was used of approximately 7 million cells. The initialization time with the solar load model was around 120 seconds. This is significantly lower compared to the initialization time of 4 and 30 days for the models with the indoor environment of the care center in this research. Because of this reason, an overview is made of parameters that are different between the model of Toparlar (2012) and the models used in this research. The overview is provided below:

- Number of cells: model 1, 2 and 3 contain respectively 29, 49.8 and 25.3 million cells. This is much more than the 7 million cells used for the CFD model of Toparlar (2012);
- Number of boundaries: in the model of Toparlar (2012), walls and roofs are not specified as separate boundaries. Furthermore, grass surfaces have also not been specified separately in his research. The model of the care center also contains much more boundaries because of the inclusion of the indoor environment of the care center;
- Number of interfaces: in the study by Toparlar (2012), 2 interfaces have been defined. In this research, model 1 contains 26 interfaces (26 vertical), model 2 in this research contains 26 interfaces (4 horizontal, 22 vertical), model 3 contains 5 interfaces (4 horizontal, 1 vertical);
- Walls: in Toparlar (2012) walls are modeled as faces in Gambit which are given a thickness in the thermal boundary conditions section of Fluent. For the model of the care center, walls are already given a thickness in Gambit. This means there are both solid and fluid cell zones in the model. This could lead to larger initialization times;
- Ratio between smallest and largest cell size in the domain: in the models of this research, there is a large difference in cell size between the smallest and largest cell in the domain. The smallest cells in the domain at the ventilation inlets are 0.025 m while the largest cells at the borders of the computational domain are tens of meters large. This ratio between the smallest and largest cell of the domain is much smaller in the CFD model of Toparlar (2012);
- Domain height: the domain height might influence the initialization time. The domain height of the CFD model of Toparlar (2012) is 400 m. Model 1 and 2 have domain heights of 900 m. Model 3 has a smaller domain height of only 120 m;
- Number of materials: the building envelope of the care center consists of a lot of different materials which all had to be specified in the boundary conditions section of Fluent. In Toparlar (2012), one material is chosen for the building envelope of all the buildings in the domain.
- Windows: in the model of Toparlar (2012) no windows (semi-translucent walls) are modeled. Windows are included in model 2 and 3. This might have an effect on the initialization time.

In order to investigate the effects of the above mentioned parameters on the initialization time, a simple CFD model was created of a square building of $3 \times 3 \times 3 \text{ m}^3$ (w x l x h) with a wall thickness of 0.3 m.

Dimensions of the computational domain were chosen based on the guidelines of Franke et al. (2007) and Tominaga et al. (2008).

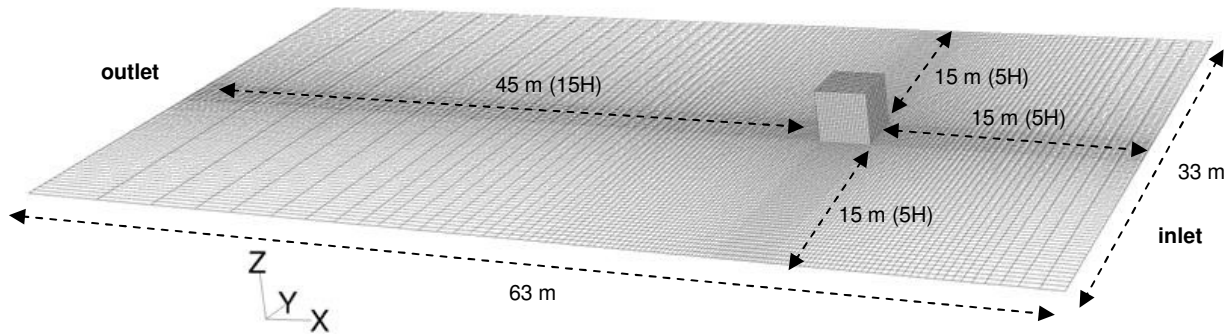


Figure 7.6: Dimensions of computational domain. The height of the domain is 18 m for the base case.

For the base case, the solar load model was set up with default settings and the initialization time was being calculated with Fluent. The initialization process took 7 seconds for the base case. Next, the effect of different parameters on the initialization time was being investigated by changing 1 parameter at a time compared to the base case, all other parameters remaining unchanged. In Table 7.1, the parameters for the base case are given as well as the variations made to these parameters for the other cases. In Figure 7.7, the calculated initialization times are given for the different variants.

Table 7.1: Applied parameters to the base case and variations made to these parameters for the other cases

Parameter	Base case	Variations
Number of cells	0.6 million	1.1, 2.4 or 3.6 million
Number of boundaries	69	10, 30, 50, 100, 200, 300, 400, 500, 600, 700 or 800
Number of horizontal interfaces	0	1, 2, 3 or 4
Number of vertical interfaces	0	1, 2, 3 or 4
Implicit walls or explicit walls (no solids, solids)	implicit walls	explicit walls
Ratio smallest - largest cell size in domain	1:35	1:17 or 1:9
Domain height	18 m	36, 54, 72 or 90 m
Number of materials	1 (concrete)	2, 4, 8 or 10
Windows/no windows	no windows	windows

From Figure 7.7, the following conclusions can be drawn. The parameters with the largest influence on the initialization time are: (1) the number of cells in the domain, (2) the number of boundaries included in the domain and (3) the presence of solid walls (explicitly modeled walls). An increasing amount of interfaces also increases the initialization time, but not significantly. The parameters that do not influence the initialization time are: (1) the ratio between the smallest and largest cell size, (2) the number of different materials used in the model and (3) the presence of windows. No clear relationship was found between the domain height and the initialization time: from 18 to 72 m domain height the initialization time slightly increases, but at 90 m the initialization decreases again.

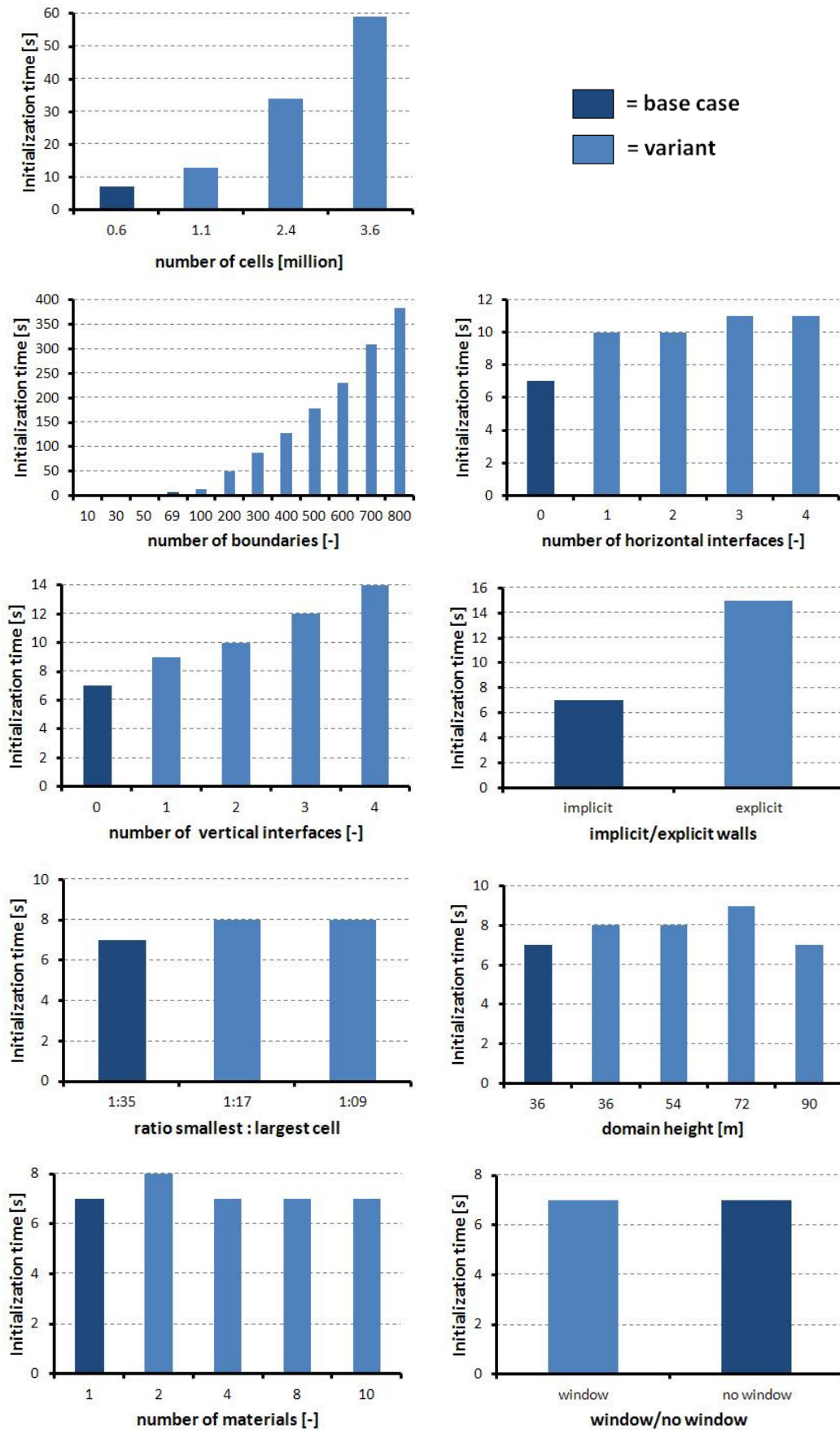


Figure 7.7: Results of parameter study. Initialization times of variants are compared to the base case.

Equations are derived from the relation between (1) the number of boundaries and the initialization time and (2) from the relation between the number of cells and the initialization time. The equations are given in the graphs of Figure 7.8.

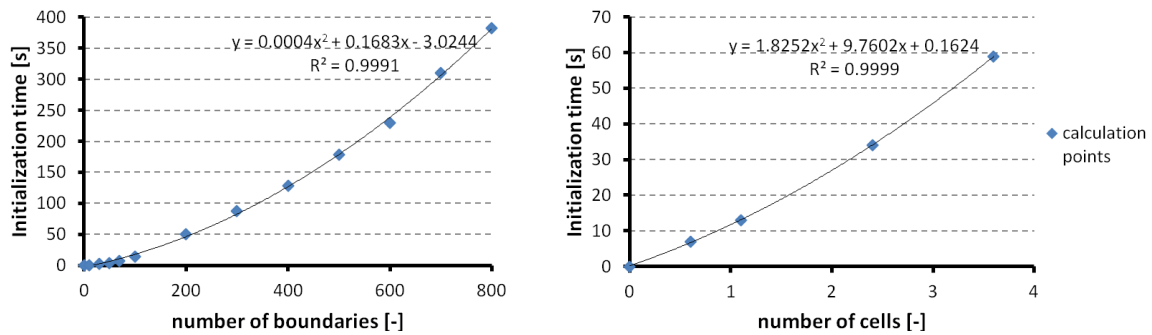


Figure 7.8: Equations for the relation between the number of boundaries and initialization time (left) and the number of cells and the initialization time (right)

In Table 7.2 and 7.3, these equations are used to calculate the initialization time for model 1, 2 and 3 based on the amount of boundaries (Table 7.2) and based on the number of cells (Table 7.3). The real initialization times are also given in these tables.

Table 7.2: Calculated initialization time based on the equation of Figure 7.8 for the amount of boundaries compared to the real initialization time

Model	Number of boundaries [-]	Calculated initialization time [s]	Real initialization time [s]
Model 1	± 210	50	± 2 hours
Model 2	± 740	341	± 30 days
Model 3	± 635	265	± 4 days

Table 7.3: Calculated initialization time based on the equation of Figure 7.8 for the number of cells compared to the real initialization time

Model	Number of cells [millions]	Calculated initialization time [s]	Real initialization time [s]
Model 1	29	1818 ≈ 30 min	± 2 hours
Model 2	49.8	5013 ≈ 84 min	± 30 days
Model 3	25.3	1415 ≈ 24 min	± 4 days

As can be seen from these Tables, the real initialization time is much larger than the ones calculated according to the formulas of Figure 7.8. The reason of this could be the fact that the models contain both a large amount of boundaries and a large number of cells. To investigate this, the base case of Figure 7.6 was adjusted by increasing both the number of cells to 3.6 million, as well as the amount of boundaries to 400. For this model, the calculated initialization time by Fluent is 845 seconds (≈ 14 minutes). When also the walls are changed from implicit to explicit walls, the initialization time calculated by Fluent is 2632 seconds (≈ 44 minutes), an increase of factor 3. This explains why the initialization times of model 2 and 3 are so long.

Table 7.4: Initialization times when more parameters are changed at the same time

Adjustments compared to base case	Initialization time [s]
3.6 million cells	59
400 boundaries	128
Explicit walls	15
3.6 million cells + 400 boundaries	845 \approx 14 min
3.6 million cells + 400 boundaries + explicit walls	2632 \approx 44 min

At the start of the development of a CFD model of an urban environment including the solar load model, attention should be paid to:

- 1) The use of explicitly modeled walls: when this is not necessary, implicitly modeled walls should be used
- 2) The total number of cells of the computational domain: except for the wall type, this is the most decisive factor in the length of the initialization time
- 3) The total number of boundaries: the number of boundaries should be kept as low as possible
- 4) The number of interfaces: a large computational domain can be split into more subdomains in order to accelerate the build up of the model. By splitting a computational in more subdomains, the amount of interfaces increases. At the same time extra boundaries are formed. When a small amount of interfaces is used, this does not seem to affect the length of the initialization time. However, a large amount of interfaces should be avoided.
- 5) Avoid the use of interfaces through a combination of fluid and solid zones: because there is a horizontal interface in the middle of the upper floor of the care center, a lot of extra boundaries are created when opening the mesh in Fluent.

Furthermore, the initialization time also might be decreased when Ansys Fluent develops a solar ray tracing algorithm that can be used in the parallel solver.

For the models in this research, it is hard to decrease the initialization time. At this stage, decreasing the amount of cells would mean that the entire grid should be meshed again from the start. The amount of boundaries was already decreased as much as possible by merging boundaries of the same type in Fluent. The best way to decrease the initialization time for the models of this research, would be the use of implicitly modeled walls instead of explicitly modeled walls. This is left for further investigation.

8. Discussion

In this research, CFD simulations have been performed for the investigation of the UHI effect on air temperatures in and around a care center in Rotterdam. Simulations can be defined as imitations of the operation of a real process or system over time (Banks et al., 2001). During the process of this research, assumptions had to be made and some simplifications had to be applied. In this chapter, the relevance of some of these assumptions and simplifications to the accuracy of the final results is discussed.

8.1 CFD settings and parameters

In the literature chapter, causes of the UHI effect have been explained. Two of these causes are not included in the simulation models. First of all, anthropogenic heat sources (such as building equipment and traffic) are not included because this would lead to an increased complexity of the models. Besides, large differences have been reported on the anthropogenic heat release of cities, which makes it difficult to choose a realistic value for it. However, it should be mentioned that up to 3 times lower anthropogenic heat rates have been reported for the summer period compared to the winter period (van Hove et al., 2011b). So its contribution to the UHI effect might be smaller for the simulation dates chosen in this research. Secondly, the effect of air pollution has not been taken into account. Further research is needed to investigate how it can be implemented and what the effect is on the calculated air temperatures.

Due to the occurrence of long initialization times, it was impossible to perform unsteady-RANS simulations in the timeframe of this graduation project. Therefore, the thermal buffering effect could not be taken into account. For this reason, no simulations could be performed for the night when UHI intensities appear to be the largest (van Hove et al., 2011a). Nevertheless, simulations could be performed for daytime when SHI intensities are most significant (van Hove et al., 2011a).

In order to decrease the complexity of the model and the computational costs, all building walls in the domain are given the same thermal and radiation properties. The same holds for all the building roofs in the domain. The care center forms an exception: the building construction is modeled as detailed as possible. The positions, shapes and dimensions of the buildings in the domain are adopted from drawings of the municipality of Rotterdam. Small obstacles such as trees, street lights and cars are not included. The effect of shading is taken into account by applying a lower solar absorptivity to the ground surfaces.

The ventilation outlets of the care center are modeled as small holes in the roof with a fixed velocity rate applied to it. A disadvantage of modeling the ventilation outlets in this way, is that direct solar radiation will go through the holes in the roof and heat up the indoor space when the sun is positioned high in the sky (noon). Because of the small size of the holes compared to the size of the apartments, the effect on the average indoor temperature is assumed to be negligibly small.

8.2 Validation study

In the validation study, average surface temperatures are compared to values reported in an article of Klok et al. (2012) which are based on satellite data measurements. The air temperature on a fixed location is compared to air temperature measurement of the CPC weather station. Both validation studies are valuable for the research, but not ideal. Klok et al. (2012) only provides average surface temperatures of city districts based on satellite images with a low spatial resolution of 1 x 1 km pixels. For the average temperature of the city centre, 7 pixels were chosen overlapping the city centre region. In the CFD simulation, the average surface temperature of the city centre could be calculated in more detail by selecting all the surfaces located in the city centre. The air temperature could only be validated on 1 position in the domain. Because the CPC

weather station is located on an overhang on just a few meter of a building façade, the surface properties of this building will affect the measured air temperatures.

In the future, the validation study could be extended with in-situ measurements during a summer period on different locations in the city.

8.3 UTCI equivalent temperature

8.3.1 Mean radiant temperature T_{mrt}

For the calculation of the UTCI equivalent temperature, T_{mrt} is one of the input parameters. For this value, the radiation temperature T_r is used from the CFD calculation. There was some doubt whether the mean radiant temperature T_{mrt} is equal to the radiation temperature T_r . This will be explained in more detail in this paragraph.

The formula of the radiation temperature as defined in the Fluent theory guide (2009), is given below:

$$T_r = \left(\frac{G}{4\sigma} \right)^{1/4} - 273.2 \quad (8.1)$$

In this formula, T_r is the radiation temperature [°C], σ the Stefan-Boltzmann constant ($5.67 \cdot 10^{-8} \text{ W/m}^2\text{K}^4$) and G the incident radiation [W/m^2]. The incident radiation is calculated by:

$$G = \int_{\Omega=4\pi} I d\Omega \quad (8.2)$$

with solid angle Ω [radians] and radiation intensity I [W/m^2]. The radiation intensity equals the energy per emitting surface per solid angle.

The following equation is used for the calculation of T_{mrt} from integral radiation measurements (Thorsson et al., 2007).

$$T_{mrt} = \sqrt[4]{\frac{S_{str}}{\epsilon_p \cdot \sigma}} - 273.2 \rightarrow T_{mrt} = \left(\frac{S_{str}}{\epsilon_p \cdot \sigma} \right)^{1/4} - 273.2 \quad (8.3)$$

In this formula, ϵ_p is the emissivity of the human body (0.97), σ the Stefan-Boltzmann constant ($5.67 \cdot 10^{-8} \text{ W/m}^2\text{K}^4$) and S_{str} the mean radiant flux density of the human body which is calculated by (Thorsson et al., 2007):

$$S_{str} = a_k \cdot \sum_{i=1}^n K_i \cdot \Omega_i + \epsilon_p \cdot \sum_{i=1}^n L_i \cdot \Omega_i \quad (8.4)$$

a_k is the absorption coefficient of the human body for short-wave radiation (0.7). K_i and L_i are the short-wave and long-wave radiation fluxes for solid angles Ω_i

Formula 8.1 and 8.3 have comparable forms. However the emissivity coefficient (value = 0.97) and absorption coefficient (value = 0.7) seem to be excluded from the formula of the radiation temperature as calculated by Fluent. Therefore, T_r might be different from T_{mrt} which affects the calculated UTCI equivalent temperature. Further research is needed to investigate the exact difference in T_r and T_{mrt} and the influence of the difference on the UTCI calculation.

8.3.2 Validity range UTCI calculator

In chapter 6, the UTCI equivalent temperature is calculated based on CFD input information and a MATLAB script of the online UTCI calculator. Because the UTCI calculator is based on the UTCI values calculated by complex simulation software for a set of different combinations of meteorological conditions, the UTCI equivalent temperatures can only be trusted for a certain set of input parameters. At noon, surface temperatures of sunlit façade reach values of up to 75°C. Close to these walls, the air temperature will approach the surface temperature and will therefore extend the air temperature validity range (-50 to +50°C). It was found that for air temperatures above 58°C, the calculated UTCI equivalent temperature had a negative value (corresponding to cold stress categories) instead of an expected equivalent temperature corresponding extreme heat stress. Therefore, an extra line was implemented in the UTCI script changing air temperature input values > 58°C in a value of 58°C. In this way, reliable results were also achieved for regions with high air temperatures.

Radiation temperatures and relative humidity values were all within the validity range. The validity range of the velocity magnitude at 1.1 m height is 0.3 - 11.6 m/s. For the morning case in particular, there were relatively large areas with $u_{1,1} < 0.3$ m/s. However, the calculated UTCI equivalent temperatures for $u_{1,1} < 0.3$ m/s looked plausible and therefore it is thought that also for these areas, the results can be trusted.

8.4 Initialization time

On the one hand, a high detail level was needed for modeling the care center. On the other hand, a significant part of the urban surroundings had to be modeled in order to give a good prediction of urban wind flow and the UHI effect. This results in a complex model which on its turn leads to long simulation times. For this reason, focus was on keeping the number of cells in the domains as low as possible. In the end of this research, it was found that the focus should also have been on keeping the number of boundaries and number of interfaces as low as possible. Although implicitly modeled walls are less realistic and are advised to be used when the wall thickness is small compared to the overall geometry, it should have been a better choice to model the walls of the care center implicitly.

At this stage, having already generated a complete mesh, there are several options for decreasing the initialization time:

- 1) Decreasing the number of cells: because the urban region is split up into more subdomains, the northern subdomain (subdomain 1) could be exchanged by an empty domain containing fewer cells. This domain is expected to have the least influence on the air temperatures around the care center.
- 2) Replacing all the solid zones by fluid zones and modeling the walls implicitly by giving them a thickness in Fluent. A disadvantage of this method is that the material layers in the wall cannot be modeled separately.

Both of the above mentioned options are left for further research.

8.5 Recommendations for further research

Based on the simulations performed in this research and the points of discussion as mentioned in the previous paragraph, the following recommendations for further research can be made:

- Investigate how air pollution and anthropogenic heat sources can be modeled with CFD and investigate their contribution to the UHI effect.

- The validation study could be extended with in-situ measurements on different locations around the care center.
- More accurate results could be achieved when transient simulations are performed for the validation study. In this way the thermal buffering effect can be included.
- An investigation of the difference in and relation between the radiation temperature T_r and mean radiant temperature T_{mrt} could be of great value for the use of CFD for thermal comfort studies.
- Try to reduce the initialization time of the CFD models described in this research by one of the mentioned options and investigate the UHI effect of Rotterdam on the indoor temperatures of the care center.
- Because the urban region is placed in a circular subdomain, the UHI effect on outdoor (and indoor) temperatures and thermal comfort could also be evaluated for different wind directions.
- Start with a very simple model of the indoor environment of a building situated in an urban setting and calculate the UHI effect on indoor temperatures. Add more details step by step.

9. Conclusions

In this research, CFD is used for the computation of the UHI effect during the heat wave of 2006 for a case study, being a care center and its surroundings situated in the Dutch city Rotterdam. The effects on thermal comfort of the elderly have been investigated as well. The advantage of CFD for the investigation of the UHI effect compared to other investigation methods is its possibility to look at the UHI distribution over the entire urban area rather than looking at the UHI intensity at fixed positions (air temperature measurements) or average values (thermal infrared remote sensing techniques). This project is unique, because of the combination of both the outdoor environment and indoor environment in the same CFD model. In this research, 3 models have been developed with great care and guidelines have been adopted accordingly.

An extensive validation study has been performed of both average surface temperatures and the local air temperature based on satellite measurement data as reported in Klok et al. (2012) and air temperature measurements on a fixed position in Rotterdam city centre as reported by the CPC project: heat stress in the city (CPC, 2009). Good results were found for the average surface temperatures of the morning case. For the noon case, surface temperatures are overestimated, while the surface temperatures for the late afternoon case are underestimated. Better results might be achieved with transient simulations. For the validation study of the air temperature, the CFD results were in relatively good correspondence with the local air temperature measurements.

Both, SHI and UHI intensities have been calculated for the region around the care center for 3 moments during a hot day of the 2nd heat wave of July 2006. For all cases, UHI intensities were lower than the SHI intensities and also the variation was smaller. In the morning, UHI intensities ranged from +0.5 to +3.5°C and SHI intensities ranged between 0 and +15°C. The UHI effect is most significant at noon with UHI intensities varying from +1 to +6.5°C and SHI intensities ranging between +4 and +38°C. It should be noted here, that Fluent overestimates the surface temperatures for this time so the real SHI intensity range might be smaller but still significant. Lowest SHI and UHI intensities were found for the late afternoon case. The UHI intensity range was -1.5 to +0.5°C and SHI intensities ranged between +1 to +8.5°C. When looking at the local variation in SHI intensities, surface temperatures are mostly affected by solar radiation and the surface properties: the effect of shading was clearly visible for all cases. Higher surface temperatures were observed in regions with low air velocities. The negative correlation between air velocities and surface temperatures was more visible for the sunlit surfaces than shadowed surfaces. The local distribution in UHI intensities is more dependent on air velocities and the distance from building facades than whether these positions are in sunlit or shaded areas.

As a performance indicator for the outdoor thermal comfort of the elderly, the Universal Thermal Climate Index is used. This, because UTCI takes all heat transfer mechanisms of the human heat balance into account, it is especially developed for outdoor settings and it has proven to show good results for the thermal comfort assessment of elderly as well (Bröde et al., 2011b). Furthermore, the characteristics of the reference person of the underlying Fiala model are comparable to the characteristics of Dutch elderly > 65 years old (DINED anthropometric database). The UTCI equivalent temperatures are calculated for the region around the care center for a morning, noon and late afternoon case of a hot day of the 2nd heat wave of July 2006. For the morning case, thermal stress categories varied between no thermal stress (+9 to +26°C) and moderate thermal stress (+26 to +32°C). Strong (+32 to +38°C) to very strong heat stress (+38 to +46°C) is only visible in the vicinity of sunlit building facades. Thermal stress is strongest for the noon case with strong heat stress in most of the regions surrounding the care center. Only moderate heat stress is visible in regions with higher air velocities. Finally, in the late afternoon heat stress varied from no thermal stress to moderate heat stress. Although UHI intensities and SHI intensities were higher for the morning case, the area with no

thermal stress is smaller for the evening case because of higher air temperatures and a lower relative humidity level. It is also shown for the evening case, that thermal comfort is highly dependent on the relative humidity. This is especially true for heat waves, when ambient air temperatures are high.

In this research, a first step is made to the prediction of the UHI effect on indoor temperatures and thermal comfort for a care center in Rotterdam. The geometry of the upper floor as well as building material characteristics, surface properties, ventilation inlets/outlets and windows are included. The complexity of the model was reduced, by keeping the amount of cells as low as possible and by simplifying the geometry of care center. Some initial results for the care center in the rural area were obtained. The distribution of the temperatures was considered to be reliable, but the values were highly overestimated. Further research on this is needed.

Large initialization times were found for the models including the indoor environment of the care center because of the use of the solar load model. From the parameter study, the following conclusions about the initialization time can be drawn. The initialization time is highly dependent on the combination of 3 parameters: the type of walls, the number of cells in the domain and the number of boundaries in the domain. The higher the number of cells and boundaries in the domain, the higher the initialization time is. The use of solid walls (explicitly modeled in Gambit) increases the initialization time extensively. Furthermore, an increase of interfaces also leads to a slight increase of the initialization time. When using the solar load model for large models of urban settings including indoor environments, the number of boundaries and cells should be kept as low as possible and the use of solid zones should be avoided. Furthermore, the initialization time could be decreased if a next release of ANSYS Fluent software includes a solar ray tracing algorithm for use on parallel nodes. In this way, solar data does not have to be generated in the serial mode.

Nomenclature

Table N.1: Abbreviations

Abbreviation	Description
ABP	Architecture, Building and Planning
ASHRAE	American Society of Heating, Refrigerating and Air conditioning Engineers
ATG	Adaptive Temperature Limit Indicator
AVHHR	Advanced Very High Resolution Radiometer
BPS	Building Physics and Services
BSA	Body Surface Area
CFD	Computational Fluid Dynamics
CLEAR	Comfortable Low Energy ARchitecture
DTS	Dynamic Thermal Sensation
GMT	Greenwich Mean Time
HVAC	Heating, Ventilation and Air Conditioning
KNMI	Koninklijk Nederlands Meteorologisch Instituut
MEMI	Munich Energy-balance Model for Individuals
NOAA	US National Oceanic and Atmospheric Administration
PET	Physiological Equivalent Temperature
PMV	Predicted Mean Vote
PPD	Predicted Percentage of people being Dissatisfied
RANS	Reynolds Averaged Navier-Stokes
SHI	Surface urban Heat Island
SVF	Sky View Factor
TU/e	Eindhoven University of Technology
UBL	Urban Boundary Layer
UCL	Urban Canopy Layer
UHI	(atmospheric) Urban Heat Island
UTCI	Universal Thermal Climate Index
VVZS	Verzorging- Verpleeg- Ziekenhuizen en Serviceflats

Table N.2: Greek symbols (part 1)

Symbol	Description	Dimension
α	constant in turbulent kinetic energy profile	-
α	absorptivity	-
α_k	absorption coefficient of the human body for short-wave radiation	-
β	thermal expansion coefficient	K^{-1}
ϵ	turbulence dissipation rate	m^2/s^3
ϵ	emissivity	-
ϵ_p	emissivity of the human body	-

Table N.3: Greek symbols (part 2)

Symbol	Description	Dimension
θ	wind direction	$^{\circ}$ (N= 0°, E= 90°, S= 180°, W= 270°)
κ	von Karman constant	-
λ	thermal conductivity	W/mK
ρ	density	[kg/m ³]
σ	Stefan-Boltzmann constant	W/m ² K ⁴
τ	transmittance	-
σ_s	scattering coefficient	-
Ω	solid angle	radians

Table N.4: Latin symbols (part 1)

Symbol	Description	Dimension
c_p	specific heat capacity	J/kgK
clo	clothing insulation	Clo (1 Clo = 0.155 Km ² /W)
d	thickness	m
h	height	m
htc	heat transfer coefficient	W/m ² K
k	turbulent kinetic energy	m ² /s ²
k_s	equivalent sand-grain roughness height	m
l	length	m
p_a	water vapor pressure	Pa
q_{ev}	evaporation rate	W/m ²
s	length scale of domain	-
u^*_{ABL}	friction velocity in ABL log-law	m/s
u	air velocity magnitude	m/s
u_a	local air velocity	m/s
u_{ref}	reference air velocity	m/s
w	width	m
x, y, z	Cartesian co-ordinates	m
z_0	aerodynamic roughness length	m
z_p	distance from point p to the wall	m
z_{ref}	reference height	m
C	convective heat transfer	W/m ²
C_s	roughness constant	-
E_d	heat loss by water vapor diffusion through skin	W/m ²
E_{re}	latent heat loss due to respiration	W/m ²
E_{sw}	evaporation heat loss due to sweating	W/m ²
G	global radiation	W/m ²
G	incident radiation	W/m ²
H	building height	m

Table N.5: Latin symbols (part 2)

Symbol	Description	Dimension
I	radiation intensity	W/m ²
I_u	stream-wise turbulent intensity	%
K_i	short-wave radiation flux	W/m ²
L	sensible (dry) heat loss due to respiration	W/m ²
L_i	long-wave radiation flux	W/m ²
LAD	Leaf Area Density	m ² /m ³
LAI	Leaf Area Index	m ² /m ²
M	rate of metabolic heat production	W/m ²
MET	measuring unit for the amount of energy required for a certain physical activity compared to the amount of energy required at rest.	MET (1 MET = 3.5 ml O ₂ per kg body weight per minute)
P_c	cooling power	W/m ³
Q	heat transfer rate	W/m ²
Q_e	latent heat flux	W/m ²
R	heat loss by radiation	W/m ²
R_c	thermal resistance of a construction	m ² K/W
RH	relative humidity	%
S_{str}	mean radiant flux density of the human body	W/m ²
T_{air}	air temperature	°C
T_e	outdoor temperature	°C
T_i	indoor temperature	°C
T_l	lower temperature limit of comfort band	°C
T_{max}	maximum air temperature	°C
T_{mrt}	mean radiant temperature	°C
T_n	neutral temperature	°C
T_o	operating temperature	°C
T_r	radiation temperature	°C
T_{rural}	rural surface temperature	°C
T_{surf}	surface temperature	°C
T_{upper}	upper temperature limit of comfort band	°C
U	wind velocity	m/s
U_{ref}	reference mean wind speed	m/s
W	rate of mechanical work accomplished	W/m ²

References

2011. *Adresboek VVZS (Verzorgings- Verpleeg- Ziekenhuizen en Serviceflats in Nederland)*. Redactie Adresboek, Capelle a/d IJssel

Air foundation, 2013. *Maaspad Rotterdam*. [Online] Available at: <http://www.airfoundation.nl/stedenbouw/v1/plugins/files/download.php> [Consulted on 7th of November, 2013]

ANSYS FLUENT, 2006. *User's guide*, ANSYS Inc. chapter 13.9 [Online]. Available at: <http://cdlab2.fluid.tuwien.ac.at/LEHRE/TURB/Fluent.Inc/fluent6.3.26/help/html/ug/node583.htm> [consulted on 26th of July, 2013]

ANSYS FLUENT 12.0, 2009. *Theory guide*. ANSYS Inc., p. 15 - 19 and p. 15 - 20

ANSYS FLUENT 12.0, 2009. *User's guide*. ANSYS Inc., p. 7 - 46, 7 - 47 and 7 - 130, chapter 13, 26 - 14 and 26 - 15

ASHRAE 2005, *Fundamentals Handbook*. Table 5 chapter 3

ASHRAE, 2010. *Standard 55: thermal environmental conditions for human occupancy*.

Banks, J., Carson, J., Nelson, B. and Nicol, D., 2001. *Discrete-event system simulation*. Prentice hall, p. 3

Blazejczyk, K., Epstein, Y., Jendritzky, G., Staiger, H. and Tinz, B., 2011. *Comparison of UTCI to selected thermal indices*. International Journal of Biometeorology 56 (3), p. 515 - 535

Blazejczyk, K., Jendritzky, G., Bröde, P., Fiala, D., Havenith, G., Epstein, Y., Psikuta, A. and Kampmann, B., 2013. *An introduction to the universal thermal climate index (UTCI)*. Geographia Polonica 86 (1), p. 5 - 10

Blocken, B., 2011. *CFD in building engineering - fundamentals and applications in urban physics and wind engineering*. Eindhoven University of Technology, p. 2, 12 and 28

Blocken, B., and Gualtieri, C., 2012. *Ten iterative steps for model development and evaluation applied to Computational Fluid Dynamics for Environmental Fluid Mechanics*. Environmental Modeling and Software 33, p. 1 - 22

Blocken, B., Stathopoulos, T., and Carmeliet, J., 2007. *CFD simulation of the atmospheric boundary layer: wall function problems*. Atmospheric Environment 41 (2), p. 238 - 252

Bone, A.H.L.G., 2007. *Bouwkunde tabellenboek*. Wolters Noordhoff, p. 206 - 209

Brandsma, T., 2010. *Warmte-eilandeffect van de stad Utrecht*. Zenit, p. 501

Bröde, P., Fiala, D., Blazejczyk, K., Holmér, I., Jendritzky, G., Kampmann, B., Tinz, B. and Havenith, G., 2011a. *Deriving the operational procedure for the Universal thermal climate index UTCI*. International Journal of Biometeorology 56 (3), p. 481 - 494

Bröde, P., Krüger, E.L., Rossi, F.A., and Fiala, D., 2011b. *Predicting urban outdoor thermal comfort by the universal thermal climate index UTCI - A case study in southern Brazil*. International Journal of Biometeorology 56 (3), p. 471 - 480

Buildings department Hong Kong, Document: *General Principles of Control of Overall Thermal Transfer Value*. [Online] Available at: <http://www.bd.gov.hk/english/documents/code/OTTV-02.pdf> [consulted on 25th of July, 2013]

Cajoto, V.I., Peromingo, J.A., Vicdeo, G.V., Leira, J.S., and Frojan, S., 2005. *Health impact of 2003 heat wave at Hospital de Riveira (A Coruna)*. *Annals of Internal Medicine* 22 (1), p. 15 - 20

Cebeci, T. and Bradshaw, P., 1977. *Momentum transfer in boundary layers*. New York: Hemisphere Publishing Corporation

CFD Online forum. Available at: <http://www.cfd-online.com/> [consulted at 15th of October, 2013]

Choi, J., Kim, J., and Woo, J., 2009. *A numerical study on the effects of skyscrapers on flow and dispersion in a metropolis*. The seventh International Conference on Urban Climate in Yokohoma, p. 1

Climate Proof Cities Consortium, project: Heat stress in the city of Rotterdam. Project leaders: Nijhuis, E.W.J.T. and Streng, J.M.A. Data received from: Elbers, J. Project website: <http://www.climatexchange.nl/sites/rotterdam/index.htm> [consulted on 15th of October]

Daanen, H.A.M., 2004. *Warm aanbevolen*. Rede, in verkorte vorm uitgesproken bij de aanvaarding van het ambt van bijzonder hoogleraar Thermofysiologie vanwege de Stichting het Vrije Universiteitsfonds, aan de faculteit der Bewegingswetenschappen van de Vrije Universiteit Amsterdam.

Daanen, H.A.M., and Herweijer, J., 2012. *Short high-intensity heat acclimation does not lead to adaptations in Young and elderly females - manuscript draft*. *European Journal of Applied Physiology*, p. 3

Daanen, H.A.M., Heusinkveld, B., van Hove, B., and van Riet, N., 2011. *Heat strain in elderly during heat waves in the Netherlands*. In: Kounalakis, S., Koskoulou, M. (Eds). *Abstract book XIV International Conference on Environmental Ergonomics Nafplio Greece 2011*, p.168 - 170

De Dear, R.J., Brager, G., and Cooper, D., 1997. *Developing and adaptive model of thermal comfort and preference*. Final report ASHRAE RP- 884.

De Nijs, T., Crommentuijn, L., Farjon, H., Leneman, H., Ligtoet, W., De Niet, W., and Schotten, K., 2002. *Vier scenario's van het landgebruik in 2030, achtergrondrapport bij de Nationale Natuurverkenning 2*, RIVM rapport 408764003, RIVM

Defraeye, T., Blocken, B. and Carmeliet, J., 2011. *An adjusted temperature wall function for turbulent forced convective heat transfer for bluff bodies in the atmospheric boundary layer*. *Building and Environment* 46 (11), p. 2130 - 2141

Diaz, J., Garcia, R., Velazquez De Castro, F., Hernandez, E., Lopez, C. and Otero, A., 2002. *Effects of extremely hot days on people older than 65 years in Seville (Spain) from 1986-1987*. *International Journal of Biometeorology* 46 (3), p. 145 - 149

DINED anthropometric database [Online] available at: <http://dined.io.tudelft.nl/nl/geron1998,204> [consulted on 15th of October, 2013]

Döpp, S., 2011. *Kennismontage: Hitze en Klimaat in de Stad*. TNO-publicatie, p. 5 - 13, 16 - 23

Dorland and Saunders, W.B., 2007. *Dorland's Medical Dictionary for Health*. Imprint of Elsevier

Duijm, F., Hendriks, U., and Meijer, G., 2007. *Lekker fris in school 2*. GGD Groningen.

Engineeringtoolbox [Online] available at: http://www.engineeringtoolbox.com/emissivity-coefficients-d_447.html [consulted on 26th of July 2013]

Fanger, P.O., 1972. *Thermal comfort*. New York: Mc Graw-Hill

Fiala, D., Lomas, K.J., and Stohrer, M., 1999. *A computer model of human thermoregulation for a wide range of environmental conditions: The passive system*. *Journal of Applied Physiology* 87 (5), p. 1957 - 1972

Fiala, D., Havenith, G., Bröde, P., Kampmann, B., and Jendritzky, G., 2011. *UTCI-Fiala multi-node model of human heat transfer and temperature regulation*. International Journal of Biometeorology 56 (3), p. 429 -4 41

Fluent tutorial, 2007. *Tutorial: using solar load model for indoor ventilation*. Fluent Inc.

Fluke corporation, 2009. *Emissivity values of common materials*. [Online] Available at: <http://www.emlab.com/m/store/Fluke%20Thermal%20Camera%20Emissivity%20Values.pdf> [consulted on 25th of July, 2013]

Franke, J., Hellsten, A., Schlünzen, H., and Carissimo, B., 2007. *Best practice guideline for the CFD simulation of flows in the urban environment*. COST Action 732

Gruyter, C., 2007. *Duizend doden bij hittegolf 2006*. nrc.nl

Haak, A., 2012. *Climate change and heat stress in residential buildings - evaluation of adaptation measures*. University of Technology Eindhoven, p. 31

Hansen, A., Bi, P., Ryan, P., Nitschke, M., Pisaniello, D. and Tucker, G., 2008. *The effect of heat waves on hospital admissions for renal disease in a temperate city in Australia*. International Journal of Epidemiology 37 (6), p. 1359 - 1365

Havenith, G., Fiala, D., Blazejczyk, K., Richards, M., Bröde, P., Holmér, I., 2011. *The UTCI-clothing model*. International Journal of Biometeorology 56 (3), p. 461 - 470

Heusinkveld, B.G., van Hove, L.W.A., Jacobs, C.M.J., Steeneveld, G.J., Elbers, J.A., Moors, E.J. and Holtslag, A.A.M., 2010. *Use of a mobile platform for assessing urban heat stress in Rotterdam*. Proceedings of the 7th Conference on Biometeorology in Freiburg, p. 433 - 438

Hirsch, C., Bouffieux, V., and Wilquem, F., 2002. *CFD simulation of the impact of new buildings on wind comfort in an urban area*. In: Augusti, G., Borri, C., and Sacre, C. (editors), 2002. *Impact of Wind and Storm on City life and Built Environment*, Proceedings of the Workshop CSTB in Nantes, p. 164 - 171

Höppe, P., 1999. *The physiological equivalent temperature - a Universal index for the assessment of the thermal environment*. International Journal of Biometeorology 43 (2), p. 71 - 75

Van Hove, B., Elbers, J., Jacobs, C., Heusinkveld, B., and Jans, W., 2011a. *Het stadsklimaat in Rotterdam. Een eerste analyse van de meetgegevens van het meteorologisch meetnet*. WUR publication

Van Hove, L.W.A., Steeneveld, G.J., Jacobs, C.M.J., Heusinkveld, B.G., Elbers, J.A., Moors, E.J., and Holtslag, A.A.M., 2011b. *Exploring the Urban Heat Island Intensity of Dutch cities*. Alterra report 2170, p. 7, 30 - 32

Huynen, M.M., Martens, P., Schram, D., Weijenberg, M.P., and Kunst, A.E., 2001. *The impact of heat waves and cold spells on mortality rates in the Dutch population*. Environmental Health Perspectives 109 (5), p. 463 - 470

ISSO, 2004. *Thermische behaaglijkheid; eisen voor de binnentemperaturen in gebouwen*. ISSO 74, Rotterdam

Jacobs, A.F.G., and Palland, C.L., 1982. *Indirect measurement of the latent heat flux of meadow grass from the energy balance - The sensible heat flux being measured by using the correlation technique*. Journal of Hydrology 58 (1-2), p. 159 - 166

KemTek Thermal Solutions, 2013. *Hot pavement*. [Online] Available at: http://www.kemtekthermal.com/pdfs/Hot_pavement.pdf [Consulted on 7th of November, 2013]

Kim, Y., and Baik, J. 2004. *Daily maximum urban heat island intensity in large cities in Korea*. Theoretical and Applied Climatology 79, p. 151 - 164

Koninklijk Nederlands Meteorologisch Instituut [Online] Available at: <http://www.knmi.nl/cms/content/37321/hittegolf> [Consulted on 14th of June, 2013]

- Koninklijk Nederlands Meteorologisch Instituut [Online] Available at: <http://www.knmi.nl/klimatologie/weeramateurs/UHL/> [Consulted on 14th of June, 2013]
- Koninklijk Nederlands Meteorologisch Instituut [Online] Available at: <http://www.knmi.nl/klimatologie/windrozen/> [Consulted on 8th of July, 2013]
- Klok, L., Zwart, S., Verhagen, H., and Mauri, E., 2012. *The surface heat island of Rotterdam and its relationship with urban surface characteristics*. Resources, Conservation and Recycling 64, p. 23 - 29
- Kovats, R.S., and Hajat, S., 2008. *Heat stress and public health: a critical review*. Annual Review of Public Health 29, p. 41 - 55
- Kunst, A.E., Looman, C.W.N., and Mackenbach, J.P., 1991. *The decline in winter excess mortality in the Netherlands*. International Journal of Epidemiology 20 (4), p. 971 - 977
- Lauder, B. and Spalding, D., 1974. *The numerical computation of turbulent flows*. Computer Methods in Applied Mechanics and Engineering 3 (2), p. 269 - 289
- Linden, P., 1999. *The fluid mechanics of natural ventilation*. Annual Review of Fluid Mechanics 31, p. 201 - 238
- Mackenbach, J.P., Borst, V. and Schols, J., 1997. *Heat-related mortality among nursing-home patients*. Lancet 349, p. 1297 - 1298
- Merema, B.J., 2013. *Computational analysis of climate change adaptation measures at the building and street scale focused on vegetative measures - Case study for the city of Arnhem*. University of Technology Eindhoven
- Mosteller, R.D., 1987. *Simplified calculation of body surface area*. The New England Journal of Medicine 317, p.1098
- NEN-EN 12464, 2011. *Licht en verlichting - verlichting van werkruimten - deel 1: werkruimten binnen*.
- Ocean Biochemistry lab. *Lecture on Advanced Very High Resolution Radiometer and Moderate resolution Imaging Spectrometer* [Online]. Available at: <http://ocean.stanford.edu/courses/EESS8/> (consulted on 15th of October, 2013)
- Oke, T.R., 1987. *Boundary Layer Climates*. 2nd edition. Routledge
- Oke, T.R., 1988. *The urban energy balance*. Progress in Physical Geography 12 (4), p. 471 - 508
- Oke, T.R., 1995. *The heat island of the urban boundary layer: characteristics, causes and effects*. In: J.E. Cermak (Editor), *Wind Climate in Cities* 277, p. 81 - 107
- Onmura, S., 2001. *Study on Evaporative Cooling Effect of Roof Lawn Gardens*. Energy and Buildings 33 (7), p. 653 - 666
- Oudin Astrom, D., Forsberg, B., and Rocklov, J. 2011. *Heat wave impact on morbidity and mortality in the elderly population: a review of recent studies*. Maturitas 69 (2), p. 99 - 105
- Parsons, K.C., and Webb, L.B., 1997. *Thermal Comfort Requirement for People with Physical Disabilities*.
- Parsons, N., Odumenya, M., Edwards, A., Lecky, F., and Pattison, G., 2011. *Modelling the effects of the weather on admissions to UK trauma units: A cross-sectional study*. Emergency Medicine Journal 28 (10), p. 851 - 855
- Peeters, L., de Dear, R., Hensen, J., and D'haeseleer, W., 2009. *Thermal comfort in residential buildings: Comfort values and scales for building energy simulation*. Applied Energy 86 (5), p. 772 - 780

Priyadarsini, R., Hien, W. N., and David, C.K.W., 2008. *Microclimatic modeling of the urban thermal environment of Singapore to mitigate urban heat island*. Solar Energy 82 (8), p. 727 - 745

Protek USA, *reflectance and emittance of building materials*. [Online] Available at: <http://www.protek-usa.com/pdf-new/SolarReflectanceEmittanceBldgMaterialsGraph.pdf> [consulted on 26th of July, 2013]

Rahola, B.S., van Oppen, P., and Mulder, K., 2009. *Heat in the city: an inventory of knowledge deficiencies regarding heat stress in Dutch cities and options for its mitigation*. National Research Programme Climate changes Spatial Planning, p. 4, 9 - 14

Ramponi, R. and Blocken, B., 2012. *CFD simulation of cross-ventilation for a generic isolated building: Impact of computational parameters*. Building and Environment 53, p. 34 - 48

2010. *Reader Lighting technology course 7S630*, Eindhoven University of Technology

Richards, P.J., and Hoxey, R.P., 1993. *Appropriate boundary conditions for computational wind engineering models using the k- ϵ turbulence model*. Journal of Wind Engineering and Industrial Aerodynamics 46 - 47, p. 145 - 153

Robitu, M., Musy, M., Inard, C., and Groleau, D., 2006. *Modeling the influence of vegetation and water pond on urban microclimate*. Solar Energy 80 (4), p. 435 - 447

Roodenburg, J., 1983. *Adaptation of rural minimum temperature forecasts to an urban environment*. Archives for Meteorology, Geophysics, and Bioclimatology Series B 32 (4), p. 395 - 401

Rutten, P.G.S., and Hensen, J.L.M. 2002. *Thermische behaaglijkheid in verpleeghuizen in Nederland in de zomersituatie*. Prelude B.V. 01

Schellen, L., Loomans, M.G.L.C., Kingma, B.R.M., de Wit, M.H., Frijns, A.J.H., and Marken Lichtenbelt, W.D., 2013. *The use of a thermophysiological model in the built environment to predict thermal sensation: Coupling with the indoor environment and thermal sensation*. Building and Environment 59, p. 10 - 22

Sørensen, D.N., and Nielsen, P.V., 2003. *Quality control of computational fluid dynamics in indoor environments*. Indoor Air 13 (1), p. 2 - 17

Spagnolo, J., and de Dear, R., 2003. *A field study of thermal comfort in outdoor and semi-outdoor environments in subtropical Sydney Australia*. Building and Environment 38 (5), p. 721 - 738

Steenefeld, G.J., and Hove, L.W.A., 2010. *Een eerste inschatting van het 'Urban Heat Island' effect voor Rotterdam en omgeving: Een modelstudie*. WUR publication, p. 7

Steenefeld, G.J., Koopmans, S., Heusinkveld, B.G., van Hove, L.W.A., and Holtslag, A.A.M., 2011. *Quantifying Urban Heat Island effects and outdoor human comfort in relation to urban morphology by exploring observations from hobby-meteorologists in the Netherlands*. Submitted to Journal of Geophysical Research

Stone, K., Daanen, H.A.M., Jonkhoff, W., and Bosch, P., 2013. *Quantifying the sensitivity of our urban systems - impact functions for urban systems*. National Research Programme Knowledge for Climate, p. 53

Takahashi, K., Yoshida, H., Tanaka, Y., Aotake, N. and Wang, F., 2003, *Heat flux measurement of urban boundary layers in Kyoto city and its prediction by CFD simulation*, 8th International IBPSA Conference Eindhoven

Thorsson, S., Lindberg, F., Eliasson, I., and Holmer, B., 2007. *Different methods for estimating the mean radiant temperature in an outdoor urban setting*. International Journal of Climatology 27 (14), p. 1983 - 1993

Tominaga, Y., Mochida, A., Yoshie, R., Kataoka, H., Nozu, T., Yoshikawa, M., and Shirasawa, T., 2008. *AJG guidelines for practical applications of CFD to pedestrian wind environment around buildings*. Journal of Wind Engineering and Industrial Aerodynamics 96 (10-11), p. 1749 - 1761

Toparlar, Y., 2012. *Computational analysis of climate change adaptation measures at the building and street scale focused on evaporative cooling: case study for Bergpolder Zuid*. University of Technology Eindhoven.

University of Giessen Germany, *Plant Parameter Data*. [Online] Available at: <http://www.uni-giessen.de/~gh1461/plapada/php/list/content.php> [consulted on 15th of October, 2013]

UTCI, UTCI-calculator. Available at: <http://www.utci.org/> [consulted on 15th of October, 2013]

Van Hoof, J. and Hensen, J.L.M., 2006. *Thermal comfort and older adults*. *Gerontechnology* 4 (4), p. 223-228

Van Hooff, T. and Blocken, B., 2010. *Coupled urban wind flow and indoor natural ventilation modelling on a high-resolution grid: A case study for the Amsterdam ArenA stadium*. *Environmental Modelling and Software* 25 (1), p. 51 - 65

Van Hooff, T., van der Heijden, M.G.M., Blocken, B., Hensen, J.L.M., and Timmermans, H.J.P., 2012. *Notes on performance indicators for Climate Proof Cities*. Unit Building Physics and Services, Eindhoven University of Technology.

Vanhems P., Gambotti L., and Fabry J. 2003. *Excess rate of in-hospital death in Lyons, France, during the August 2003 heat wave*. *New England Journal of Medicine* 349, p. 2077 - 2078

Wieringa, J., 1992. *Updating the Davenport roughness classification*. *Journal of Wind Engineering and Industrial Aerodynamics* 41 (1-3), p. 357 - 368

Wong, E., Hogan, K., Rosenberg, J., and Andrea, D., 2008. *Reducing Urban Heat Islands: Compendium of Strategies*. Publication of the US Environmental Protection Agency, p. 7, 13 - 16

Zulovich, J., 1993. *Active Solar Collectors for Farm Buildings - University of Missouri*. [Online] Available at: <http://extension.missouri.edu/publications/DisplayPub.aspx?P=G1971> [Consulted on 25th of July 2013]

Appendix 1: subdomains

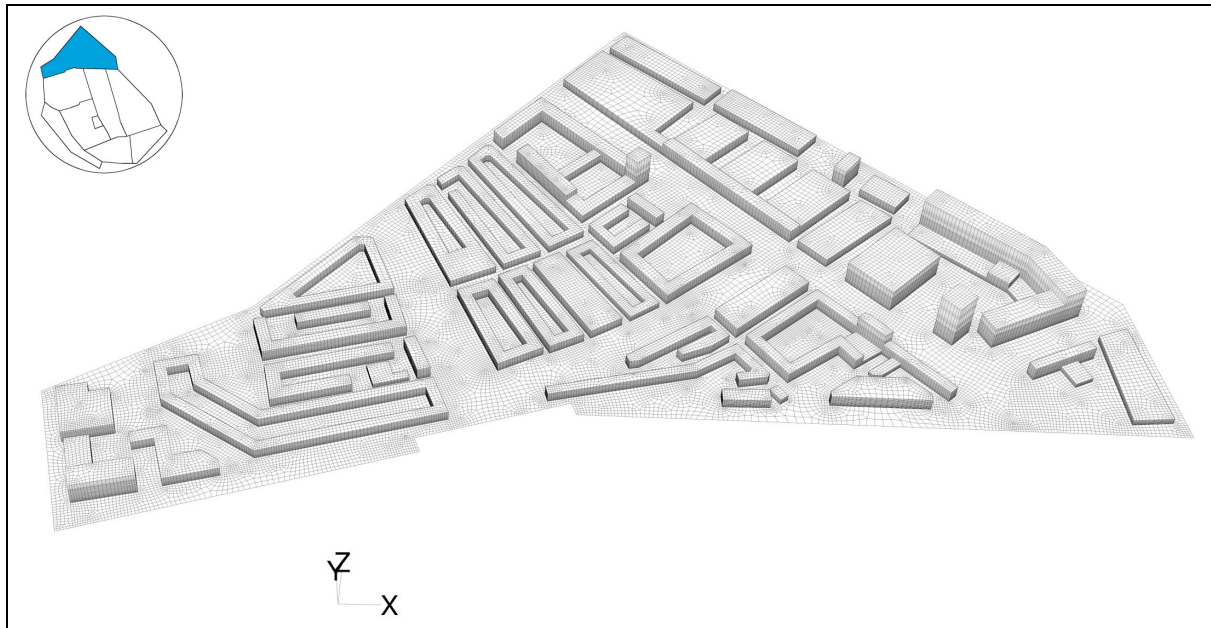


Figure A1.1: Subdomain 1 with 3.1 million cells

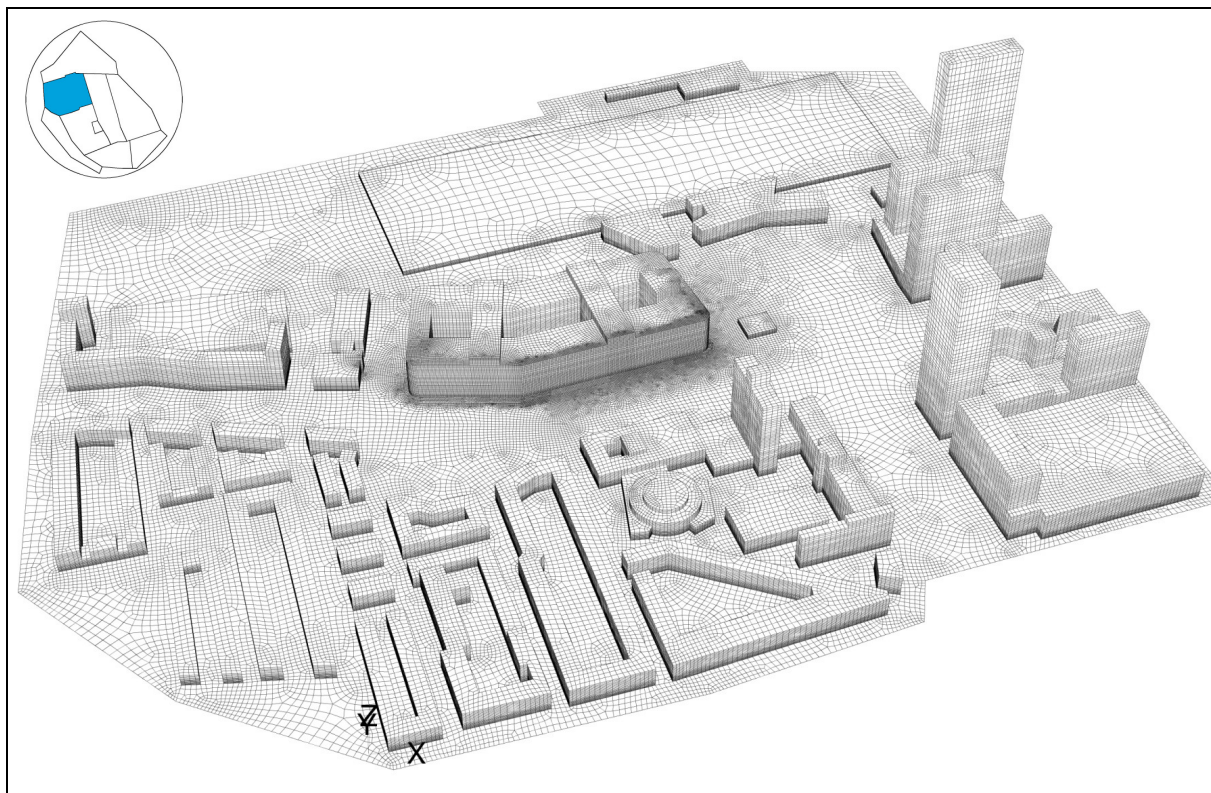


Figure A1.2: Subdomain 2 with 4.7 million cells

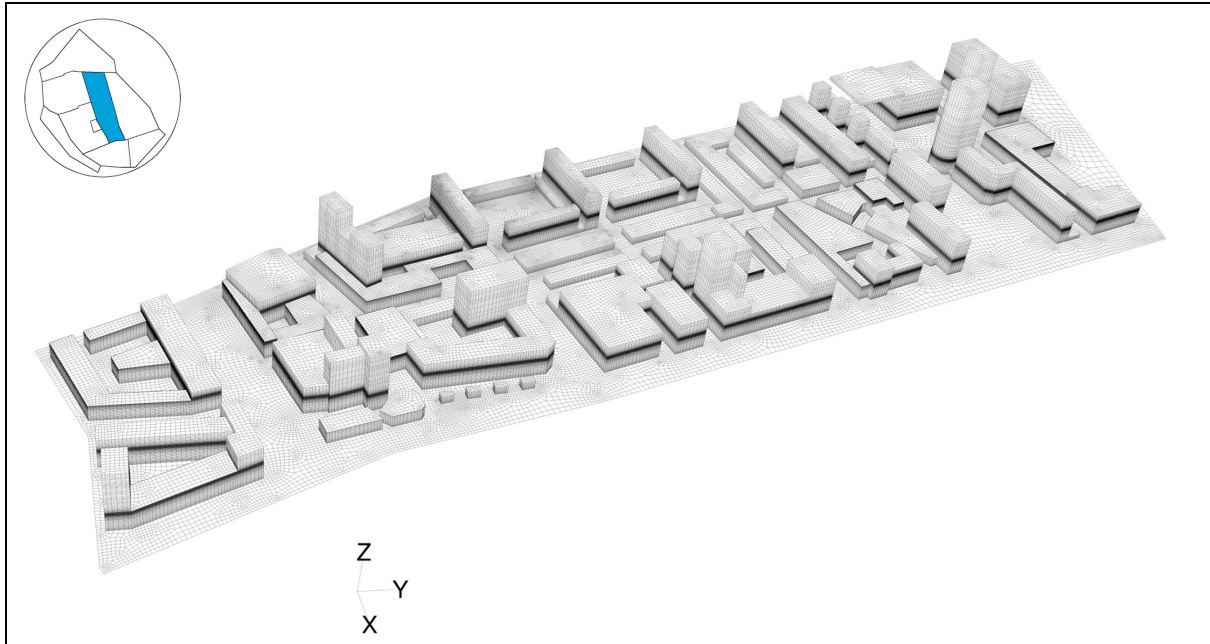


Figure A1.3: Subdomain 3 with 6.0 million cells

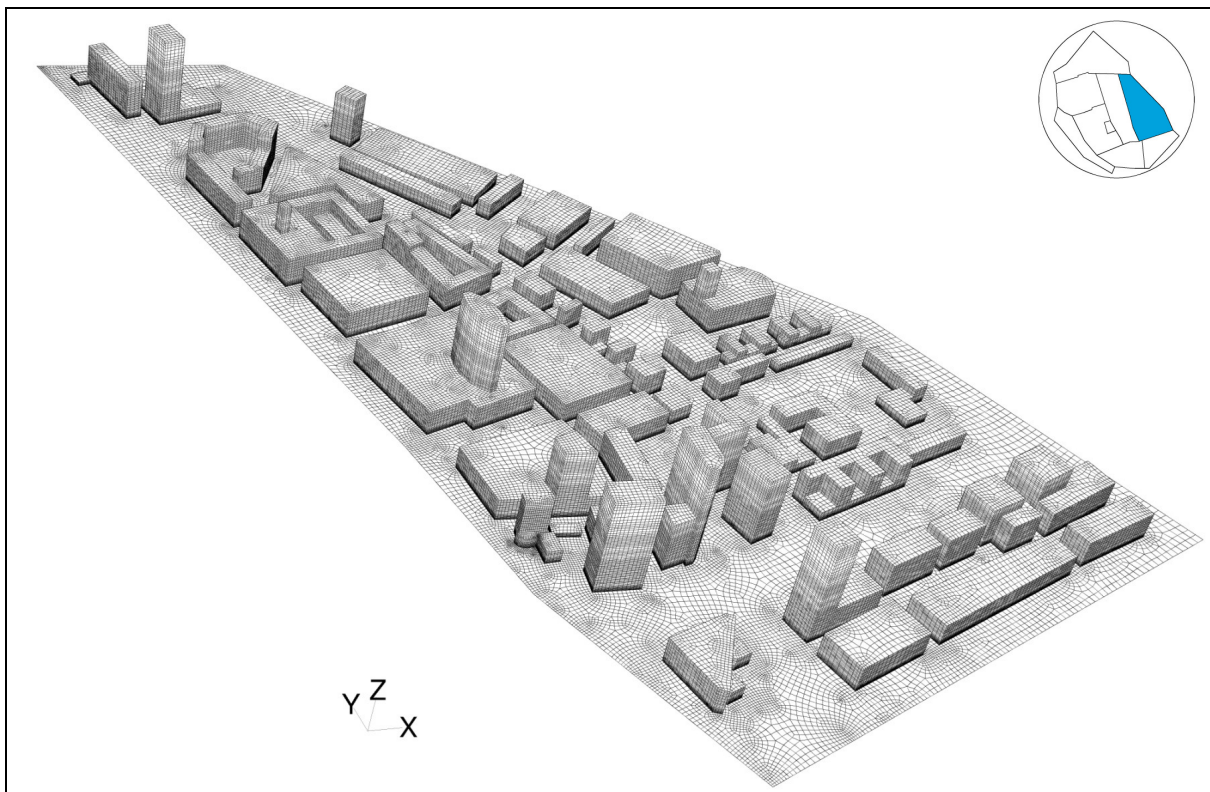


Figure A1.4: Subdomain 4 with 3.7 million cells

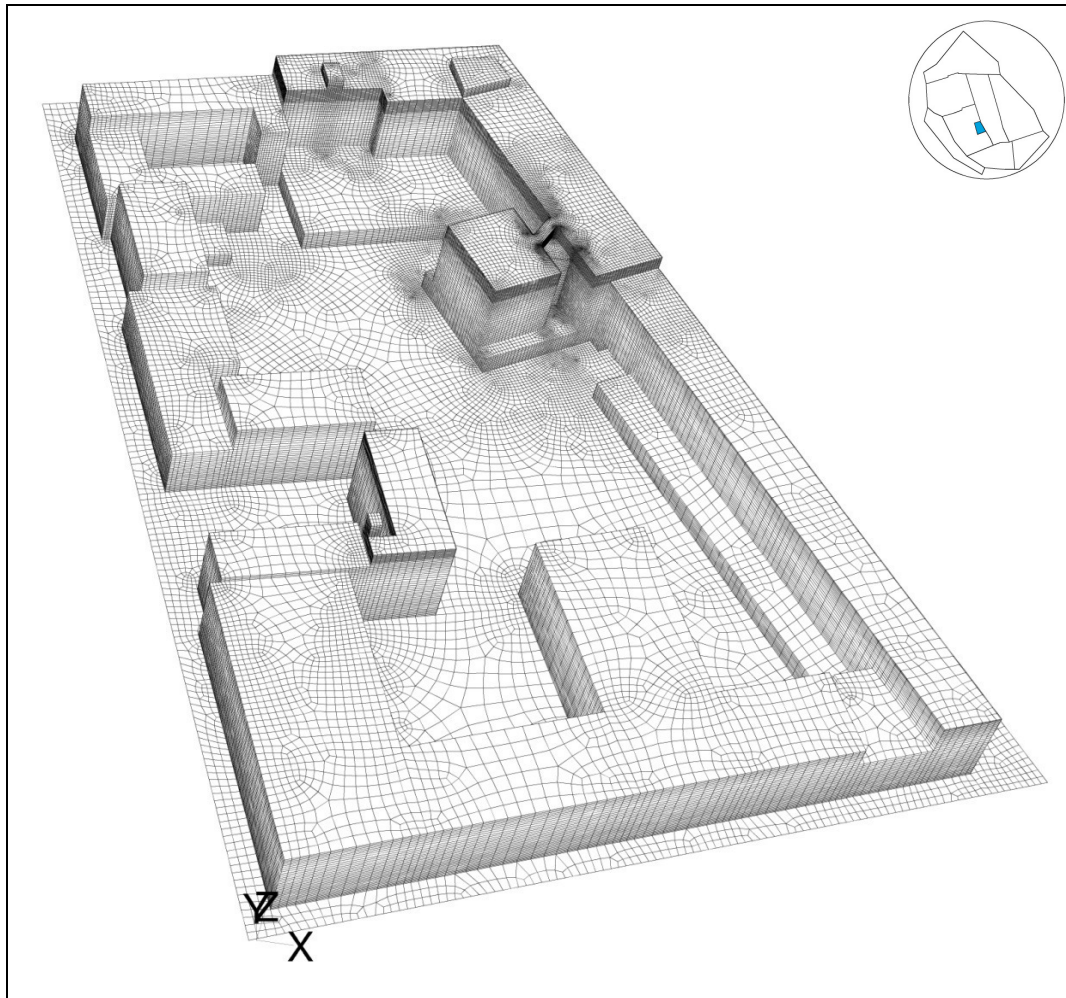


Figure A1.5: Subdomain 5 with 2.2 million cells

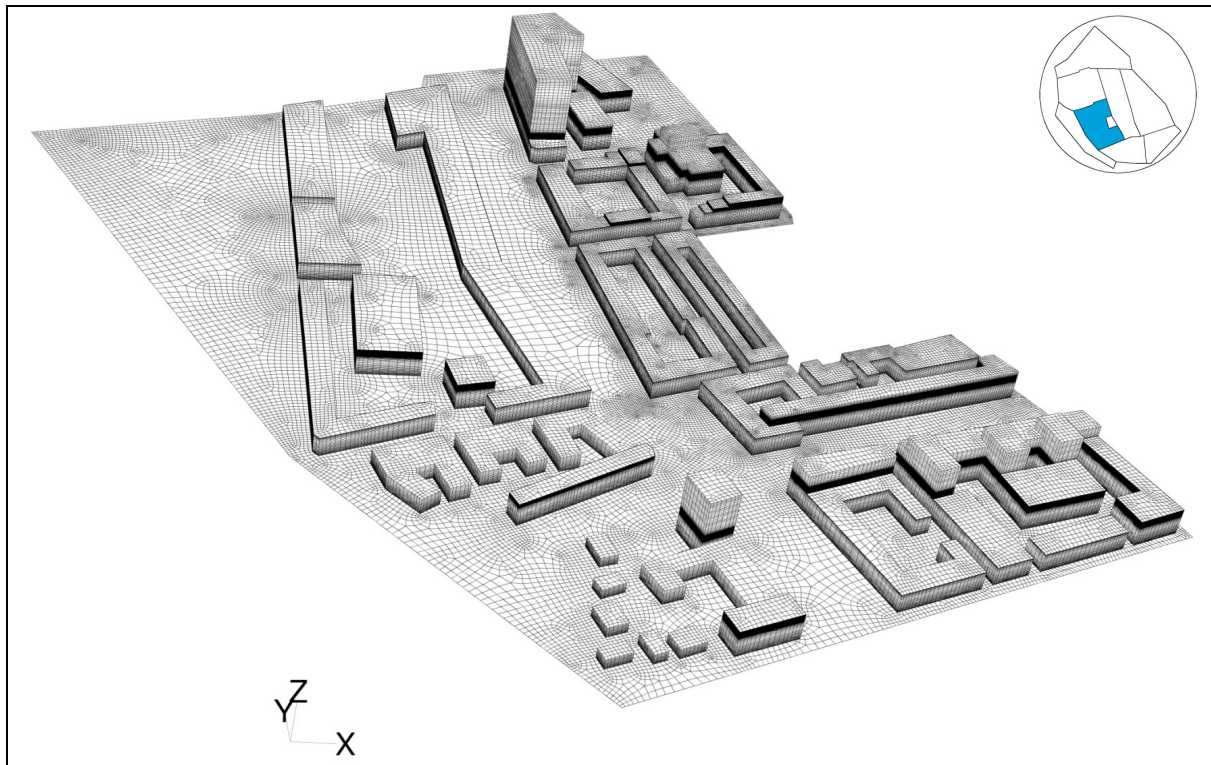


Figure A1.6: Subdomain 6 with 4.6 million cells

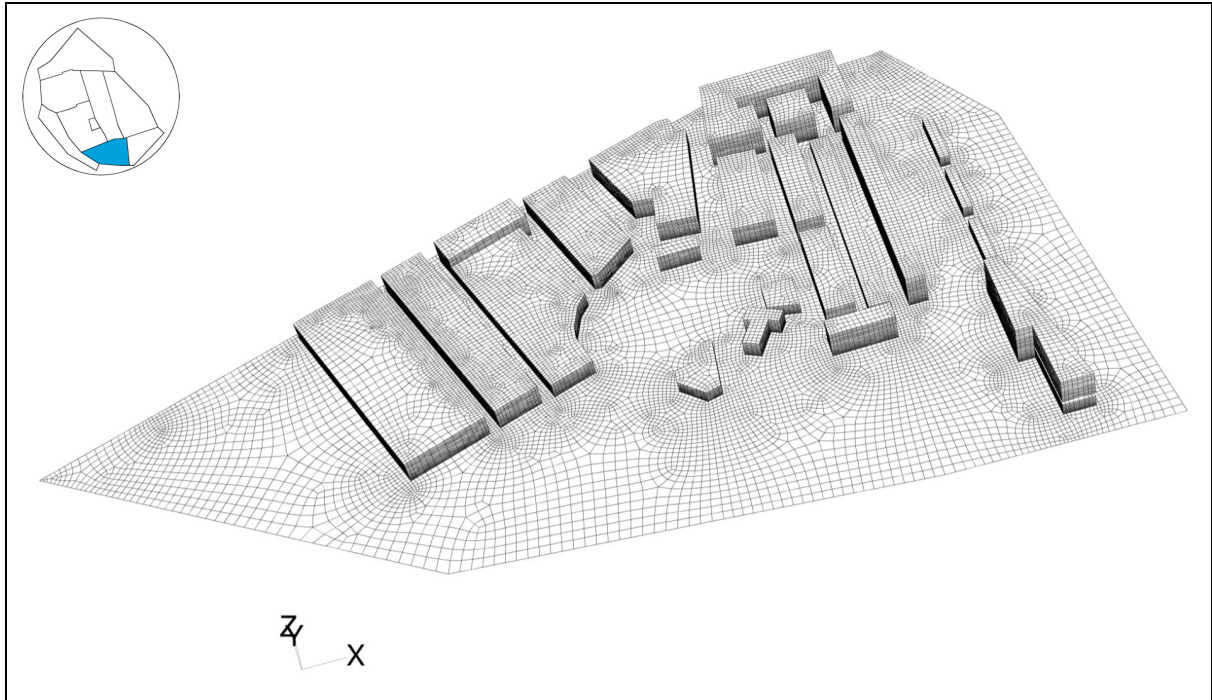


Figure A1.7: Subdomain 7 with 1.3 million cells

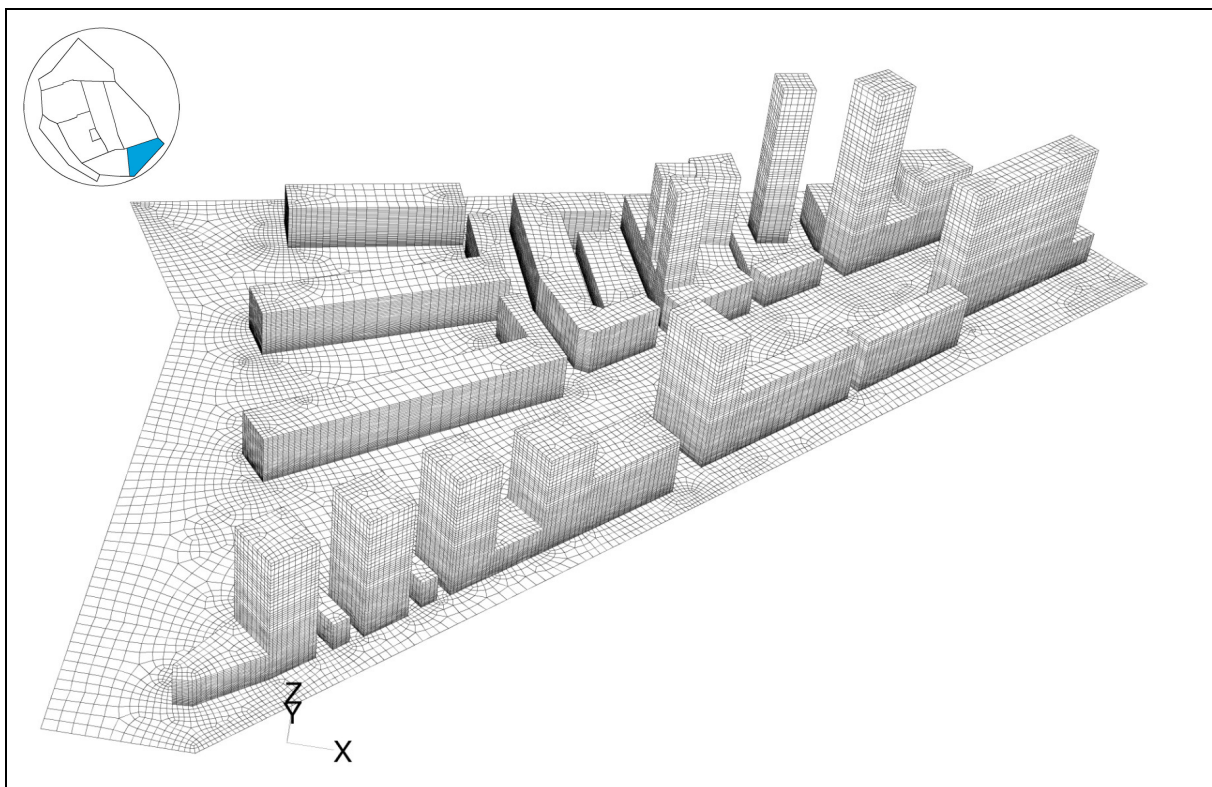


Figure A1.8: Subdomain 8 with 1.2 million cells

Appendix 2: inlet profiles

Inlet profiles for model 1 and 2

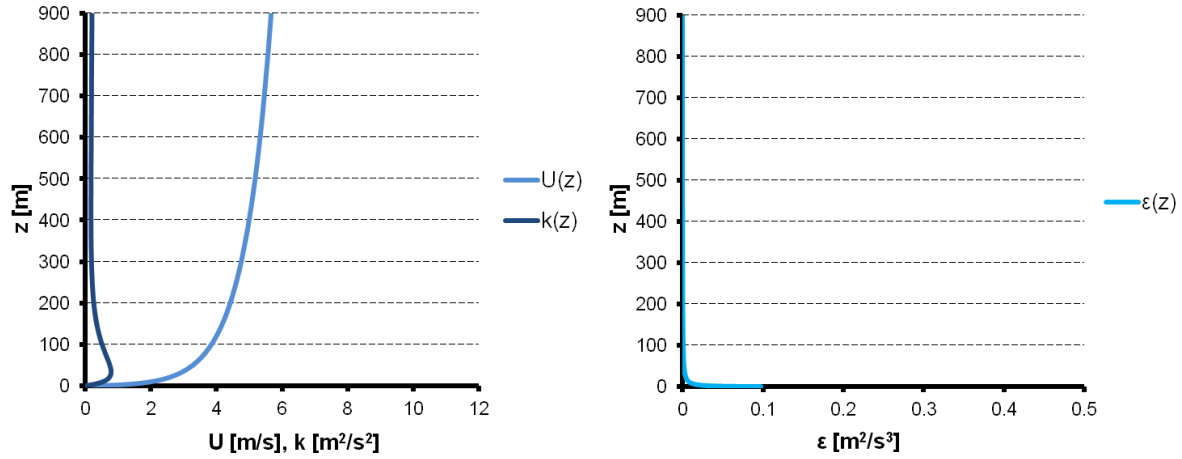


Figure A2.1: Inlet profiles for wind velocity, turbulent kinetic energy and turbulent dissipation rate for $U_{ref} = 2$ m/s and $z_0 = 1.0$ m

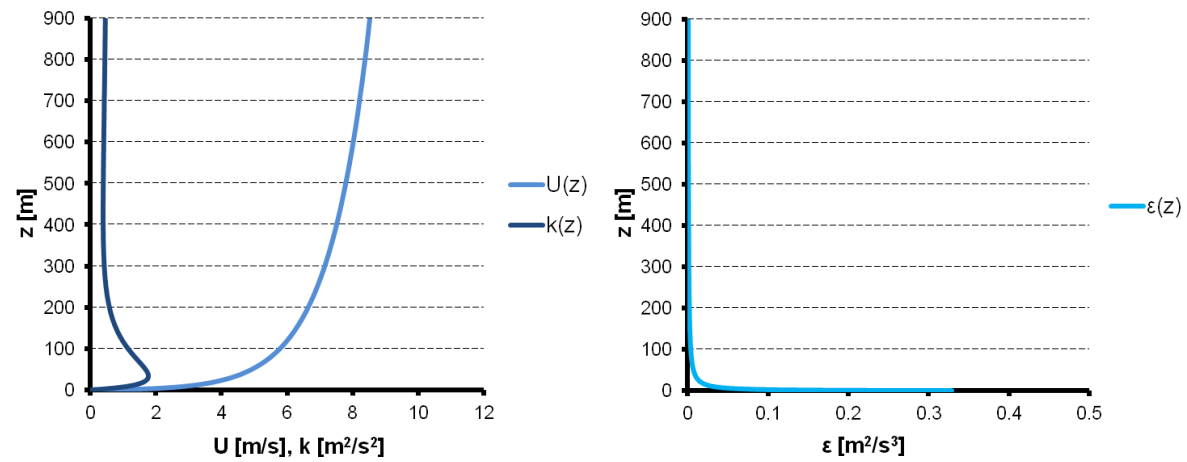


Figure A2.2: Inlet profiles for wind velocity, turbulent kinetic energy and turbulent dissipation rate for $U_{ref} = 3$ m/s and $z_0 = 1.0$ m

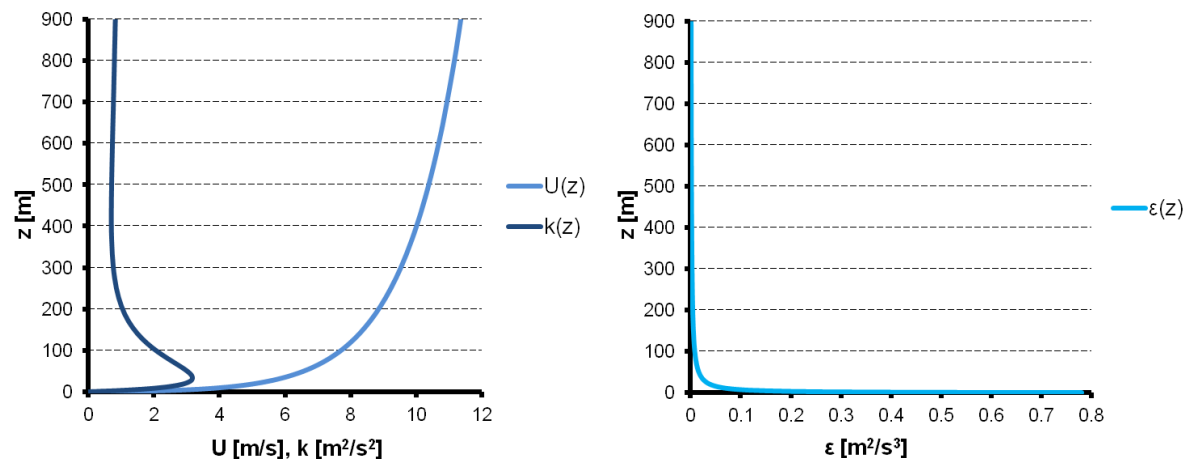


Figure A2.3: Inlet profiles for wind velocity, turbulent kinetic energy and turbulent dissipation rate for $U_{ref} = 4$ m/s and $z_0 = 1.0$ m

Inlet profiles for model 3

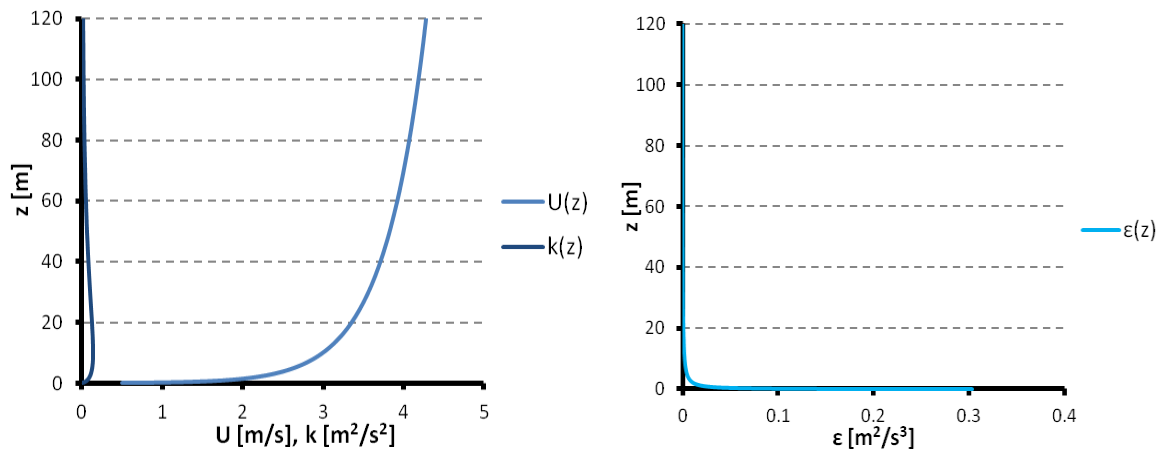


Figure A2.4: Inlet profiles for wind velocity, turbulent kinetic energy and turbulent dissipation rate for $U_{ref} = 3$ m/s and $z_0 = 0.03$ m

Appendix 3: UTCI MATLAB script

```

% MATLAB script based on:
% UTCI, Version a 0.002, October 2009
% Copyright © 2009 Peter Broede
% Program for calculating UTCI Temperature (UTCI)
% released for public use after termination of COST Action 730
%
% The above mentioned script was adjusted to be readable by MATLAB
% A different formula for the calculation of the water vapor pressure is
% used
%
% Input parameters (all of type DOUBLE PRECISION)
% Ta      : air temperature, degree Celsius
% RH: Relative Humidity (%)
% ehPa    : water vapour presure, hPa=hecto Pascal
% D_Tmrt  : T-mrt (mean radiant temperature, degree Celsius) - Ta
% val0m   : wind speed 10 m above ground level in m/s

clear all

importdata('D:\My Documents\data UTCI\UTCI_case1_input.txt');
xcoordinater = ans.data(:,2);
ycoordinater = ans.data(:,3);
Tar = ans.data(:,7);
D_Tmrtr = ans.data(:,6);
var = ans.data(:,5);

fid_out = fopen(['D:\My Documents\data UTCI\UTCI_case1_output.txt'],'w'); %
Open file for reading (default)

for i=1:length(Tar);
    xcoordinate=xcoordinater(i);
    ycoordinate=ycoordinater(i);
    Ta=Tar(i);
    if Ta>=58.01
        Ta=58;
    end
    D_Tmrt=D_Tmrtr(i);
    RH=34;
    %RH depends on date/time
    va=var(i);
    if va==0
        va=0.01;
    end
    psat=611*exp(17.08*Ta/(234.18+Ta));
    Pa=psat*(RH/100);
    kPa=Pa/1000;

    UTCI_approx=Ta+...
        ( 6.07562052E-01 ) + ...
        ( -2.27712343E-02 ) * Ta + ...
        ( 8.06470249E-04 ) * Ta*Ta + ...
        ( -1.54271372E-04 ) * Ta*Ta*Ta + ...
        ( -3.24651735E-06 ) * Ta*Ta*Ta*Ta + ...
        ( 7.32602852E-08 ) * Ta*Ta*Ta*Ta*Ta + ...
        ( 1.35959073E-09 ) * Ta*Ta*Ta*Ta*Ta*Ta + ...
        ( -2.25836520E+00 ) * va + ...
        ( 8.80326035E-02 ) * Ta*va + ...

```

```

( 2.168444454E-03 ) * Ta*Ta*va + ...
( -1.53347087E-05 ) * Ta*Ta*Ta*va + ...
( -5.72983704E-07 ) * Ta*Ta*Ta*Ta*va + ...
( -2.55090145E-09 ) * Ta*Ta*Ta*Ta*Ta*va + ...
( -7.51269505E-01 ) * va*va + ...
( -4.08350271E-03 ) * Ta*va*va + ...
( -5.21670675E-05 ) * Ta*Ta*va*va + ...
( 1.94544667E-06 ) * Ta*Ta*Ta*va*va + ...
( 1.14099531E-08 ) * Ta*Ta*Ta*Ta*va*va + ...
( 1.58137256E-01 ) * va*va*va + ...
( -6.57263143E-05 ) * Ta*va*va*va + ...
( 2.22697524E-07 ) * Ta*Ta*va*va*va + ...
( -4.16117031E-08 ) * Ta*Ta*Ta*va*va*va + ...
( -1.27762753E-02 ) * va*va*va*va + ...
( 9.66891875E-06 ) * Ta*va*va*va*va + ...
( 2.52785852E-09 ) * Ta*Ta*va*va*va*va + ...
( 4.56306672E-04 ) * va*va*va*va*va + ...
( -1.74202546E-07 ) * Ta*va*va*va*va*va + ...
( -5.91491269E-06 ) * va*va*va*va*va*va + ...
( 3.98374029E-01 ) * D_Tmrt + ...
( 1.83945314E-04 ) * Ta*D_Tmrt + ...
( -1.73754510E-04 ) * Ta*Ta*D_Tmrt + ...
( -7.60781159E-07 ) * Ta*Ta*Ta*D_Tmrt + ...
( 3.77830287E-08 ) * Ta*Ta*Ta*Ta*D_Tmrt + ...
( 5.43079673E-10 ) * Ta*Ta*Ta*Ta*Ta*D_Tmrt + ...
( -2.00518269E-02 ) * va*D_Tmrt + ...
( 8.92859837E-04 ) * Ta*va*D_Tmrt + ...
( 3.45433048E-06 ) * Ta*Ta*va*D_Tmrt + ...
( -3.77925774E-07 ) * Ta*Ta*Ta*va*D_Tmrt + ...
( -1.69699377E-09 ) * Ta*Ta*Ta*Ta*va*D_Tmrt + ...
( 1.69992415E-04 ) * va*va*D_Tmrt + ...
( -4.99204314E-05 ) * Ta*va*va*D_Tmrt + ...
( 2.47417178E-07 ) * Ta*Ta*va*va*D_Tmrt + ...
( 1.07596466E-08 ) * Ta*Ta*Ta*va*va*D_Tmrt + ...
( 8.49242932E-05 ) * va*va*va*D_Tmrt + ...
( 1.35191328E-06 ) * Ta*va*va*va*D_Tmrt + ...
( -6.21531254E-09 ) * Ta*Ta*va*va*va*D_Tmrt + ...
( -4.99410301E-06 ) * va*va*va*va*D_Tmrt + ...
( -1.89489258E-08 ) * Ta*va*va*va*va*D_Tmrt + ...
( 8.15300114E-08 ) * va*va*va*va*va*D_Tmrt + ...
( 7.55043090E-04 ) * D_Tmrt*D_Tmrt + ...
( -5.65095215E-05 ) * Ta*D_Tmrt*D_Tmrt + ...
( -4.52166564E-07 ) * Ta*Ta*D_Tmrt*D_Tmrt + ...
( 2.46688878E-08 ) * Ta*Ta*Ta*D_Tmrt*D_Tmrt + ...
( 2.42674348E-10 ) * Ta*Ta*Ta*Ta*D_Tmrt*D_Tmrt + ...
( 1.54547250E-04 ) * va*D_Tmrt*D_Tmrt + ...
( 5.24110970E-06 ) * Ta*va*D_Tmrt*D_Tmrt + ...
( -8.75874982E-08 ) * Ta*Ta*va*D_Tmrt*D_Tmrt + ...
( -1.50743064E-09 ) * Ta*Ta*Ta*va*D_Tmrt*D_Tmrt + ...
( -1.56236307E-05 ) * va*va*D_Tmrt*D_Tmrt + ...
( -1.33895614E-07 ) * Ta*va*va*D_Tmrt*D_Tmrt + ...
( 2.49709824E-09 ) * Ta*Ta*va*va*D_Tmrt*D_Tmrt + ...
( 6.51711721E-07 ) * va*va*va*D_Tmrt*D_Tmrt + ...
( 1.94960053E-09 ) * Ta*va*va*va*D_Tmrt*D_Tmrt + ...
( -1.00361113E-08 ) * va*va*va*va*D_Tmrt*D_Tmrt + ...
( -1.21206673E-05 ) * D_Tmrt*D_Tmrt*D_Tmrt + ...
( -2.18203660E-07 ) * Ta*D_Tmrt*D_Tmrt*D_Tmrt + ...
( 7.51269482E-09 ) * Ta*Ta*D_Tmrt*D_Tmrt*D_Tmrt + ...
( 9.79063848E-11 ) * Ta*Ta*Ta*D_Tmrt*D_Tmrt*D_Tmrt + ...
( 1.25006734E-06 ) * va*D_Tmrt*D_Tmrt*D_Tmrt + ...
( -1.81584736E-09 ) * Ta*va*D_Tmrt*D_Tmrt*D_Tmrt + ...

```



```

( -3.52197671E-10 ) * Ta*Ta*va*D_Tmrt*D_Tmrt*D_Tmrt + ...
( -3.36514630E-08 ) * va*va*D_Tmrt*D_Tmrt*D_Tmrt + ...
( 1.35908359E-10 ) * Ta*va*va*D_Tmrt*D_Tmrt*D_Tmrt + ...
( 4.17032620E-10 ) * va*va*va*D_Tmrt*D_Tmrt*D_Tmrt + ...
( -1.30369025E-09 ) * D_Tmrt*D_Tmrt*D_Tmrt*D_Tmrt + ...
( 4.13908461E-10 ) * Ta*D_Tmrt*D_Tmrt*D_Tmrt*D_Tmrt + ...
( 9.22652254E-12 ) * Ta*Ta*D_Tmrt*D_Tmrt*D_Tmrt*D_Tmrt + ...
( -5.08220384E-09 ) * va*D_Tmrt*D_Tmrt*D_Tmrt*D_Tmrt + ...
( -2.24730961E-11 ) * Ta*va*D_Tmrt*D_Tmrt*D_Tmrt*D_Tmrt + ...
( 1.17139133E-10 ) * va*va*D_Tmrt*D_Tmrt*D_Tmrt*D_Tmrt + ...
( 6.62154879E-10 ) * D_Tmrt*D_Tmrt*D_Tmrt*D_Tmrt*D_Tmrt + ...
( 4.03863260E-13 ) * Ta*D_Tmrt*D_Tmrt*D_Tmrt*D_Tmrt*D_Tmrt + ...
( 1.95087203E-12 ) * va*D_Tmrt*D_Tmrt*D_Tmrt*D_Tmrt*D_Tmrt + ...
( -4.73602469E-12 ) * D_Tmrt*D_Tmrt*D_Tmrt*D_Tmrt*D_Tmrt*D_Tmrt +
...
( 5.12733497E+00 ) * kPa + ...
( -3.12788561E-01 ) * Ta*kPa + ...
( -1.96701861E-02 ) * Ta*Ta*kPa + ...
( 9.99690870E-04 ) * Ta*Ta*Ta*kPa + ...
( 9.51738512E-06 ) * Ta*Ta*Ta*Ta*kPa + ...
( -4.66426341E-07 ) * Ta*Ta*Ta*Ta*Ta*kPa + ...
( 5.48050612E-01 ) * va*kPa + ...
( -3.30552823E-03 ) * Ta*va*kPa + ...
( -1.64119440E-03 ) * Ta*Ta*va*kPa + ...
( -5.16670694E-06 ) * Ta*Ta*Ta*va*kPa + ...
( 9.52692432E-07 ) * Ta*Ta*Ta*Ta*va*kPa + ...
( -4.29223622E-02 ) * va*va*kPa + ...
( 5.00845667E-03 ) * Ta*va*va*kPa + ...
( 1.00601257E-06 ) * Ta*Ta*va*va*kPa + ...
( -1.81748644E-06 ) * Ta*Ta*Ta*va*va*kPa + ...
( -1.25813502E-03 ) * va*va*va*kPa + ...
( -1.79330391E-04 ) * Ta*va*va*va*kPa + ...
( 2.34994441E-06 ) * Ta*Ta*va*va*va*kPa + ...
( 1.29735808E-04 ) * va*va*va*va*kPa + ...
( 1.29064870E-06 ) * Ta*va*va*va*va*kPa + ...
( -2.28558686E-06 ) * va*va*va*va*va*kPa + ...
( -3.69476348E-02 ) * D_Tmrt*kPa + ...
( 1.62325322E-03 ) * Ta*D_Tmrt*kPa + ...
( -3.14279680E-05 ) * Ta*Ta*D_Tmrt*kPa + ...
( 2.59835559E-06 ) * Ta*Ta*Ta*D_Tmrt*kPa + ...
( -4.77136523E-08 ) * Ta*Ta*Ta*Ta*D_Tmrt*kPa + ...
( 8.64203390E-03 ) * va*D_Tmrt*kPa + ...
( -6.87405181E-04 ) * Ta*va*D_Tmrt*kPa + ...
( -9.13863872E-06 ) * Ta*Ta*va*D_Tmrt*kPa + ...
( 5.15916806E-07 ) * Ta*Ta*Ta*va*D_Tmrt*kPa + ...
( -3.59217476E-05 ) * va*va*D_Tmrt*kPa + ...
( 3.28696511E-05 ) * Ta*va*va*D_Tmrt*kPa + ...
( -7.10542454E-07 ) * Ta*Ta*va*va*D_Tmrt*kPa + ...
( -1.24382300E-05 ) * va*va*va*D_Tmrt*kPa + ...
( -7.38584400E-09 ) * Ta*va*va*va*D_Tmrt*kPa + ...
( 2.20609296E-07 ) * va*va*va*va*D_Tmrt*kPa + ...
( -7.32469180E-04 ) * D_Tmrt*D_Tmrt*kPa + ...
( -1.87381964E-05 ) * Ta*D_Tmrt*D_Tmrt*kPa + ...
( 4.80925239E-06 ) * Ta*Ta*D_Tmrt*D_Tmrt*kPa + ...
( -8.75492040E-08 ) * Ta*Ta*Ta*D_Tmrt*D_Tmrt*kPa + ...
( 2.77862930E-05 ) * va*D_Tmrt*D_Tmrt*kPa + ...
( -5.06004592E-06 ) * Ta*va*D_Tmrt*D_Tmrt*kPa + ...
( 1.14325367E-07 ) * Ta*Ta*va*D_Tmrt*D_Tmrt*kPa + ...
( 2.53016723E-06 ) * va*va*D_Tmrt*D_Tmrt*kPa + ...
( -1.72857035E-08 ) * Ta*va*va*D_Tmrt*D_Tmrt*kPa + ...
( -3.95079398E-08 ) * va*va*va*D_Tmrt*D_Tmrt*kPa + ...

```

(-3.59413173E-07) * D_Tmrt*D_Tmrt*D_Tmrt*kPa + ...
 (7.04388046E-07) * Ta*D_Tmrt*D_Tmrt*D_Tmrt*kPa + ...
 (-1.89309167E-08) * Ta*Ta*D_Tmrt*D_Tmrt*D_Tmrt*kPa + ...
 (-4.79768731E-07) * va*D_Tmrt*D_Tmrt*D_Tmrt*kPa + ...
 (7.96079978E-09) * Ta*va*D_Tmrt*D_Tmrt*D_Tmrt*kPa + ...
 (1.62897058E-09) * va*va*D_Tmrt*D_Tmrt*D_Tmrt*kPa + ...
 (3.94367674E-08) * D_Tmrt*D_Tmrt*D_Tmrt*D_Tmrt*kPa + ...
 (-1.18566247E-09) * Ta*D_Tmrt*D_Tmrt*D_Tmrt*D_Tmrt*kPa + ...
 (3.34678041E-10) * va*D_Tmrt*D_Tmrt*D_Tmrt*D_Tmrt*kPa + ...
 (-1.15606447E-10) * D_Tmrt*D_Tmrt*D_Tmrt*D_Tmrt*D_Tmrt*kPa + ...
 (-2.80626406E+00) * kPa*kPa + ...
 (5.48712484E-01) * Ta*kPa*kPa + ...
 (-3.99428410E-03) * Ta*Ta*kPa*kPa + ...
 (-9.54009191E-04) * Ta*Ta*Ta*kPa*kPa + ...
 (1.93090978E-05) * Ta*Ta*Ta*Ta*kPa*kPa + ...
 (-3.08806365E-01) * va*kPa*kPa + ...
 (1.16952364E-02) * Ta*va*kPa*kPa + ...
 (4.95271903E-04) * Ta*Ta*va*kPa*kPa + ...
 (-1.90710882E-05) * Ta*Ta*Ta*va*kPa*kPa + ...
 (2.10787756E-03) * va*va*kPa*kPa + ...
 (-6.98445738E-04) * Ta*va*va*kPa*kPa + ...
 (2.30109073E-05) * Ta*Ta*va*va*kPa*kPa + ...
 (4.17856590E-04) * va*va*va*kPa*kPa + ...
 (-1.27043871E-05) * Ta*va*va*va*kPa*kPa + ...
 (-3.04620472E-06) * va*va*va*va*kPa*kPa + ...
 (5.14507424E-02) * D_Tmrt*kPa*kPa + ...
 (-4.32510997E-03) * Ta*D_Tmrt*kPa*kPa + ...
 (8.99281156E-05) * Ta*Ta*D_Tmrt*kPa*kPa + ...
 (-7.14663943E-07) * Ta*Ta*Ta*D_Tmrt*kPa*kPa + ...
 (-2.66016305E-04) * va*D_Tmrt*kPa*kPa + ...
 (2.63789586E-04) * Ta*va*D_Tmrt*kPa*kPa + ...
 (-7.01199003E-06) * Ta*Ta*va*D_Tmrt*kPa*kPa + ...
 (-1.06823306E-04) * va*va*D_Tmrt*kPa*kPa + ...
 (3.61341136E-06) * Ta*va*va*D_Tmrt*kPa*kPa + ...
 (2.29748967E-07) * va*va*va*D_Tmrt*kPa*kPa + ...
 (3.04788893E-04) * D_Tmrt*D_Tmrt*kPa*kPa + ...
 (-6.42070836E-05) * Ta*D_Tmrt*D_Tmrt*kPa*kPa + ...
 (1.16257971E-06) * Ta*Ta*D_Tmrt*D_Tmrt*kPa*kPa + ...
 (7.68023384E-06) * va*D_Tmrt*D_Tmrt*kPa*kPa + ...
 (-5.47446896E-07) * Ta*va*D_Tmrt*D_Tmrt*kPa*kPa + ...
 (-3.59937910E-08) * va*va*D_Tmrt*D_Tmrt*kPa*kPa + ...
 (-4.36497725E-06) * D_Tmrt*D_Tmrt*D_Tmrt*kPa*kPa + ...
 (1.68737969E-07) * Ta*D_Tmrt*D_Tmrt*D_Tmrt*kPa*kPa + ...
 (2.67489271E-08) * va*D_Tmrt*D_Tmrt*D_Tmrt*kPa*kPa + ...
 (3.23926897E-09) * D_Tmrt*D_Tmrt*D_Tmrt*D_Tmrt*kPa*kPa + ...
 (-3.53874123E-02) * kPa*kPa*kPa + ...
 (-2.21201190E-01) * Ta*kPa*kPa*kPa + ...
 (1.55126038E-02) * Ta*Ta*kPa*kPa*kPa + ...
 (-2.63917279E-04) * Ta*Ta*Ta*kPa*kPa*kPa + ...
 (4.53433455E-02) * va*kPa*kPa*kPa + ...
 (-4.32943862E-03) * Ta*va*kPa*kPa*kPa + ...
 (1.45389826E-04) * Ta*Ta*va*kPa*kPa*kPa + ...
 (2.17508610E-04) * va*va*kPa*kPa*kPa + ...
 (-6.66724702E-05) * Ta*va*va*kPa*kPa*kPa + ...
 (3.33217140E-05) * va*va*va*kPa*kPa*kPa + ...
 (-2.26921615E-03) * D_Tmrt*kPa*kPa*kPa + ...
 (3.80261982E-04) * Ta*D_Tmrt*kPa*kPa*kPa + ...
 (-5.45314314E-09) * Ta*Ta*D_Tmrt*kPa*kPa*kPa + ...
 (-7.96355448E-04) * va*D_Tmrt*kPa*kPa*kPa + ...
 (2.53458034E-05) * Ta*va*D_Tmrt*kPa*kPa*kPa + ...
 (-6.31223658E-06) * va*va*D_Tmrt*kPa*kPa*kPa + ...

```
( 3.02122035E-04 ) * D_Tmrt*D_Tmrt*kPa*kPa*kPa + ...
( -4.77403547E-06 ) * Ta*D_Tmrt*D_Tmrt*kPa*kPa*kPa + ...
( 1.73825715E-06 ) * va*D_Tmrt*D_Tmrt*kPa*kPa*kPa + ...
( -4.09087898E-07 ) * D_Tmrt*D_Tmrt*D_Tmrt*kPa*kPa*kPa + ...
( 6.14155345E-01 ) * kPa*kPa*kPa*kPa + ...
( -6.16755931E-02 ) * Ta*kPa*kPa*kPa*kPa + ...
( 1.33374846E-03 ) * Ta*Ta*kPa*kPa*kPa*kPa + ...
( 3.55375387E-03 ) * va*kPa*kPa*kPa*kPa + ...
( -5.13027851E-04 ) * Ta*va*kPa*kPa*kPa*kPa + ...
( 1.02449757E-04 ) * va*va*kPa*kPa*kPa*kPa + ...
( -1.48526421E-03 ) * D_Tmrt*kPa*kPa*kPa*kPa + ...
( -4.11469183E-05 ) * Ta*D_Tmrt*kPa*kPa*kPa*kPa + ...
( -6.80434415E-06 ) * va*D_Tmrt*kPa*kPa*kPa*kPa + ...
( -9.77675906E-06 ) * D_Tmrt*D_Tmrt*kPa*kPa*kPa*kPa + ...
( 8.82773108E-02 ) * kPa*kPa*kPa*kPa*kPa + ...
( -3.01859306E-03 ) * Ta*kPa*kPa*kPa*kPa*kPa + ...
( 1.04452989E-03 ) * va*kPa*kPa*kPa*kPa*kPa + ...
( 2.47090539E-04 ) * D_Tmrt*kPa*kPa*kPa*kPa*kPa + ...
( 1.48348065E-03 ) * kPa*kPa*kPa*kPa*kPa*kPa
```

```
fprintf(fid_out, '%1.3f, %1.3f, %1.2f\r\n', xcoordinate,
ycoordinate, UTCI_approx);
```

```
end
```